1972

An engineering analysis of fluid amplifiers and development of an air velocity sensor

Gian Sagar Aneja

Department:

111

AN ENGINEERING ANALYSIS OF FLUID AMPLIFIERS AND DEVELOPMENT OF AN AIR VELOCITY SENSOR

by

GIAN SAGAR ANEJA, 1948-

A

THESIS

Presented to the Faculty of the Graduate School of the

UNIVERSITY OF MISSOURI-ROLLA

In Partial Fulfillment of the Requirements for the Degree

MASTER OF SCIENCE IN MECHANICAL ENGINEERING

1972

Approved by

D. L. Gyorey (Advisor) Virgil J. Flanigan

Xavier R Avula

ABSTRACT

Fluidics, the new control technique finds its use amongst the conventional electronics and pneumatics due to some of its impressive features. Selected literature about bistable and proportional amplifiers has been presented for better understanding of the element behavior.

Sensors; typical applications of fluidics have been described separately. An air flow velocity sensor has been set-up. Basically it consists of a cylinder placed across the air flow that sheds vortices in the wake due to 'Von Karman Vortex Street' phenomenon. The frequency of vortices gives a measure of velocity. The velocities obtained from the sensor have been compared to the ones obtained using a pitot tube.

ACKNOWLEDGEMENTS

The author wishes to extend his sincere thanks and appreciation to his advisor, Dr. D. A. Gyorog, for the guidance, encouragements and valuable suggestions throughout the course of this thesis.

The author is grateful to Dr. V. J. Flanigon. His assistance in reviewing the manuscript made this report possible.

TABLE OF CONTENTS

TABLE OF CONTENTS (Continued)

LIST OF ILLUSTRATIONS

LIST OF ILLUSTRATIONS (Continued)

LIST OF ILLUSTRATIONS (Continued)

LIST OF ILLUSTRATIONS (Continued)

LIST OF ILLUSTRATIONS (Continued)

LIST OF TABLES

LIST OF SYMBOLS

A	area
A,B	correspond to the two ports of an amplifier (control or the output)
c	control ports
C	capacitance of a fluid line
C_D	coefficient of drag
d	diameter of sensor tubes
d'	distance between free vortex layers
e	ambient conditions
f	frequency of vortices shed
D	drag force
h	depth of channels for the fluid elements
k	ratio of control nozzle width to power nozzle width
K	ratio of control mass flow to power mass flow
K_P	amplification factor
l	feedback cavity length for a fluidic oscillator
L	inductance of a fluid line
M	momentum of a fluid jet
o	receivers of fluid amplifiers
P	pressure
P_S	static pressure in the wind tunnel test section
q_c	dimensionless control flow
Q	volume flow
r	radii of the latched vortex vent
R	resistance of a fluid line

LIST OF SYMBOLS (Continued)

R_e	Reynolds Number
s	laplace operator s-domain
S	Strouhal Number
t	thickness of the power nozzle width of fluid amplifiers
T	temperature
T_t	transport time
u	velocity of vortices with respect to the flowing liquid
U	tangential velocity in vortex chamber of vortex amplifier
v_s	vent width for a jet attachment amplifier
V	velocity of air flow
W	weight flow of fluid
X,Y	rectangular coordinates
$\overline{X},\overline{Y}$	dimensionless rectangular coordinates
X_s	splitter location
X_v	vent location
Z	impedence of a fluid line
β	control pulse strength
γ	ratio of specific heats
θ	jet deflection angle
τ	time constant
ρ	density of air
μ	viscosity of air
Φ	vent terminal crossing angle
ω	uncertainty

I INTRODUCTION

Fluidic devices are being used as a new mode of control similar to electronics and pneumatics. Active research in Fluidics started with initiation by Harry Diamond Laboratories in 1960. Basically all the technologies depend on a medium to transmit energy which in case of Fluidics is gases e.g., air and liquids also are equally useful. There are fluidic control components such as bistable amplifiers, proportional amplifiers; elements such as resistors, capacitors and devices such as OR/NOR, AND/NAND; all these components find similar use to the ones employed in electronic circuits.

The fluidic control applications have been growing rapidly because of their impressive features such as higher reliability, lower cost of production, environmental tolerance, reducing the number of transducers etc. Fluidic applications include liquid level sensing, temperature sensing, rotational speed measurement and object sensing. It has also been used for process control, steam turbine speed control, hydrofoil lift control, aircraft pitch rate damper and fluid transmission control for diesel locomotive. Recently, fluid operational amplifiers have also been developed. The limitations of the fluidic components are slow response, noise problem, filtration of supply flow, load sensitivity, difficulty in cascading, thereby limiting the design of complicated circuits. In modern control techniques, Fluidics has come to stay with electronics and pneumatics and there has to be a compromise in their respective use as none of them is perfect in itself when economic considerations are included with the design considerations.

Out of the many fluidic components bistable and proportional

amplifiers play an active role in Fluidics. Wall attachment amplifier and turbulence amplifier, both come under bistable amplifiers. Similarly, under proportional amplifiers, there come jet deflection (interaction) and vortex amplifiers.

Wall attachment amplifier is basically an application of the Coanda Effect. If a jet of fluid, coming out of a nozzle, finds a straight or curved wall with in a certain range of distance, the jet attaches to the wall (Fig. 1) and travels along it. Switching it to the opposite wall is done through a low pressure control input. If the jet is again stable in the new position, the element is called a bistable amplifier. The two output pressures could be recovered separately by inserting a splitter in the downstream flow. On the other hand if there are no Coanda Walls by the side of the power jet (Fig. 2), it deflects on interaction with the control jet. The output from the amplifier depends on the strength of the control signal prior to saturation. Literature has been cited in the following chapters, to furnish more details about bistable and proportional amplifiers. Different types of switching, switching time analysis, special design configurations and cascading amplifiers have been dicsussed for jet attachment amplifiers. To analyse a jet interaction amplifier a lumped parameter technique and an equivalent electrical circuit has been presented. Also included are the design steps for cascading amplifiers and development of an operational amplifier and its applications in fluidic control circuits.

Different fluid sensors have been described and their practical design feasibilities considered. The primary object of the present

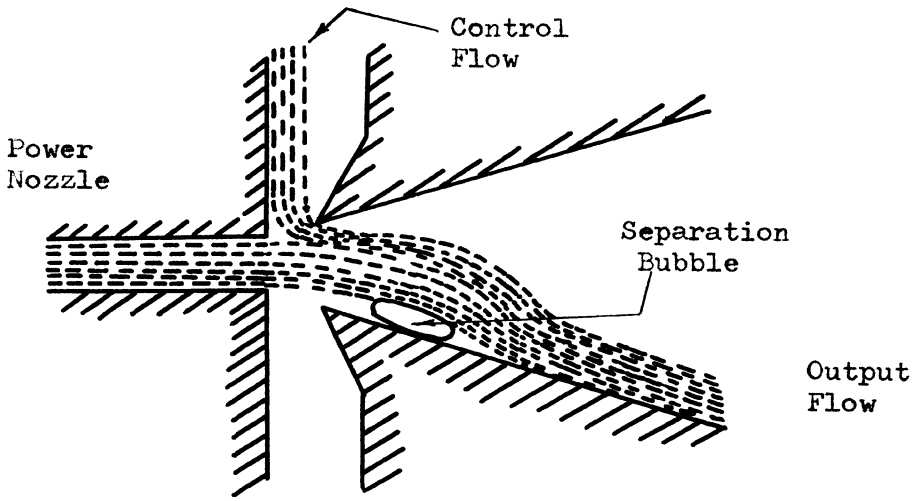

Fig. 1. A Wall Attachment Amplifier

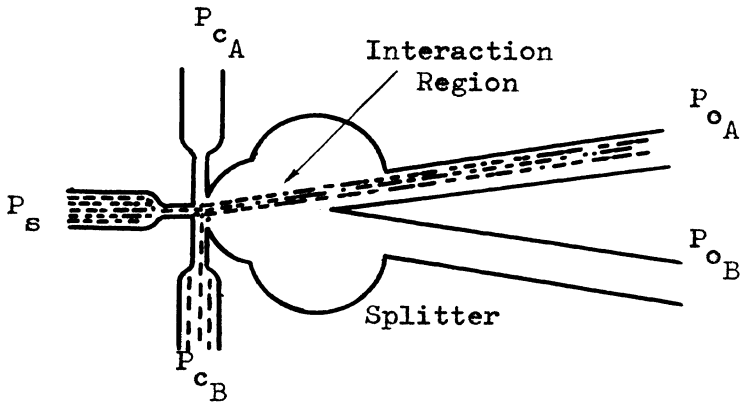

Fig. 2. A Jet Deflection Amplifier

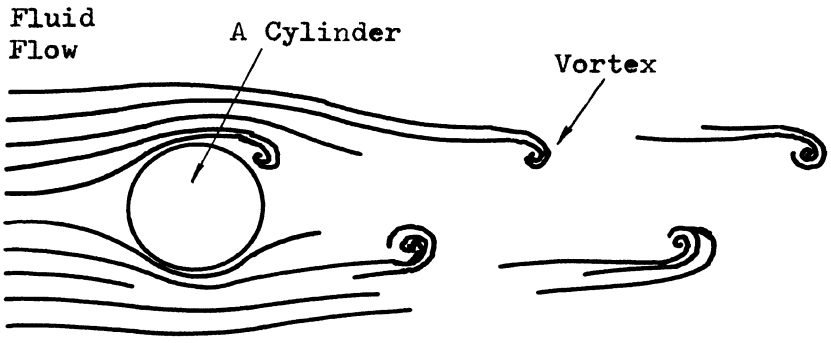

Fig. 3. Vortex Shedding Illustration

investigation was to analyse 'An Air Flow Velocity Sensor' and test it experimentally. The principal behind this sensor is that a cylinder immersed in an air flow sheds vortices in its wake (Fig. 3) due to 'Von Karman Vortex Street', the frequency of vortices shed gives a measure for the velocity of air flow.

II BISTABLE AMPLIFIERS

An element, which gives two discrete levels of amplified output on application of relatively small input signal, is known as a bistable amplifier.

There are different fluidic components such as jet attachment amplifiers, turbulence amplifiers, induction amplifiers which all come under bistable amplifiers. In this chapter jet attachment and turbulence amplifiers have been described with reference to available literature.

A. Jet Attachment Amplifiers

It has already been mentioned in the Introduction that the operation of a jet attachment amplifier is based on the Coanda Effect. A fluid jet exiting a nozzle entrains the surrounding air. Due to a free replacement of air surrounding the jet, there is no pressure gradient set up across the jet. However, the presence of a wall restricts the replacement of the entrained air and results in a drop in pressure in the region. Thus, the jet leans towards the wall forming a small low pressure separation bubble. This phenomenon was historically found by Henry Coanda, a Rumanian Engineer. In the case of no control flow, the power jet attaches to one of the walls at random and remains stable. On application of a low pressure control flow, the pressure in the separation bubble increases and the power jet eventually detaches and flips to the other wall forming a new separation bubble. There are three kinds of switching gains for the amplifier which are defined as follows;

$$\text{Pressure Gain,} \quad G_P = \frac{p_{OA} - p_{OB}}{p_{CA} - p_{CB}}$$

$$\text{Flow Gain,} \quad G_Q = \frac{q_{OA} - q_{OB}}{q_{CA} - q_{CB}}$$

$$\text{Power Gain,} \quad G_{PQ} = \frac{p_{OA} \cdot q_{OA} - p_{OB} \cdot q_{OB}}{p_{CA} \cdot q_{CA} - p_{CB} \cdot q_{CB}}$$

where p_O and q_O are changes in the output pressure and flow during the switching operation corresponding to p_C and q_C, the changes in the control pressure and flow respectively. A and B correspond to the two control ports and outputs for the amplifier.

In general, bistable amplifiers along with other active devices are vented to the atmospheric pressure so that different types of loading have a minimal effect on their normal operation.
The characteristics of a vented bistable amplifier appear in Figure 4. Fig. 4 a. illustrates the output characteristics i.e., outlet pressure vs. outlet flow corresponding to various supply pressures and the power nozzle is described by the curve supply pressure vs. supply flow (Fig. 4 b.). Normally a supply pressure of about 5 psi is chosen to limit power consumption and attain the most efficient operation. Power jet velocities are kept in the subsonic region around Mach No. equal to 0.3. The switching characteristics (Fig. 5) take into account different supply pressures and the curves correspond to right control signals as well as left control signals. These plora may differ slightly due to possible unsymmetry in manufacture of the two control ports and the receivers about the center line of the amplifier.

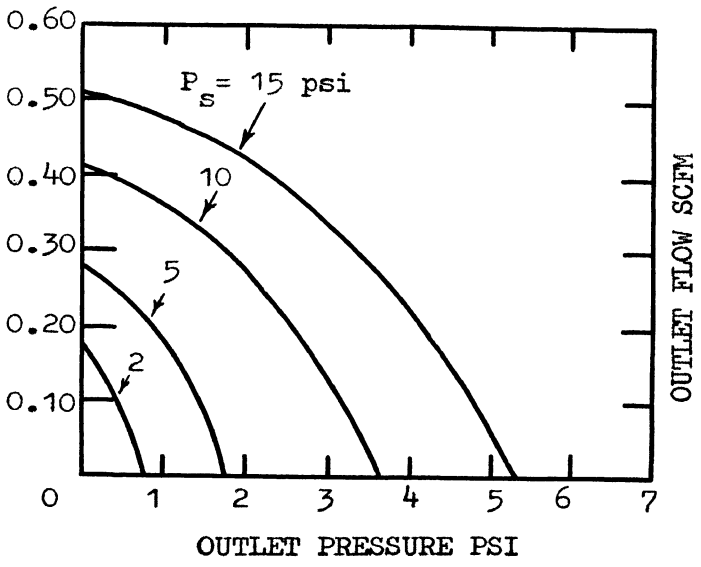

Fig. 4a. Output Characteristics of a Jet Attachment Amplifier

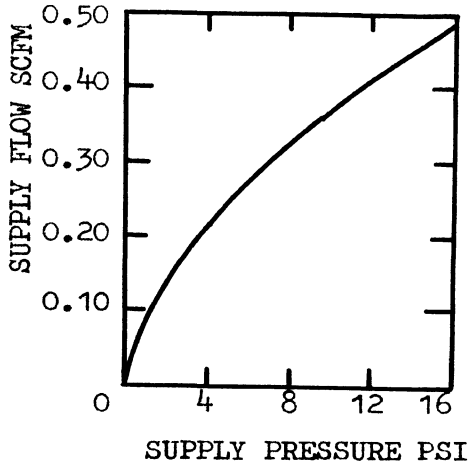

Fig. 4b. Supply Pressure and Flow Characteristics

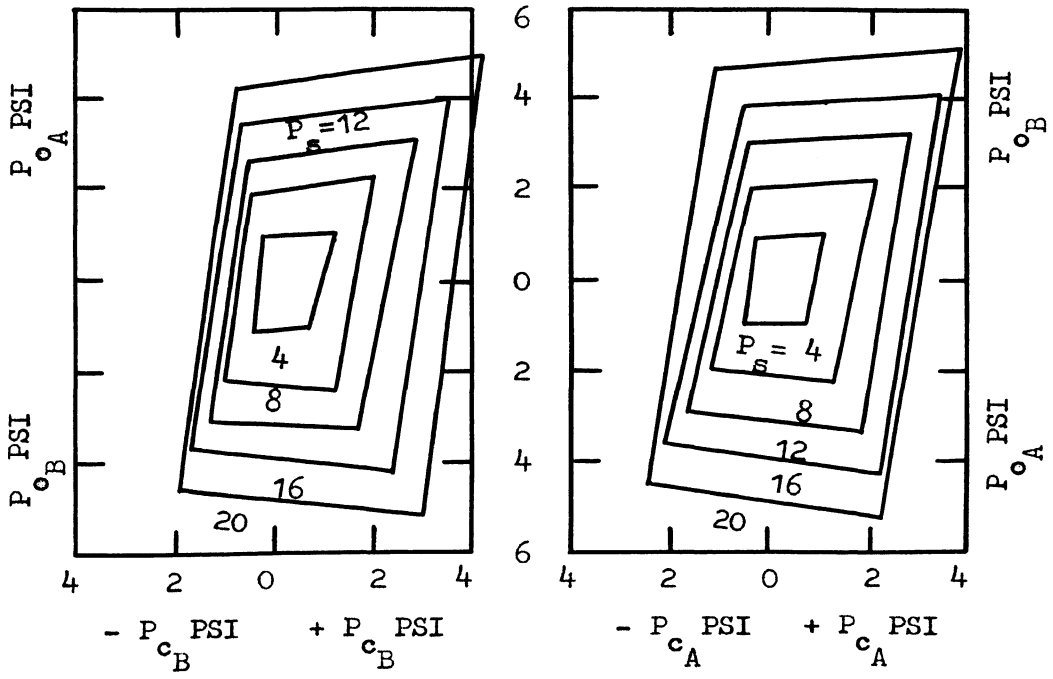

Fig. 5. Typical Switching Characteristics of a Jet Attachment Amplifier

A wide range of operational features of a jet attachment amplifier can be obtained by changing its geometrical parameters [1]. Presently a general change in performance is presented, however, in the later part of this chapter elements with specific dimensions and performance characteristics will be discussed.

1. Increasing Control-Nozzle Area:
   a. Decreases control pressure for switching
   b. Increases tendency for the power jet to oscillate
2. Increasing Coanda-Wall Divergence Angle:
   a. Decreases flow for switching
   b. Moves jet attachment point downstream
3. Increasing Receiver Aperture:
   a. Increases counter flow
   b. Increases pressure recovery
4. Moving Splitter Downstream:
   a. Increases memory
   b. Increases counter flow
   c. Decreases output energy
   d. Decreases pressure recovery
   e. Decreases tendency for the power jet to oscillate
5. Increasing Interaction Region Width (Coanda-Wall offset):
   Increases control flow, necessary for switching, up to a set back of twice the power nozzle width after that the control flow decreases
6. Increasing Depth of Flow Channels (Aspect Ratio):
   a. Increases flow
   b. For small aspect ratio (4), effect of boundary walls

increases

7. Increasing Load:

   a. Reduces control necessary for switching out of load

   b. Increases control necessary for switching into load

   c. Increases tendency for the power jet to oscillate

Switching is one of the most important aspects of a bistable amplifier yet to be analysed in detail. Several authors have tried to analyse the problem mathematically, worked with different configurations to get an efficient switching mechanism. First of all a theoretical description is given by Warren [2], where it is classified in to three types;

1. The two side walls terminate or have bleeds to separate the rest of the wall (Fig. 6). On application of control flow the separation bubble communicates with the atmospheric pressure through the bleed. The main jet straightens up, with continued control flow and entrainment of fluid on the other side causes the jet to switch to the other wall. This type of switching is called Terminated Wall or Bleed Type Switching.

2. In Contacting Both Walls type switching, the side walls are so close that on application of control flow the power jet contacts the opposite wall while still in contact with the first wall, forming two separation bubbles (Fig. 7). This happens before the power jet contacts the splitter. The first separation bubble grows in size as the pressure increases due to the control flow. Ultimately, the jet switches to the other side and switching is completed when the opposite separation bubble reaches its equilibrium state. In this type of switching the attachment walls

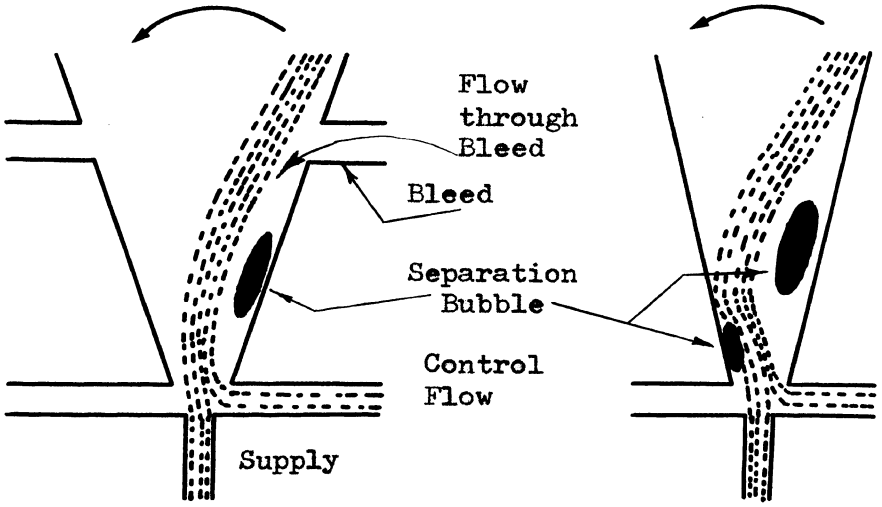

Fig. 6. Terminated Wall or Bleed Type Switching

Fig. 7. Contacting Both Walls Type Switching

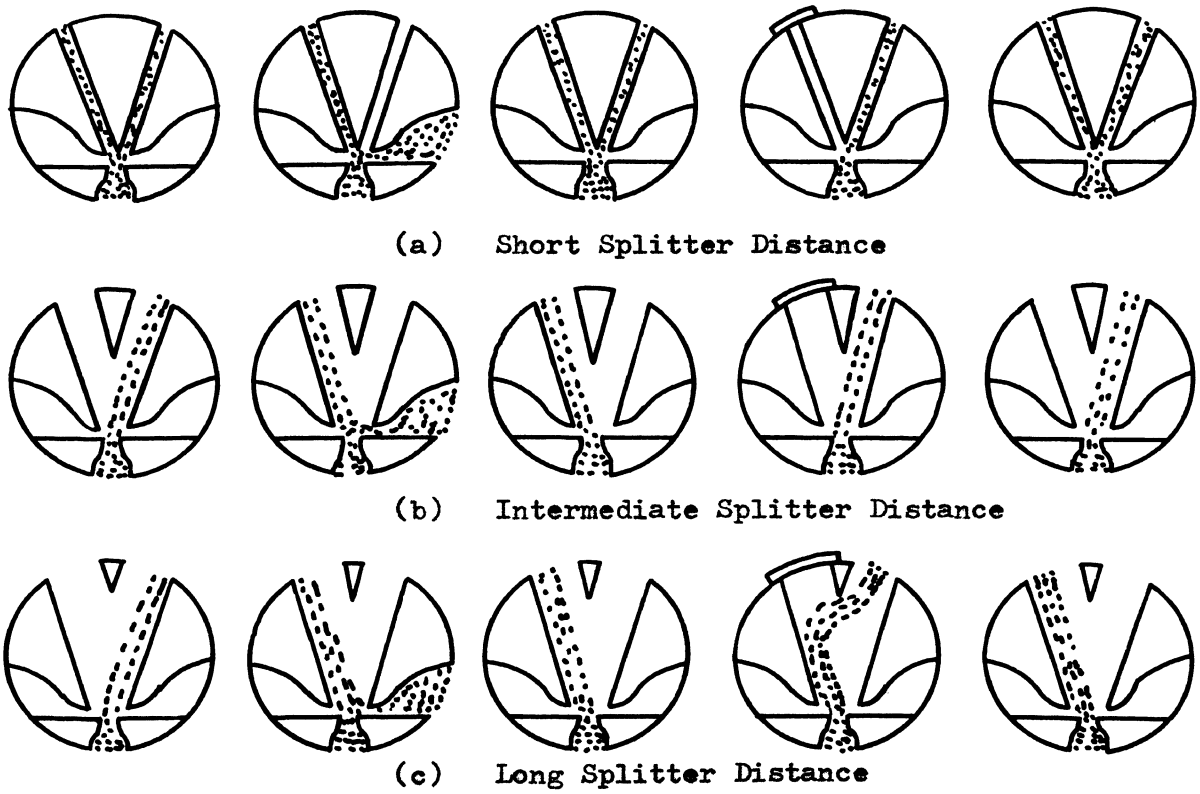

Fig. 8. Splitter Switching

are relatively long and there is limited communication of the separation bubble with the ambient pressure. However the pressure in the separation bubble is of course less than on the unattached side.

3. Splitter switching differs from the previous types in the sense that the power jet reaches the splitter before touching opposite wall. This occurs while the jet is contact with the first wall or in other words, there is a splitter penetration before the jet contacts the opposite wall or the separation bubble communicates with the atmosphere. If the splitter is located at the exit of the power nozzle, a situation similar to a pipe flow occurs and the flow is split equally in two channels (Fig. 8 a.). Control flow switches the power jet but only when it is present and so is the effect of blocking one of the outputs of the amplifier. Locating the splitter downstream (Fig. 8 b.) decreases gain and increases stability of the jet. Effects of splitter location further downstream as well as blocking one of the outputs have been shown in Fig. 8 c.

To make a rough judgement about the type of switching for an amplifier considering its geometrical parameters only, following procedure is adopted. If the wall divergence angle is more than 15° and they are located more than twice the power nozzle width apart and then if the bleed vents are located downstream of splitter, the switching is splitter type or if the bleed vents are located in the unstream, the switching will be terminated wall or bleed type. In the third case if the wall divergence angle is less than 10° and they are located less than twice the power nozzle width, further if the bleed vents and splitter locations are downstream (more than 12 times the power nozzle

width), the type of switching will be contacting both walls type.

The switching time analysis on a large scale model [3] was a special case to the amplifiers (Fig. 12) tested by Hara, Ozaki and Harda [5]. It is claimed that the present model could be scaled down from a 1" power nozzle throat width to a throat width of 0.04". The Mach No. is limited to 0.3 and minimum Reynolds No. 10^4. The switching time has been divided into three phases out of which the third phase is usually omitted.

1. Bubble growth
2. Flipping power jet to opposite wall
3. Bubble shrinkage

Lush [3] extended the theory by Borque and Newman [4] by describing the bubble growth in terms of the net flow into the separation bubble, taking into account the control flow and assuming quasi-steady flow conditions. Flipping time is essentially controlled by the control pulse strength. It is recommended for the control flow to be about twice the threshold value of flow calculated fow switching that is how the dwell time is reduced. The test were made on a large scale table model amplifier with 1" throat width (Fig. 12), throat velocity of 170 fps and Reynolds No. $9X10^4$. In the plots following variables have been used.

q_c = Non-dimensional control flow

τ = Non-dimensional time defined as:

$$\frac{\text{Mean main jet velocity at nozzle exit X time}}{\text{Throat width}}$$

β = Main jet deflection which is proportional to the control pulse strength or the control flow

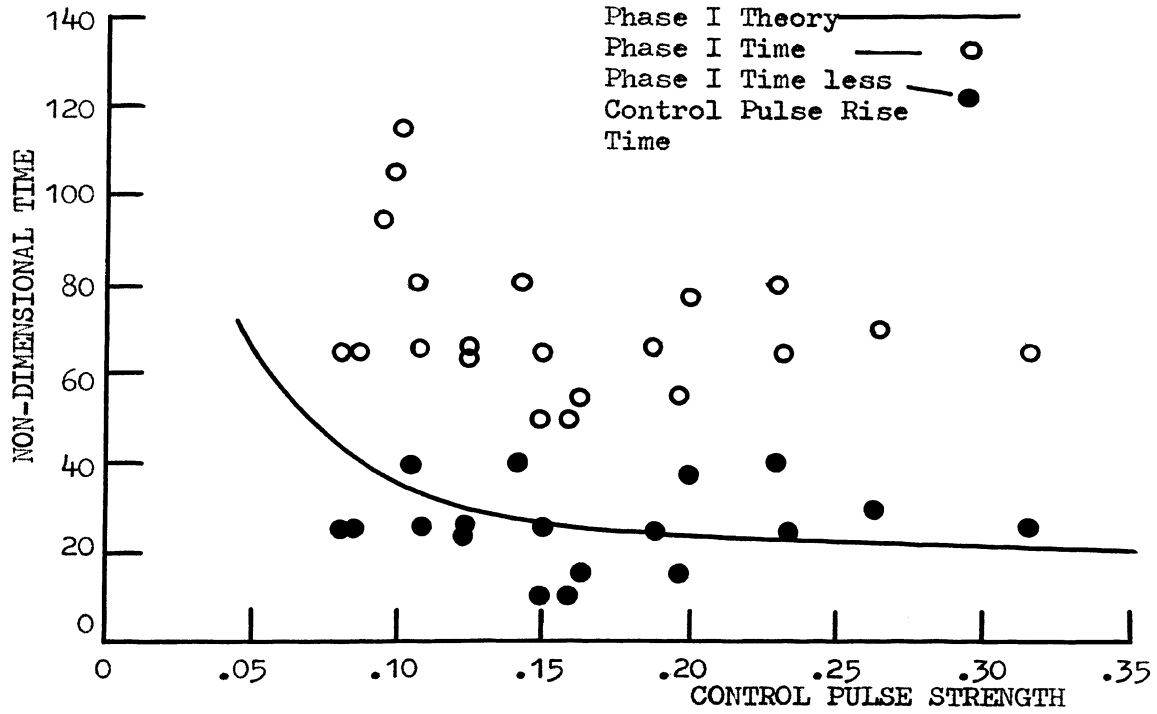

Fig. 9. Variation of Phase I Growth Time with Control Pulse Strength

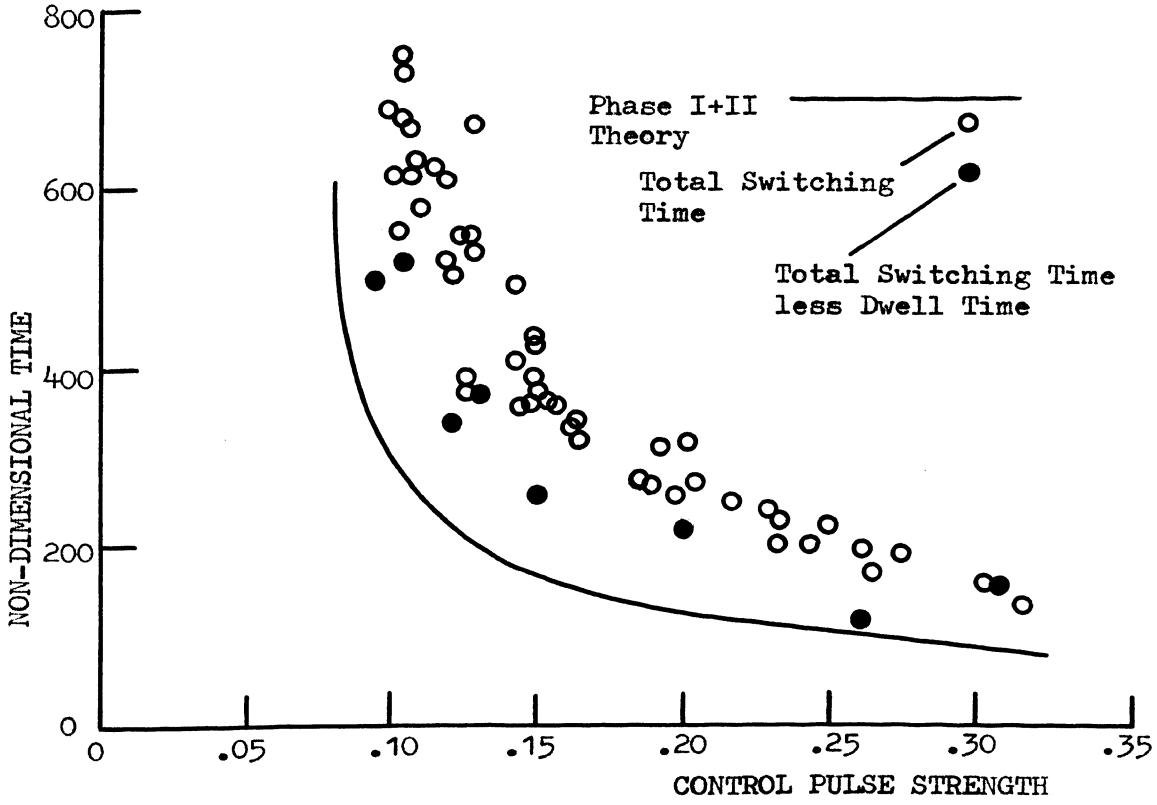

Fig. 10. Variation of Switching Time with Control Pulse Strength

Figure 9 shows the variation of phase I growth time with control pulse strength. The theoretical predictions, which do not include the finite control pulse time, don't agree with experimental data. If this time is subtracted from the experimental switching times, there seems to be a good agreement in the results.

In the second plot (Fig. 10) the time ordinate includes the flipping time of the jet. The dwell time is a maximum for control pulse strength $\beta = 0.09$ and decreases to nearly zero at $\beta = 0.3$. There is discrepancy in the results even when the dwell time is subtracted from the experimental points. This has been explained as the resulting inertia of the output columns of fluid can not be neglected, as was assumed, thereby the probes set up in the outputs measure longer time. Also, there is some effect due to the presence of opposite wall that helps in switching. Considering these points, the switching time estimates could be more precise.

More experimental tests on an amplifier (Fig. 11), geometrically similar to the one used by Lush [3] but smaller in size (0.02" power nozzle width), were done by Harda, Ozaki and Hara [5]. Primarily the analysis is aimed to investigare the effect of changing various geometrical parameters on pressure recoveries. It was found that recovery is not much effected by the vent position in case it is located downstream of the splitter (Fig. 12), however it increases by increasing the terminal crossing angle Φ(Fig. 13). Increasing the terminal angle is equivalent to closing the vent opening out of the way to receiver, that is how the recovery pressure increases. It is normally kept in the range of 75°- 90°. Also shown is the effect of

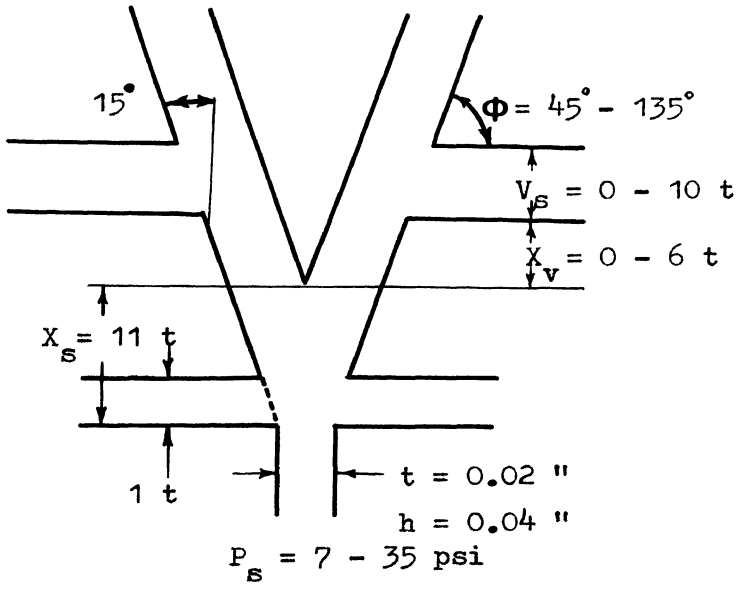

Fig. 11. Basic Pattern of the Element

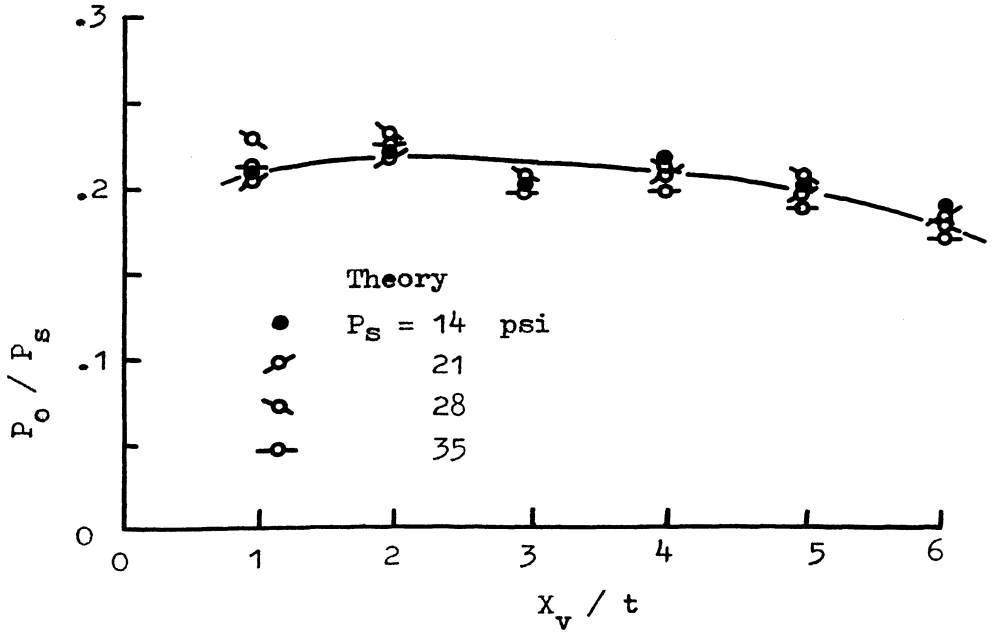

Fig. 12. Effect of the Vent Position on the Recovery Pressure

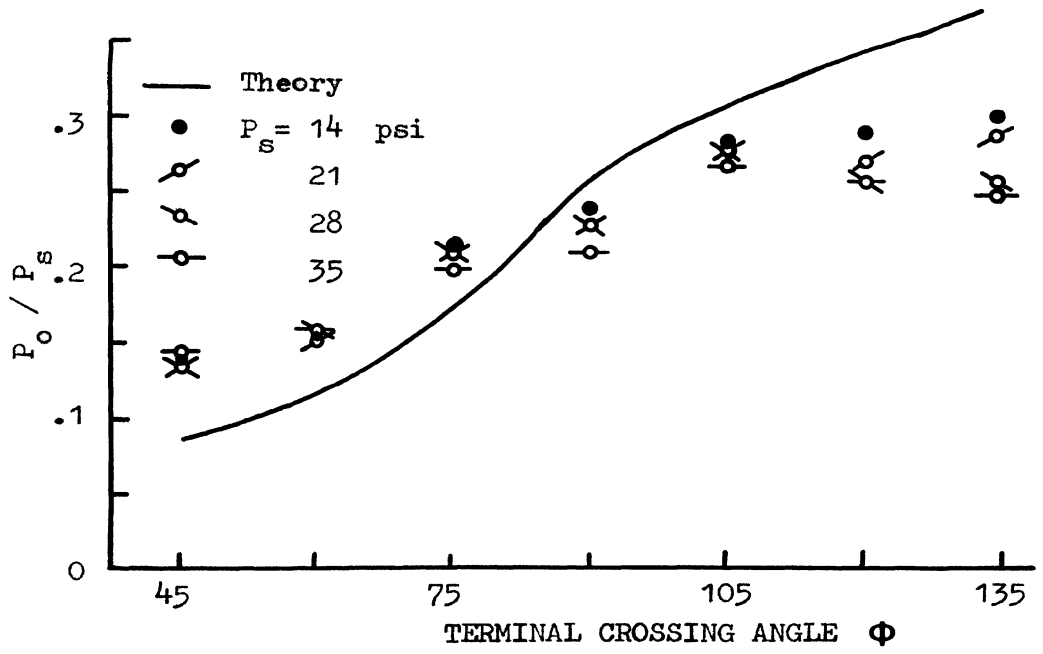

Fig. 13. Effect of the Terminal Crossing Angle on the Recovery Pressure

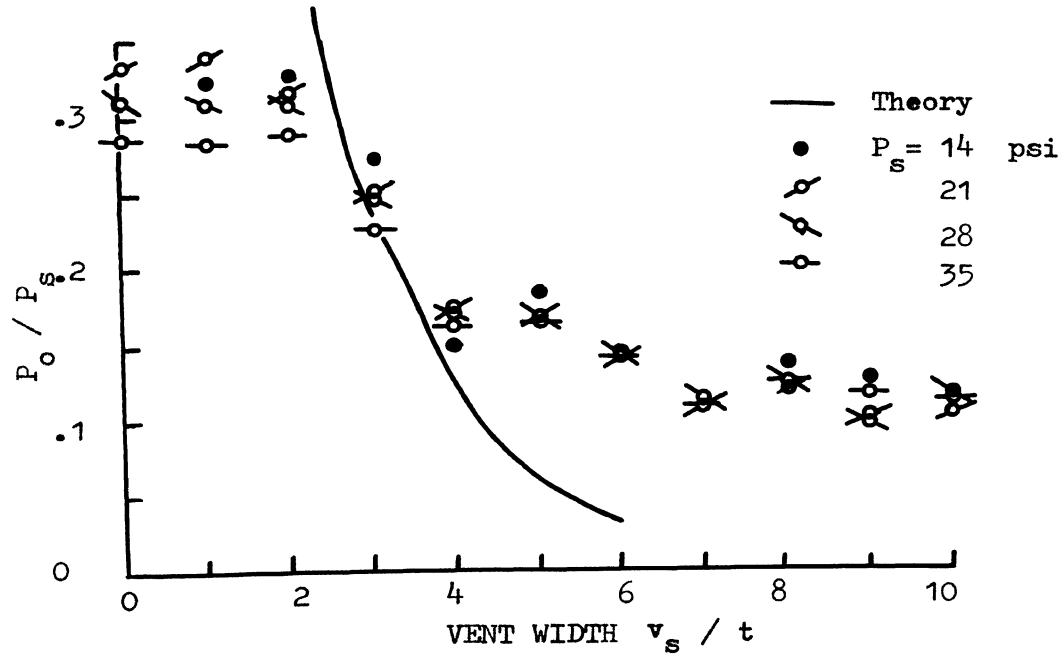

Fig. 14. Effect of the Vent Width on the Recovery Pressure

changing vent width. It plays quite a dominating role. Considering the experimental data and theoretical predictions, although they don't agree (Fig. 14), it is obvious that the pressure recovery drops considerably when the vent width exceeds twice the power nozzle width.

Most of the work on jet attachment amplifiers deal with elements having straight Coanda walls. Sarpkaya [6] tested three kinds of walls straight, concave and convex, to determine whether it was possible to have an improved performance by suitably curving the Coanda walls. Concave walls revealed poor pressure recovery curves due to a significant loss in energy due to turbulence mixing which dominates over the loss due to wall friction. Also, the pressure recovery depends on the size of the separation bubble to a large extent. In case of convex walls the separation bubble is smaller in size and overall loss in pressure recovery is considerably less (Fig. 16). Figure 15 shows a wall attachment amplifier with convex Coanda walls. The recovery pressure curves (Figs. 16 a, b & c) correspond to three power nozzle velocities 75, 300 and 460 fps respectively. The model tested was a large scale one with power nozzle width of ¼". The ideal pressure recovery is determined by assuming a subsonic power jet of an ideal gas decelerated isentropically along the curved walls, the pressure at the exit of the power nozzle to be atmospheric. Then the power nozzle and active control nozzle velocities, assuming to be uniformally distributed, are given by:

$$V_s = \frac{Q_s}{t.h} \qquad \text{and} \qquad V_c = \frac{Q_c}{1.5\ t.h} \qquad (1)$$

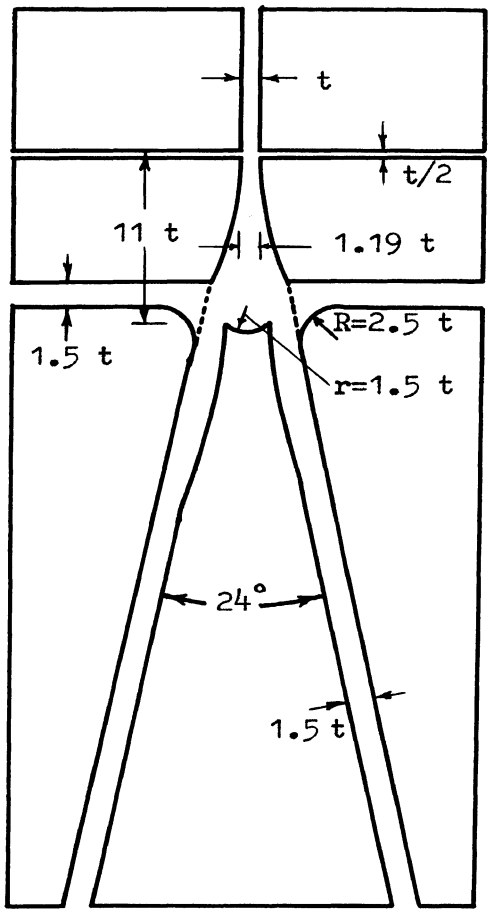

Fig. 15. Geometry of the Convex-Walled Amplifier

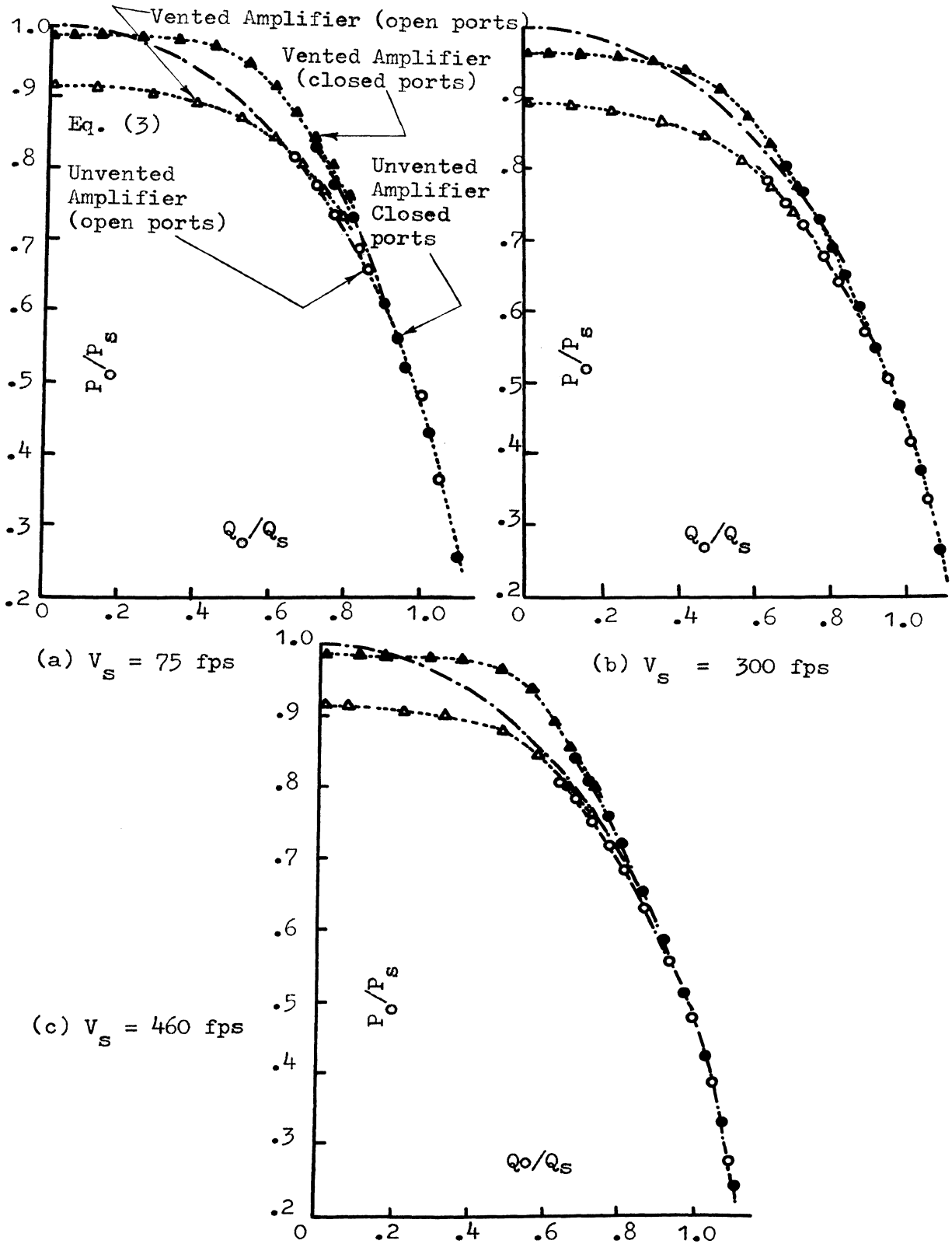

Fig. 16. Pressure Recovery vs. Normalized active-port flow for a convex walled amplifier for open and closed ports.

where 't' is the power nozzle width and 'h' is the depth of the element channels. Making use of the Bernoulli's equation and ignoring the energy correction factors;

$$P_s = \frac{\rho . V_s^2}{2} = P_o + \frac{\rho . V_o^2}{2} \qquad (2)$$

Combining equations (1) and (2) yields:

$$P_o/P_s = 1 - (1/2.25) (Q_o/Q_s)^2 \qquad (3)$$

It is apparant from the pressure recovery plots that a convex walled unit has almost ideal performance characteristics. It was also found that for a given vent and control port condition the pressure recovery vs. flow recovery relation is almost independent of the Reynolds No. and Mach No. within the range of velocities tested.

Another entirely new configuration of a jet attachment amplifier, developed under Nasa project and presented by Griffin [7], was specifically designed to handle blocked and highly capacitive loads such as a piston or bellows which normally tend to make a fluid element unstable. This amplifier (Fig. 17) is capable of driving a capacitive or reverse flowing load at high speed and with much smaller control signals. The following points were kept in mind while designing the amplifier configuration.

1. The receiver's reverse flow to be diverted away from the interaction region at the same time interaction region has to be supplied with atmospheric pressure.
2. The receiver is required to develop satisfactory pressure and flow recoveries during normal forward flowing operation.

The reverse flow from receivers escapes through vents V_3 (Fig. 17).

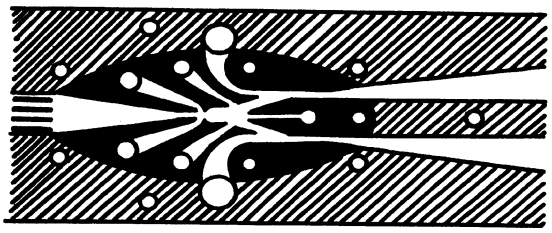

Fig. 17a. Configuration of NASA Model 7 Fluid Jet Amplifier

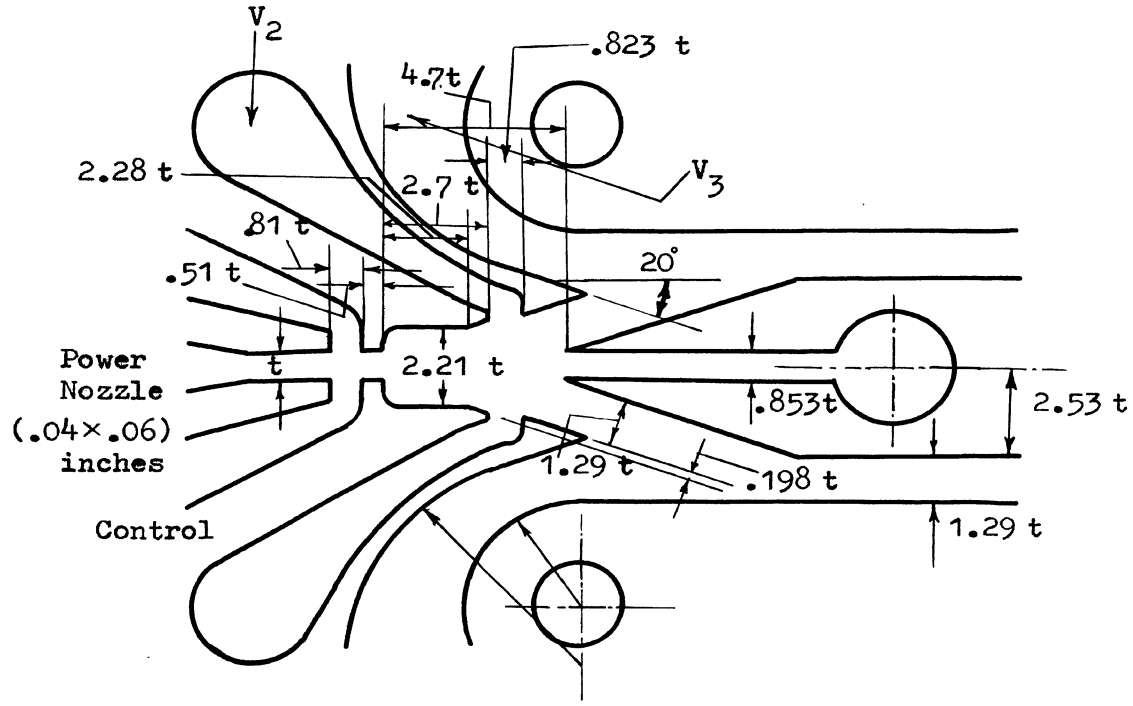

Fig. 17b. An Exploded View of the Fluid Jet Amplifier's Interaction Region

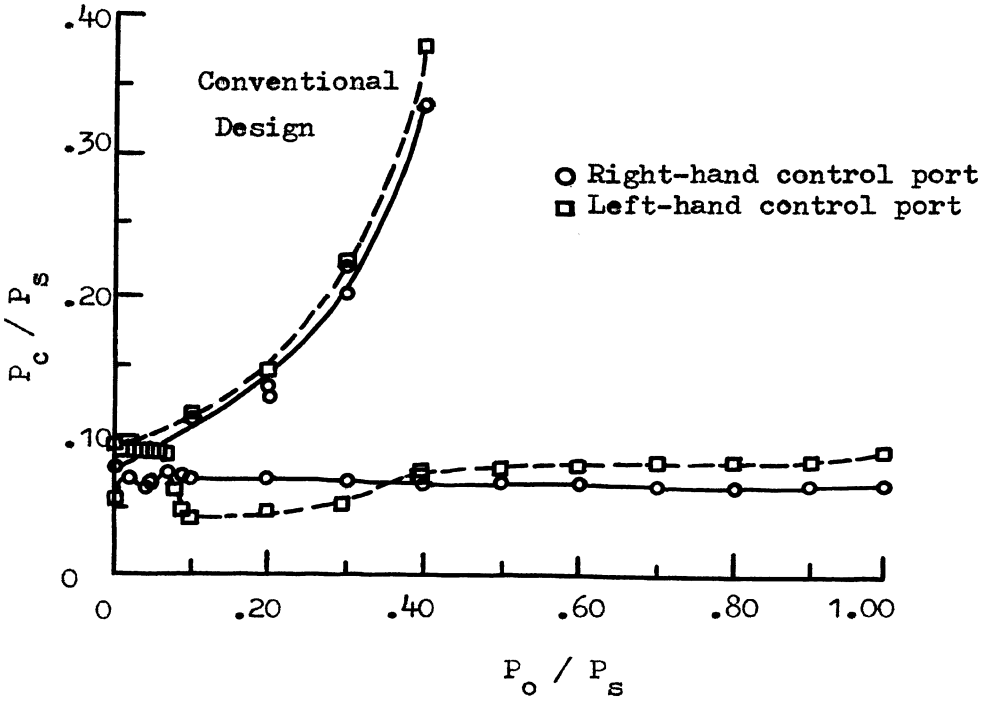

Fig. 18. Control Pressures required to switch conventional and NASA Model 7 Fluid Jet Amplifier into reverse flowing receivers. Other receiver is vented to atmosphere.

A separate vent V_2 provides the necessary entrainment flow. The baffle between V_2 and V_3 prevents the reverse flow to disturb the interaction region. It has been found that for a supply pressure of 1 psig, control flow of only 10 - 15 % of the supply is sufficient to enable the amplifier to drive a piston load under most conceivable modes of operation. Figure 18 reveals that considerably less amount of control pressure is necessary to switch the power jet into load receiver while for a conventional amplifier switching pressure usually increases with the load. The present design needs improvement in its manufacturing techniques because its interaction region is sensitive to manufacturing errors.

Cascading Amplifiers:

It is essential to develop analysis techniques for cascaded elements in fluidic circuits. Generally, the gains of individual amplifiers are limited and a greater gain can be obtained through cascading amplifiers. Belsterling [8] pointed out that input and output characteristics of the elements to be cascaded are very important considerations. The output characteristics demonstrate the way in which the amplifier will behave with a load and the input characteristics illustrate the switching flow requirements. These two characteristics are superimposed (Fig. 19). As long as the switching points of the input characteristics fall within the boundaries of the output characteristics of the driving amplifier, the elements are said to be roughly matched, however the cascading operation will be more efficient when the switching points lie close to the boundaries. In case they lie outside the output characteristics

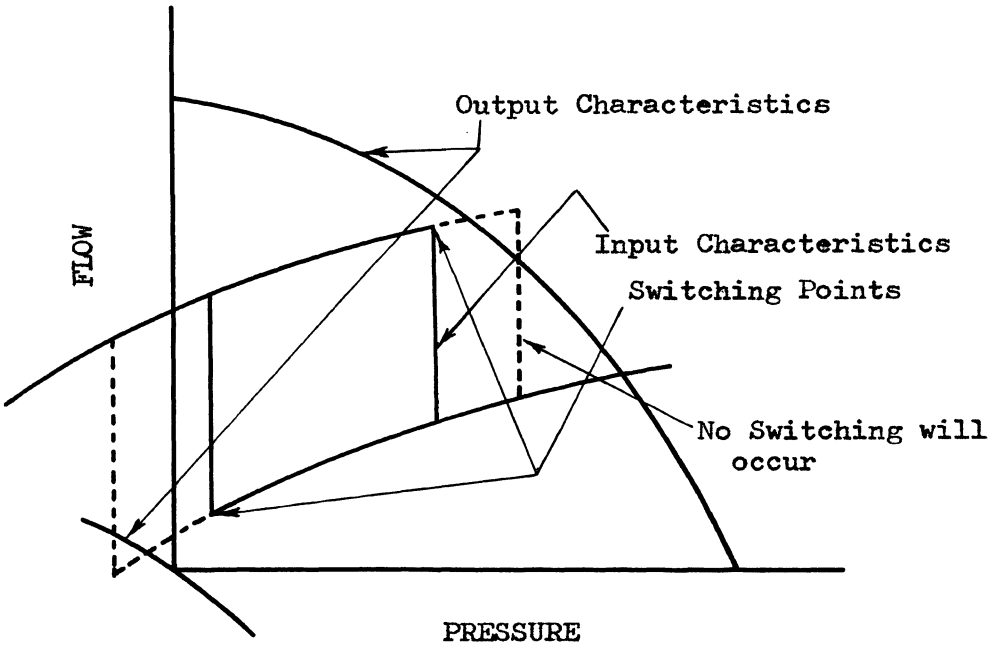

Fig. 19. Superimposition of input-output characteristics of Jet Attachment Amplifiers to test the cascading operation

of the driving element, the elements are not cascaded as the driven element does not receive strong enough signals for switching. In most digital circuits, an important requirement for the amplifiers is to have high fan-out capability. It is defined as the number of like elements an element can switch. A numerical analysis has been included to find out the fan-out capability of a jet attachment amplifier manufactured by Aviation Electric. Similarly the fan-in capability is defined as the number of like elements that can switch a given unit. It is desirable to bring all inputs directly into the jet interaction region. However, due to physical limitations it is not feasible to have fan-in greater than 4, although a fan-in of 6 has been reported.

To design a closed system (no vents) , each successive amplifier has to be made bigger to accommodate the total flow coming from the previous stage. An analysis by Hayes and Kwok [9] on latched vortex vents (Fig. 20), located between two consecutive stages, does make the cascading operation easier to some extent. In the normal operation vent flow is negligible, with gradual blocking of output or even in case of reversed flow to some extent, the flow escapes through the vent without switching the main jet. In other words, as the output is loaded, static pressure inside the chamber goes on increasing while the vortex vent resistance goes on decreasing, thereby the flow through the vortex vent increases. This element has a wide range of operation along with the cascaded stages. It has appreciable pressure recoveries but has a draw back, that compression pulses propagate back into amplifier's interaction region. The pressure and velocity distribution flow equations for the outer annulus region as well as

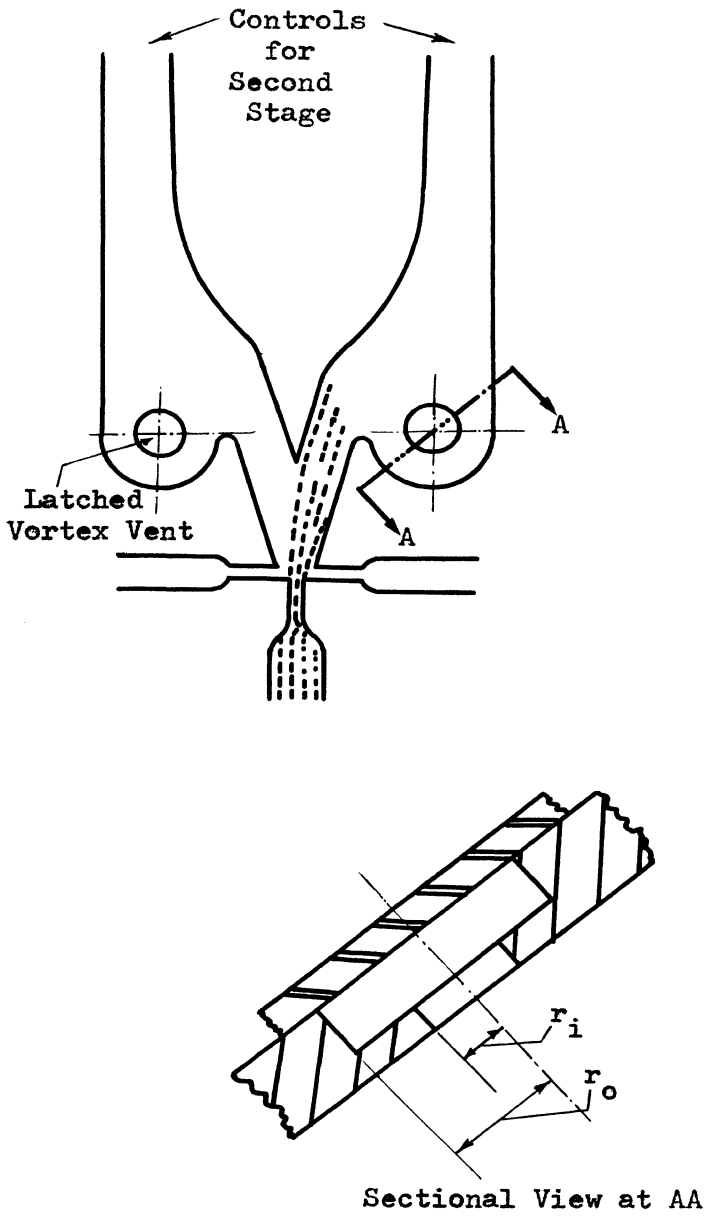

Fig. 20. Latched Vortex Vent Configuration as applied to a Fluid Amplifier

inner core flow region of the vent were derived in cylindrical coordinates basically starting from the Navier-Stokes equations with assumptions such as; the flow in the vent is steady, symmetrical with respect to Z-axis, incompressible and it is fully established and defined by the velocity vector in the annulus region $r_i < r < r_o$.

Experimentally, a large scale model was under test that proved the theory with water as the working fluid. Its flow pattern was visualized and water velocities were determined from the length of light streakes from the time exposure photographs of the water flow.

A Numerical Example for Cascading Amplifiers:

An Aviation Electric wall attachment amplifier (line matched), has been used to test the normal staging of amplifiers and also to find its fan-out capability. Refer to Figure 4 for its characteristics. Following is some information for the amplifier;

	Max.	Nominal	Min.
Input pressure	15 psig	5.0 psig	2.0 psig
Power consumption		4.1 watts	1.0 watt
Pressure Recovery (Blocked)		35 %	
Flow Recovery (Open)		125 %	
Frequency response	800 cps		
Response time		0.0004 sec	
Switching flow	0.110 scfm	0.060 scfm	0.035 scfm
Switching pressure	1.15 psig	0.68 psig	0.31 psig

Assuming a supply pressure to the first amplifier to be 2.0 psig for which switching flow is 0.035 scfm and switching pressure is 0.31 psig. Further assuming that supply press to the second stage is 5.0

psig which requires a switching flow of 0.60 scfm and switching pressure 0.68 psig. It is observed from Figure 4 a. that the switching requirement for the second stage cannot be met from the first stage corresponding to a supply pressure of 2.0 psig since the switching points lie outside the output characteristics of the first amplifier. Increasing the supply to 5.0 psig would be more than enough. Since the amplifiers have been equiped with vented vortex that can take care of the extra pressure and flow to allow a successful cascading operation.

The fan-out capability of the above mentioned amplifier can be determined from the flow criterion. Corresponding to a supply of 5.0 psig and its switching pressure of 0.68 psig, the available flow from the output characteristics (Fig. 4 a.) is found to be 0.22 scfm. As the switching flow for a single element is 0.060 scfm, a fan-out of 3 is suggested.

Total switching flow required for three elements = 0.06×3

$= 0.18$ scfm

The extra flow (0.22 - 0.18) scfm escapes through various vents in the elements. Care has to be taken since it is possible that the vent flow may be larger than (0.22 - 0.18) scfm, in that case a fan-out of only two is possible.

B. Turbulence Amplifiers

It is another kind of bistable amplifiers with no moving parts. Basically it consists of two precisely aligned power tubes which have been introduced into a vented cavity along with one or more control

tubes placed across the main flow (Fig. 21).

In the absence of control signals, power stream is normally laminar, consequently there is a high pressure recovery (Figs. 22-23). As a control signal through any of the control tubes is applied, it turns the main power jet turbulent. Since the spread rate of a turbulent jet is greater than that of a laminar jet, a considerable reduction in output pressure is noticed.

Turbulence Amplifiers have a very low power consumption. Output pressure ranges from 2 inches of water (0.07 psi approx.) to less than 10 inches of water. Typical flow rates vary from 1.5 to 3.0 cubic feet per hour and Reynolds No. normally is 1400. Sensitivity increases as the Reynolds No. approaches the transition. As compared to other fluidic active components such as a jet attachment amplifier or a jet interaction amplifier, it has a very low power consumption because of;

1. Number of stages can be reduced because of high component gain.
2. Power consumption per stage is less.

Turbulence amplifiers are relatively slow. The shortest practical switching time is in the range of three milli-seconds. Improved response is obtained through;

1. Increasing power flow or approaching transition, as a consequence amplifier stability is sacrificed.
2. By using strong signals i.e., overdriving the power jet.

Turbulence Amplifiers are relatively insensitive to mis-matches with other circuit elements and have high fan-in and fan-out values. In a report by Auger [10], a fan-out approaching 20 is attainable by modification of amplifier structure or by alteration of supply

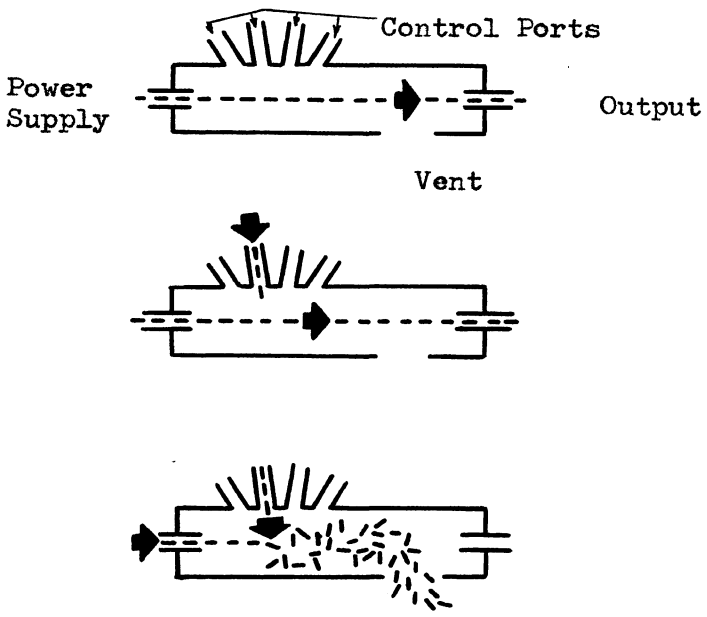

Fig. 21. The Transition in the Power Jet of a Turbulence Amplifier on application of a control signal

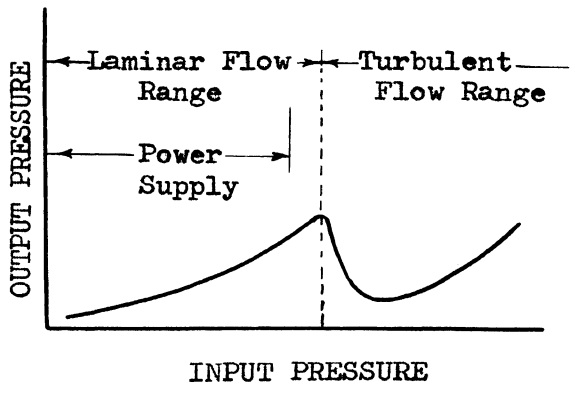

Fig. 22. A Generalized Turbulence Amplifier input-output pressure curve showing operating range and switching point.

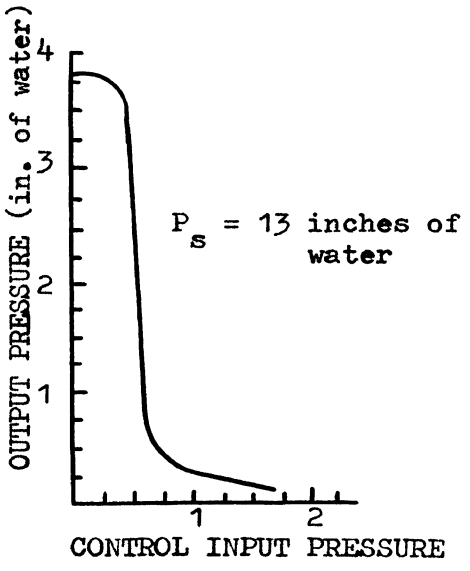

Fig. 23. Input-Output Characteristics of a Turbulence Amplifier

pressure. Turbulence caused by control signals is also effected due to geometrical parameters such as the diameters of input, output and supply tubes, changes in the power jet velocity as well as the viscosity and the density of the working fluid.

In another reference Auger [11] concluded that 0.030 inch for the input-output tubes diameter satisfies the practical suitability aspects such as power consumption, fabrication convenience, gain, output volume and size of element etc. The input-output tubes are kept 0.7 - 1.0 inches apart. If this distance exceeds 1.3 inches, sound sensitivity begins. With increasing distance, the unit becomes sensitive to high frequencies of the order of 10,000 cps. That is how at a distance of 1.9 inches with a supply of 4 inches of water, 0.2 inches is recovered when the flow gets disturbed by a dog whistle blown from a distance of 30 feet, but in case of no disturbance the pressure recovered is 0.9 inches. On the other hand when this distance is reduced below the range of high frequency sensitivity, it works fine with approximate power gain from 40 to 80. Decreasing the distance further will result in reduced gain.

Following design hints for overall description of a Turbulence Amplifier were given by Metzger and Lomas [12]:

1. Nozzle Design;
   a. To achieve a high gain the nozzle should be operated near the critical Reynolds No. range (transition).
   b. Unless sufficient length is allowed for the power nozzle, laminar flow will not be achieved prior to power nozzle exit and an earlier transition to turbulence is experienced.

2. Receiver Design;

   a. Receiving aperture should have an area about the size of the power nozzle.

   b. As much open space as feasible must be allowed on all sides of receiver to permit easy exit for the uncaptured flow.

   c. Venting is essential as any resistance in the area reduces the effective flow rate, reduces gain and increases power consumption.

3. Control Nozzle Design;

   Purpose of control nozzles is to deliver a turbulent flow disturbance to the main flow, therefore,

   a. Use very short length nozzles.

   b. Allow the control jet to expand to spread rapidly to disturb the main jet effectively.

In cascading turbulence amplifiers following characteristics need be considered (Fig. 24).

   a. Recovery pressure P_o vs. Control flow Q_c

   b. Control flow Q_c vs. Control pressure P_c

   c. Recovery pressure P_o vs. Recovery flow Q_o

First the minimum control pressure and flow required to turn off an amplifier are noted. Available flow from the output characteristics of the driver element (P_o vs. Q_o) corresponding to the switching pressure of the driven element. Then the fan-out is determined by dividing the available flow Q_o of the driver stage by the switching flow Q_c of the driven stage.

Numerically, 0.2 scfh is the control flow that can turn off the output of an amplifier (Fig. 24 a.), control pressure is determined

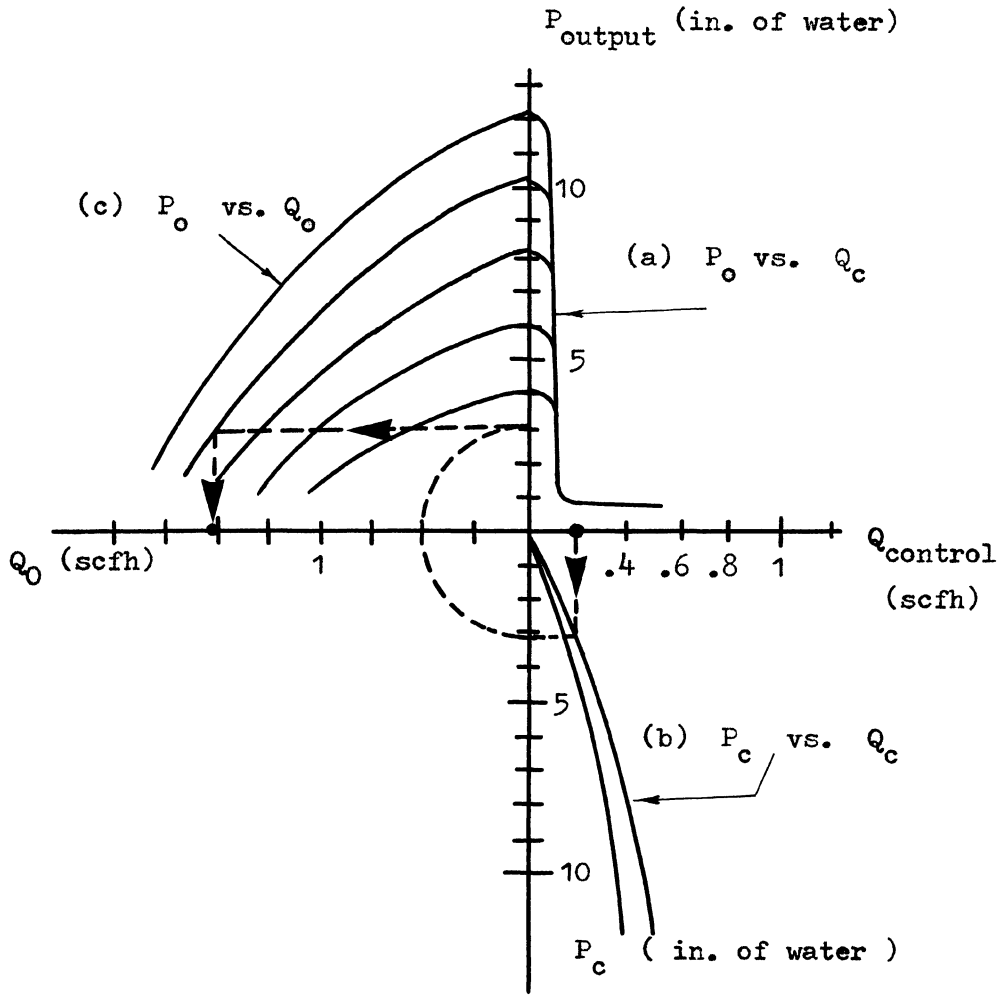

Fig. 24. Determining the Fan-out capability of a Turbulence Amplifier

from the curve P_c vs. Q_c (Fig. 24 b.) and is found to be 3 inches of water. Using this pressure and referring to the curve P_o vs. Q_o (Fig. 24 c.) for a particular supply pressure (say 10 inches of water), the available flow for driven elements is found to be 1.22 scfh.

Therefore, Fan-out $= \frac{1.22}{0.2}$

$\simeq 6$

Basically a turbulence amplifier is a NOR function device i.e., there is output when no control signal is present and vice versa. Two turbulence amplifiers could be combined to make a flip-flop device (Fig. 25) with memory similar to a jet attachment amplifier. Its operation can be studied from the following truth table:

I_1	I_2	O_1	O_2
1	0	0	1
0	0	0	1
0	1	1	0
0	0	1	0

Referring to input-output characteristics (Fig. 23), corresponding to a supply pressure of 13 inches of water, I_1 and I_2 are of the order of 1 inch of water while O_1 and O_2 are of the order of 3.75 inches of water. The time response of the flip-flop will be twice that of a single turbulence amplifier when delay in the tubings is neglected.

The switching time analysis for a jet attachment amplifier presented earlier by Lush [3] will be quite useful as was commented that the table model under test could be scaled down to one with a power nozzle width of 0.04 " while limiting Mach No. to 0.3 and

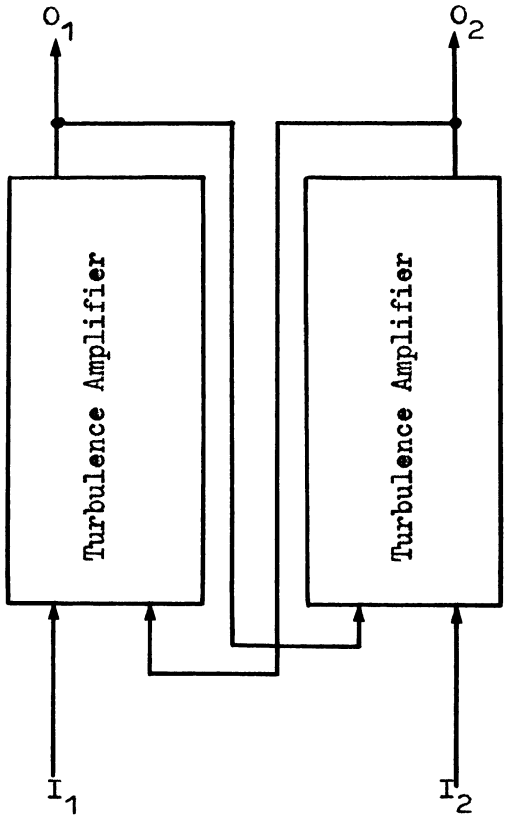

Fig. 25. A Fluidic Flip-Flop Device Consisting of Turbulence Amplifiers

minimum Reynolds No. of 10^4 . Harda, Ozaki and Hara [5] used a similar configuration but much smaller in size (0.02 " power nozzle width), to optimize its various geometrical parameters such as vent location, vent width and terminal crossing angle. Convex Coanda walls (Fig. 15) were successfully shown by Sarpkaya [6] to be more efficient as regards the pressure recovery which is described by equation (3). An entirely new configuration (Fig. 17) by Griffin [7] is no doubt more efficient, switching pressures do not increase with amplifier loading, but the only problem lies in its manufacturing complications. To illustrate cascading operation an Aviation Electric jet attachment amplifier has been used to test the normal staging as well as to determine its fan-out capability. For a successful cascading operation either the driven elements have to be large enough to accommodate extra flow or special vents like latched vortex vents (Fig. 20) have to designed. It can also be done through keeping the supply pressure for the driver stages less than that for the driven stages.

III PROPORTIONAL AMPLIFIERS

The operation of a proportional amplifier has already been described in Chapter I. Unlike bistable amplifiers, the output of a proportional device has a particular value corresponding to different input signals applied. In this chapter Jet Interaction and Vortex Amplifiers have been presented in detail. Various analysis have been included for better understanding of elements.

A. Jet Interaction Amplifiers:

For predicting the response of an amplifier, a rigorous analysis must consider the amplifier as a distributed parameter system. This is difficult, time consuming and does not permit easy generalization of results. A lumped parameter technique by Boothe [13] is presented hereby for an amplifier shown in Figure 26 a. The dynamic analysis of the amplifier is based on normalized steady-state characteristics at one operating pressure. The analysis has been divided into three regions (Fig. 26 b.) such as control region, jet region and receiver & load combined. These analysis are then combined to write the overall transfer function for the amplifier.

A small change in input signal with the operating value of control pressure $P_{c_{AO}}$, neglecting inductance and capacitance effects of control channels, is given by;

$$P'_{c_A} = P_{c_{AO}} + \frac{\delta P_{c_A}}{\delta W_{c_A}} \cdot \Delta W_{c_A} + \frac{\delta P_{c_A}}{\delta P_{c_B}} \cdot \Delta P_{c_B}' \qquad (4)$$

where $\Delta W_{c_A} = W_{c_A} - W_{c_{AO}}$,

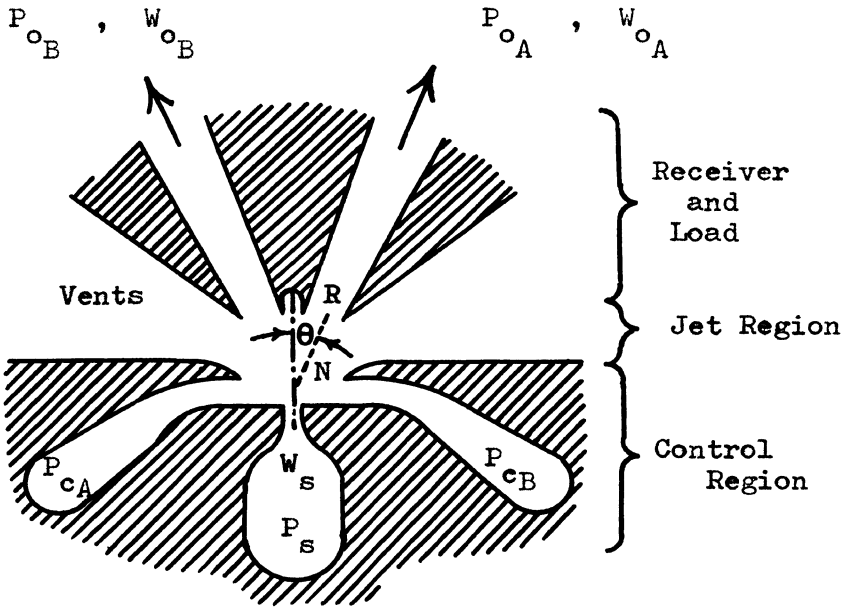

Fig. 26a. A Vented Jet Interaction Amplifier divided into three regions

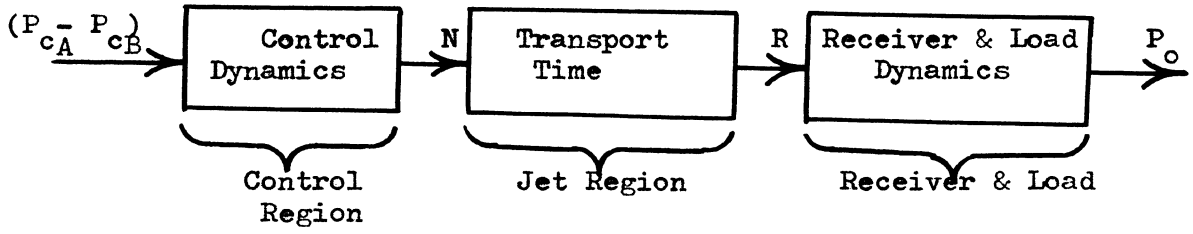

Fig. 26b. Simplified Block Diagram of Jet Interaction Amplifier

$$\Delta P_{c_A}' = P_{c_A}' - P_{c_{AO}} ,$$

and $$\Delta P_{c_B}' = P_{c_B}' - P_{c_{BO}}$$

Equation (4) is rewritten as,

$$\Delta P_{c_A}' = K_1 \cdot \Delta W_{c_A} + K_2 \cdot \Delta P_{c_B}' \qquad (5)$$

where $$K_1 = \frac{\partial P_{c_A}}{\partial W_{c_A}}\Bigg|_{P_{c_B} = \text{constant}}$$ and $$K_2 = \frac{\partial P_{c_A}}{\partial P_{c_B}}\Bigg|_{W_{c_A} = \text{const.}}$$

In above equations primed values show that the inductive and capacitive effects have been neglected, however accounted as follows;

Due to inductive effects there occurs some pressure drop in a channel that accelerates the mass of fluid present in the channel.

Pressure drop = Passage Inductance . Mass rate of flow

or, $$\Delta P_{c_A} - \Delta P_{c_A}' = L_c \cdot D\, W_{c_A}$$

or, $$\Delta P_{c_A} - \Delta P_{c_A}' = L_c \cdot s\, W_{c_A} \qquad (6)$$

where L_c = Equivalent inductance of the control passage

Inductance of a passage is given by the following expression;

$$\text{Inductance} = \frac{\text{Mass density . Length of path}}{\text{Effective cross sectional area of path}}$$

Similarly for the second control port B,

$$\Delta P_{c_B} - \Delta P_{c_B}' = L_c \cdot s\, W_{c_B} \qquad (7)$$

Deflection of power jet at the nozzle exit is defined by the the following equation;

$$\Delta\theta_N = K_3 \cdot (\Delta W_{c_A} - \Delta W_{c_B}) \qquad (8)$$

where K_3 is determined from receiver output characteristics.

Equations (4) thru (8) could be combined to get,

$$\Delta\theta_N = \frac{G_c}{(1 + \tau_c s)} \cdot (\Delta P_{c_A} - \Delta P_{c_B}) \tag{9}$$

where $$G_c = \frac{K_3}{K_1} \cdot (1 + K_2)$$

and τ_c, the control dynamics time constant = $(1 + K_2) \frac{L_c}{K_1}$

Considering the transport time T_t from nozzle receiver,

$$\Delta\theta_R = e^{-T_t s} \cdot \Delta\theta_N \tag{10}$$

where $\Delta\theta_R$ is the deflection in power jet near the receiver. Neglecting inductive effects, receiver pressure is related to the jet deflection by the equation,

$$P_{o_B}' = K_4 \cdot \Delta\theta_R - K_5 \cdot \Delta W_{o_B} \tag{11}$$

Constants K_4 and K_5 are determined from the normalized receiver characteristics.

Taking into account the inductive effects of the output channel,

$$\Delta P_{o_B} = \Delta P_{o_B}' - L_R s \Delta W_{o_B} \tag{12}$$

where L_R = Equivalent inductance of the output channel

Combining equations (11) and (12),

$$\Delta P_{o_B} = K_4 \cdot \Delta\theta_R - K_5 \left[1 + (L_R/K_5) \cdot s\right] \Delta W_{o_B} \tag{13}$$

Defining an operational impedence load Z_{o_B},

$$\Delta W_{o_B} = (1 / Z_{o_B}) \cdot \Delta P_{o_B} \tag{14}$$

From equations (13) and (14),

$$\Delta P_{o_B} = \frac{K_4 \cdot \Delta\theta_R}{\left[1 + (K_5/Z_{o_B}) + (L_R/Z_{o_B}) \cdot s\right]} \tag{15}$$

The overall transfer function is derived from equations (9), (10) and (15);

$$\Delta P_{o_B} = \frac{G_c \cdot K_4 \cdot e^{-T_t s} \quad (\Delta P_{c_A} - \Delta P_{c_B})}{(1 + \tau_c . s)\left[1 + (K_5 / Z_{o_B}) + (L_R / Z_{o_B}) . s\right]} \tag{16}$$

Frequency response data was taken in three sets. The first two sets were obtained (Figs. 27 - 28) using air with supply pressures 15 and 10 psig respectively. Both the attenuation and the phase data agree to the theory. In the second case there is a 5 cc volume dead ended load. Due to the volume there is a first order break at 33 cps. Amplitude is in agreement with in 2.5 db. except for the 680 cps. point where exists a 4 db. discrepancy. In case III using water with 5 psig supply only attenuation data was obtained (Fig. 29). Analysis predicted a first order lag at 47 cps. Tests show peaking at about 55 cps followed by a 20 db / decade drop off. The above test results show that the normalized steady state data with a lumped parameter approach is useful and it gives more exact prediction for air data with low supply pressure.

Another technique by Belsterling [14], that consists of equivalent electrical circuits depending on the graphical characteristics. This method predicts static and dynamic performance of a practical system. Considering variables such as control differential pressure, control differential flow, amplifier pressure drop and amplifier output flow; various plots appear in Figures 30-33 and they help describe the element.

The overall electrical circuit of an amplifier is shown in

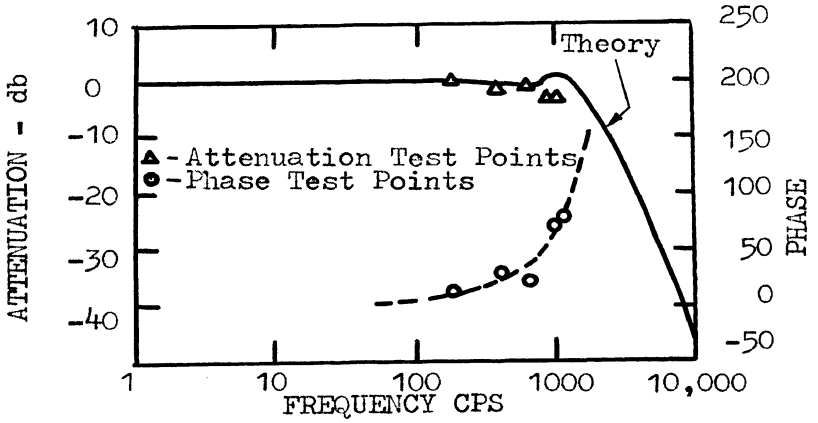

Fig. 27. Case I Frequency Response Test, Air supply at 15 psi.

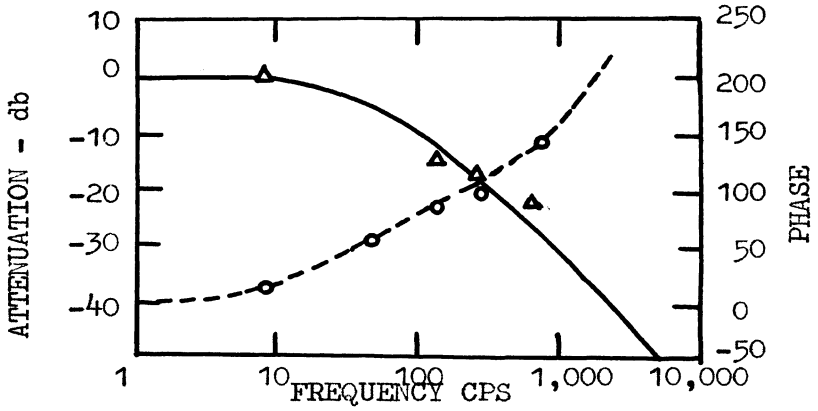

Fig. 28. Case II, Air supply at 10 psi.

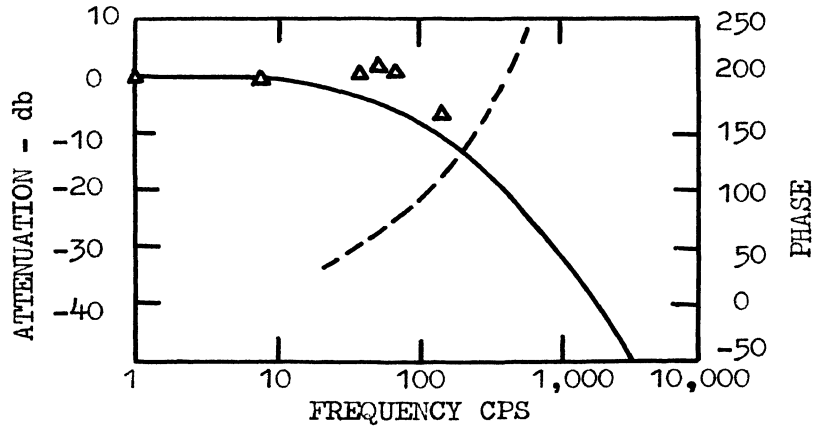

Fig. 29. Case III, Water supply at 5 psi.

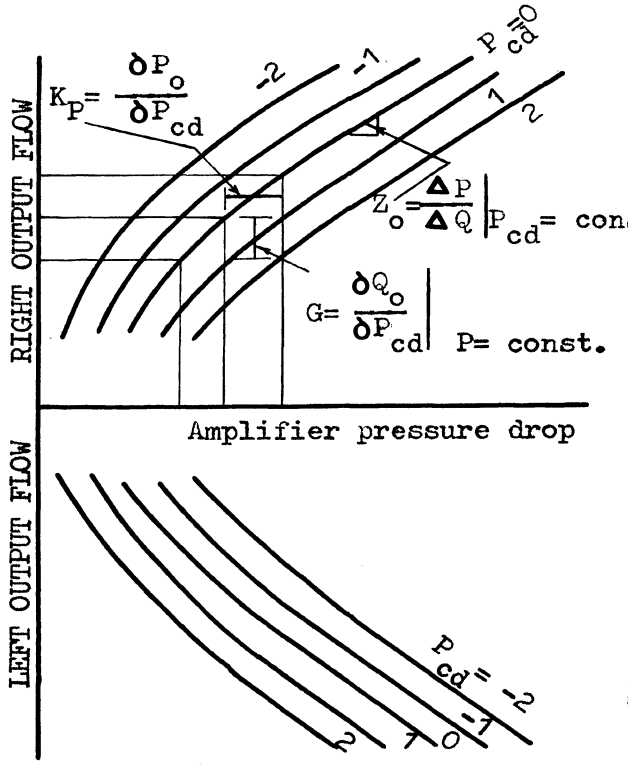

Fig. 30. Characteristic pressure-flow curves for load circuit of Fluid Amplifier

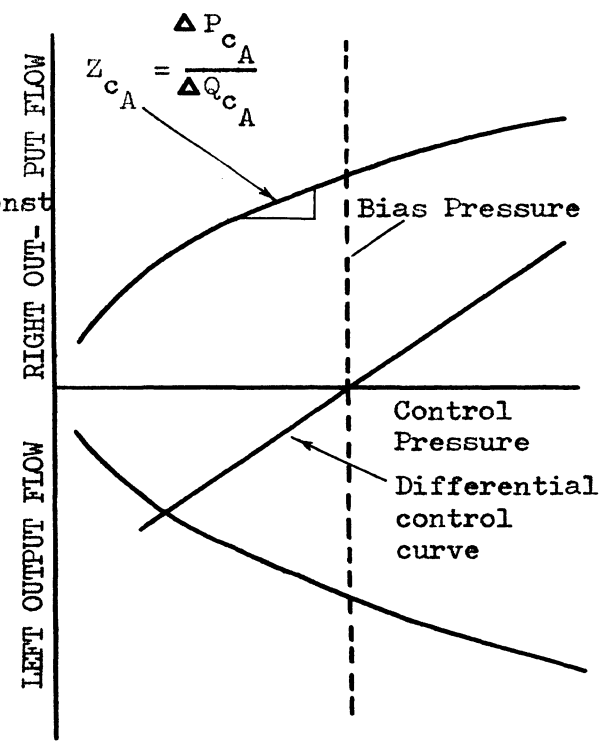

Fig. 31. Pressure-flow Characteristics of control circuit of a Fluid Amplifier

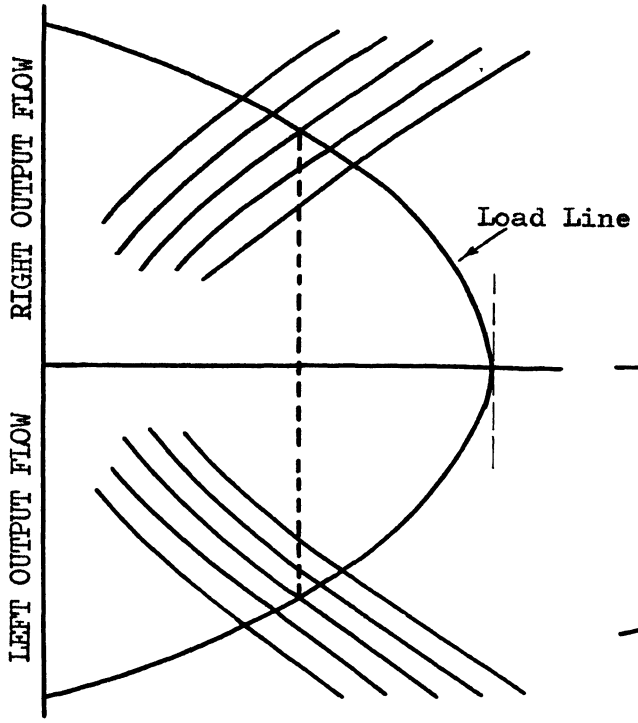

Fig. 32. Superimposing load line on load circuit curves permits graphical solution

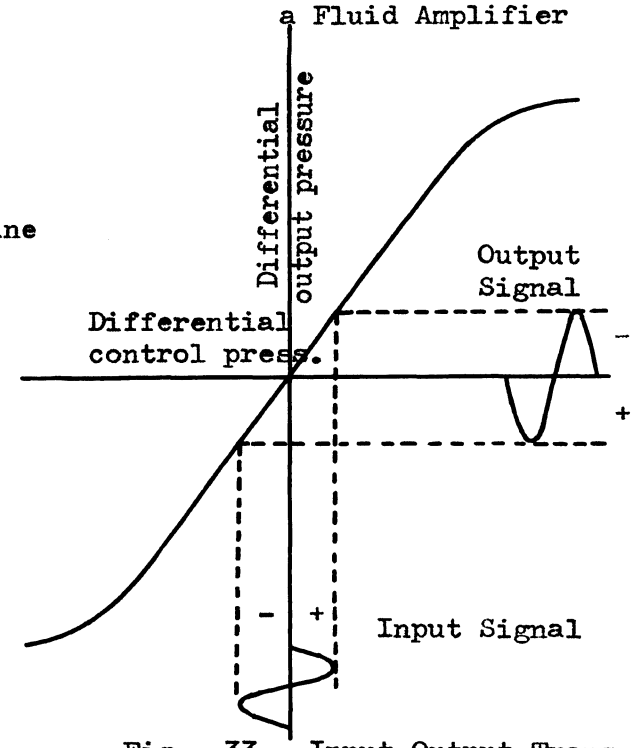

Fig. 33. Input-Output Transfer Characteristics of Fluid Amplifier

Figure 34. This circuit has been simplified further for large amplitude-high frequency signals and low amplitude-high frequency signals (Figs. 35-36). In the first case a load line technique has been used while for the second, parameters were linearized near the operating point to evaluate the various electrical equivalent elements. The transfer function in case of the low frequency signals is;

$$\frac{P_{o_d}}{P_{c_d}} = \frac{2 K_P \cdot Z_1}{Z_o + Z_1} \tag{17}$$

where K_P, the amplification factor, is calculated from the output characteristic curves at the operating point and is given by,

$$K_P = \left.\frac{\delta P}{\delta P_{c_d}}\right|_{Q=\text{constant}}$$

Z_o and Z_1 are the impedences introduced due to the amplifier output and load respectively.

At higher frequencies time delays due to transit time, wave propagation and the presence of circuit reactance like volume capacitances must be considered thereby making the transfer function more complicated;

$$\frac{P_{o_d}}{P_{c_d}} = \frac{2 K_P \cdot R_1}{R_o + R_1 \left(1 + s\frac{L_c}{R_c} + s^2 L_c C_c \right)} \cdot \frac{e^{-t_d s}}{\left[1 + s\left(\frac{C_T 2 R_o R_1}{R_o + R_1} + \frac{L_o}{R_o + R_1} \right) + \frac{s^2 C_T L_o R_1}{R_o + R_1} \right]} \tag{18}$$

where R_c and R_o are the resistances of control passage and

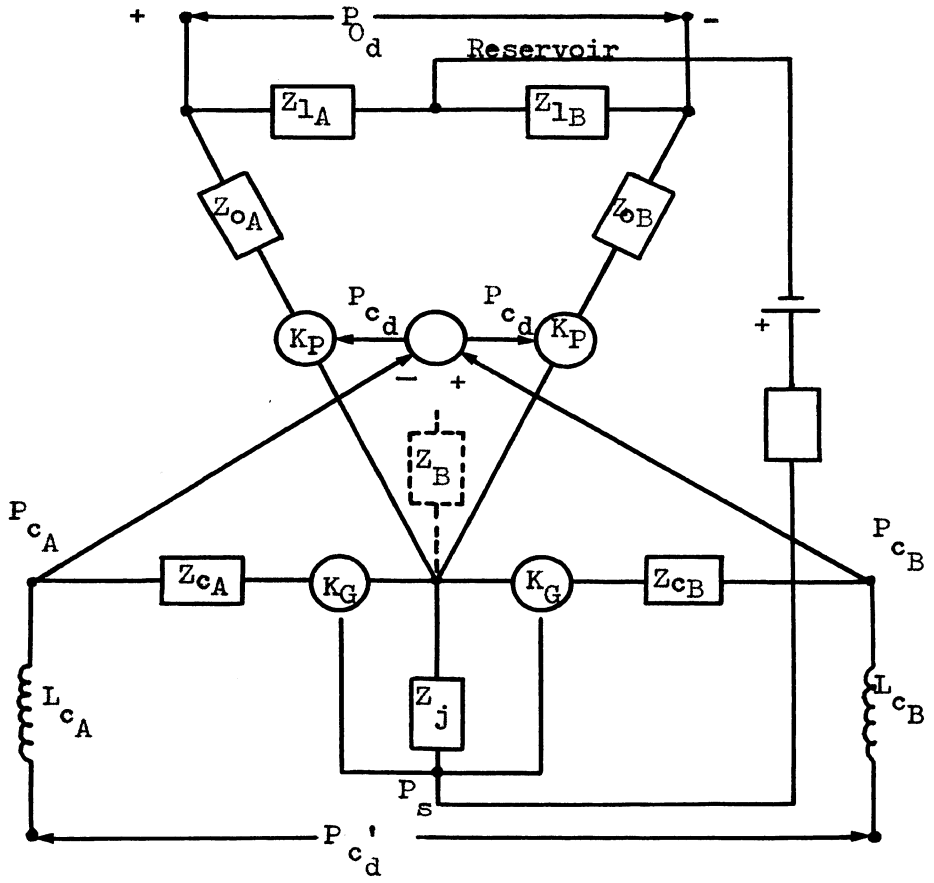

Fig. 34. Complete electrical circuit equivalent for Jet Deflection Fluid Amplifier

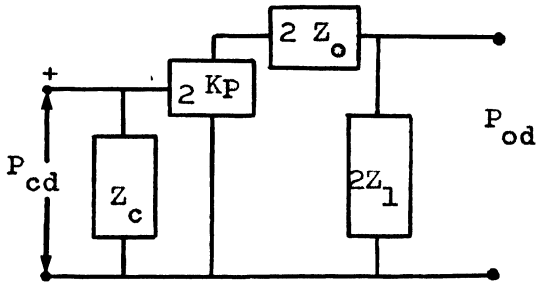

Fig. 35. Simplification for low frequency signals

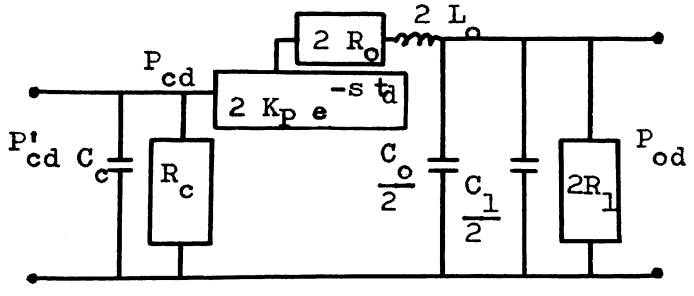

Fig. 36. Simplication for high frequency signals

output passage of the amplifier and R_l is the load resistance. The resistance is defined by pressure-flow characteristics such as,

$$R = \frac{\Delta P}{\Delta Q}$$

L_c and L_o are the equivalent inductances of the control passage and the output passage respectively. Similarly C_c and C_o are the respective capacitances of the control passage and the passage.

Capacitance C of an element is defined as,

$$C = \frac{\text{Trapped volume } V}{\text{Absolute (bias) pressure } P}$$

The capacitance C_T has been defined as;

$$C_T = \frac{C_o}{2} + \frac{C_l}{2}$$ where C_l is the load capacitance.

The effective time delay t_d consists of $t_1 + t_2 + t_3 + t_4$. where,

$$t_1 = \frac{\text{Length of control channel}}{\text{Velocity of sound + Velocity of fluid flow}}$$

$$t_2 = \frac{\text{Length of the interaction chamber}}{\text{Velocity of fluid flow}}$$

$$t_3 = \frac{\text{Length of output aperture}}{\text{Velocity of sound + Velocity of fluid flow}}$$

$$t_4 = \frac{\text{Length of output (load) tubing}}{\text{Velocity of sound}}$$

Figures 37 and 38 show the frequency response verification of theoretical predictions including the effect of variations in supply pressures.

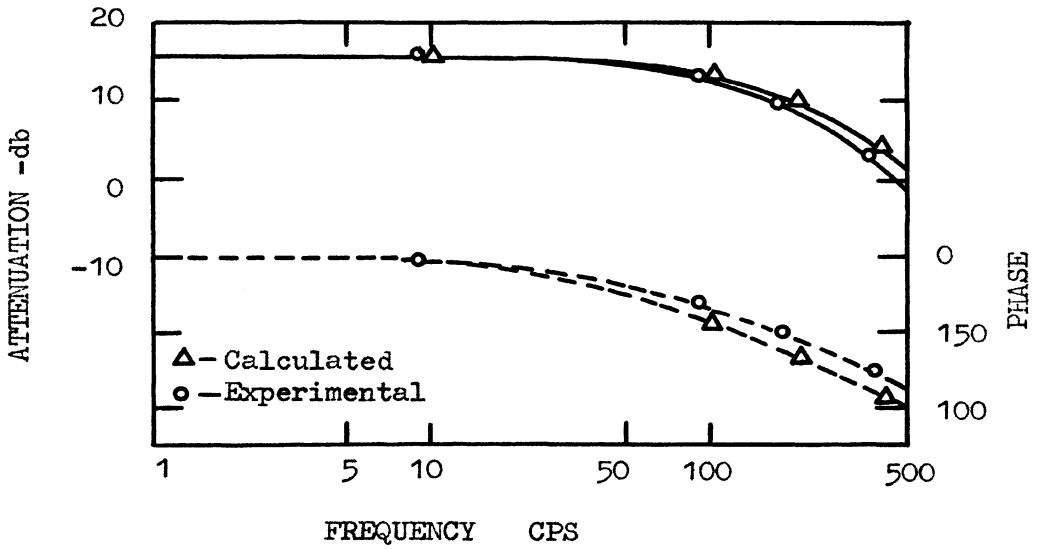

Fig. 37. Frequency Response of actual circuit with response calculated from equivalent circuit.

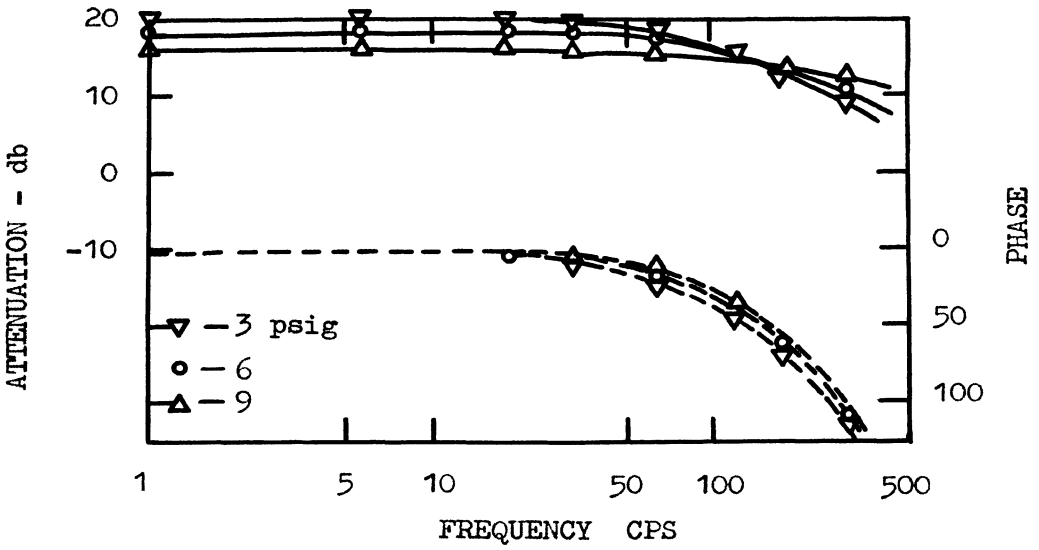

Fig. 38. Effect of variation in the Supply Pressure on Frequency Response of Fluid Amplifier

Strunk and Bowman [15] further tested the lumped parameter model, developed by Boothe and Belsterling, having three different output loads (Gain curves shown in Fig. 39) and the corresponging frequency response curves appear in Figure 40. Both magnitude ratio and phase measurements demonstrate that the amplifier follows the predicted response up to 400 cps. Above this frequency the performance departs from the predicted response in the sense that the magnitude ratio is observed to increase more than predicted which is indicative of a resonant condition developing in the output receiver. The resonant frequency is concluded to be the limit for the lumped parameter technique to be valid. Further frequency response testing is suggested by the author while changing the power jet pressure and variations in output impedences so as to find out the limiting frequency when the amplifier departs from the predicted response.

In another investigation on interaction amplifiers, Douglas and Neve [16] presented theories to predict the amplifier gains based on momentum, mass flow and power interaction criteria. In the present work the results correspond to the tests and flow visualization on a water table amplifier with 3 inch wide power nozzle, 1.6 inch control nozzle width and 7 inches walls offset.

When the power jet is deflected a distance y_1 at the splitter the extra momentum entering one of the receiver channels is given by;

$$M_o = \int_0^{y_1} \rho h . V_s^2 \, dy$$

where 'h' is the depth of flow channel, V_s the stream velocity. Using the above basic equation, following three equations describing gains G_m, G_f and G_e correspond to the criteria of momentum, mass flow

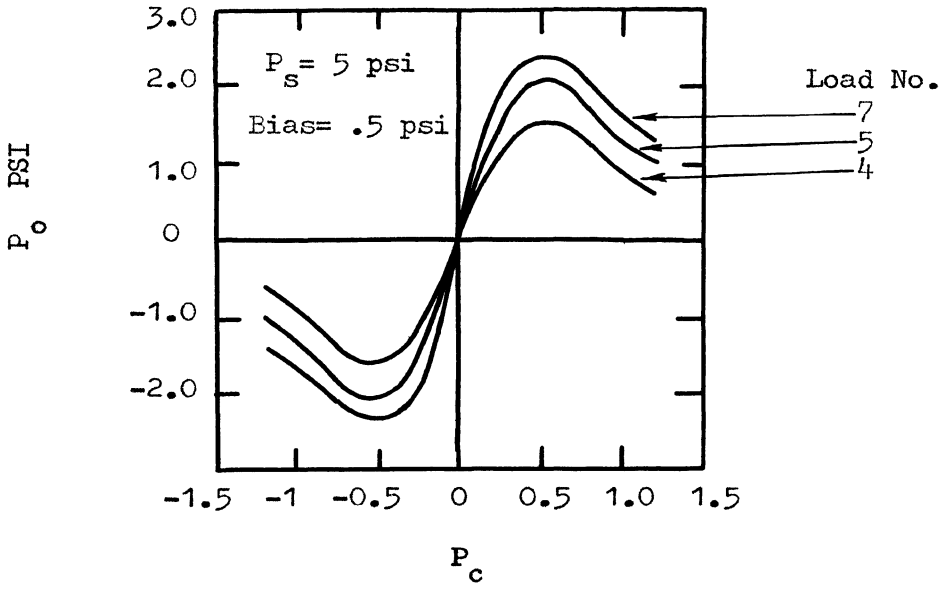

Fig. 39. Gain Curves for a Proportional Center dump Amplifier corresponding to three different loads.

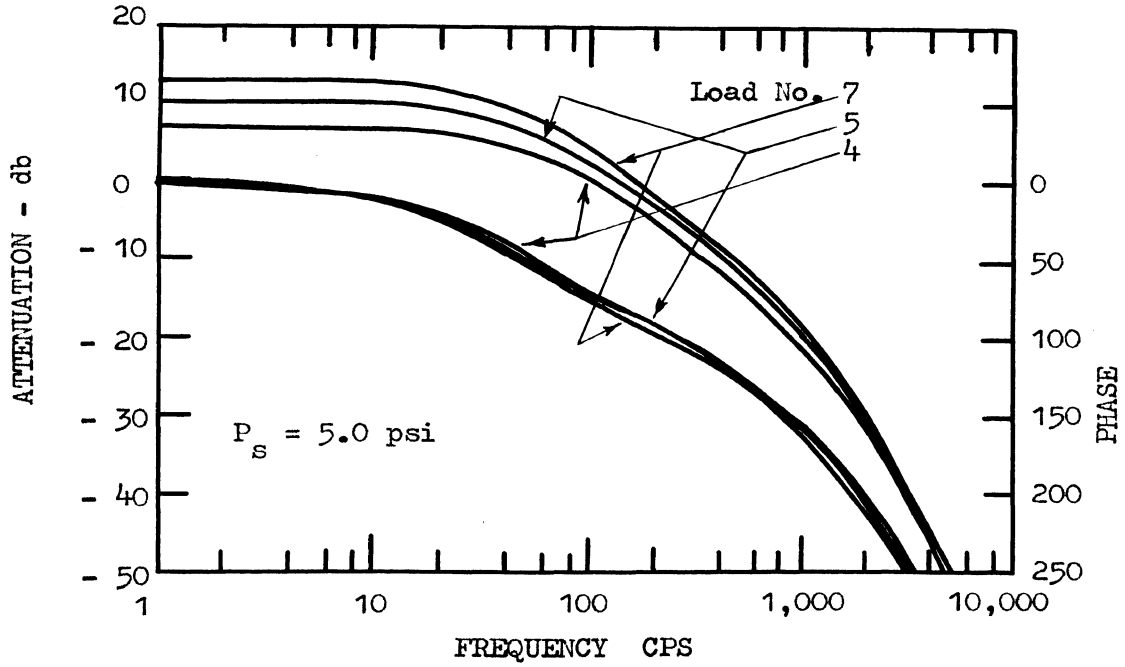

Fig. 40. Frequency Response Characteristics corresponding to three different loads for the Proportional Center dump Amplifier.

and power interaction respectively.

$$G_m = \frac{1.08\ C}{\tan \theta} \int_0^{\bar{y}_1} \bar{V}_s^2 \, dy \tag{19}$$

$$\frac{G_f}{0.451\sqrt{X_s}} = \frac{1 + K}{K} \int_0^{\bar{y}_1} \bar{V}_s \, dy \tag{20}$$

$$\frac{G_e \sqrt{X_s}}{2.574} = \frac{k^2}{K^3} \int_0^{\bar{y}_1} \bar{V}_s^3 \, dy \tag{21}$$

where $\bar{V}_s$ is the dimensionless power jet velocity, $\bar{X}$ is dimensionless downstream distance, X_s is splitter distance, $\bar{y}$ is dimensionless cross distance, K is the ratio of control mass flow to power mass flow, k is the ratio of control nozzle width to power nozzle width and C is an empirical constant.

Using a planimeter, the profiles of Figure 41 were changed to momentum differences about the assumed splitter position. The values obtained divided by the momentum input of the control jets, gives no load momentum gain (Fig. 42) which show good agreement with the theoretical curve corresponding to equation (19). Similarly other gains with mass-flow and power interaction criteria were evaluated and are described by equations (20) and (21).

The experimental tests were made on no-load conditions, the gains will decrease slightly under application of loads.

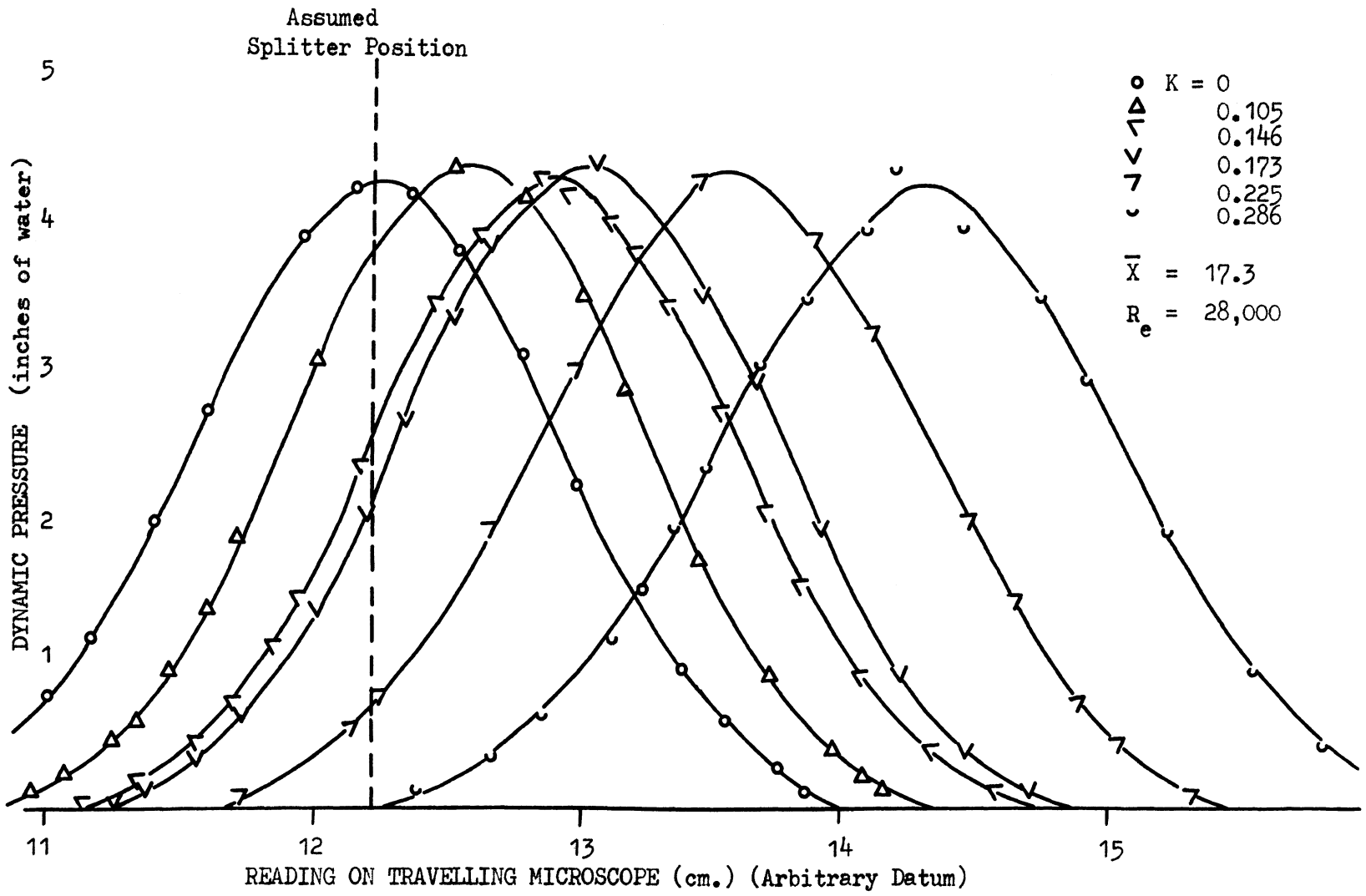

Fig. 41. Jet Profiles for Various Deflections

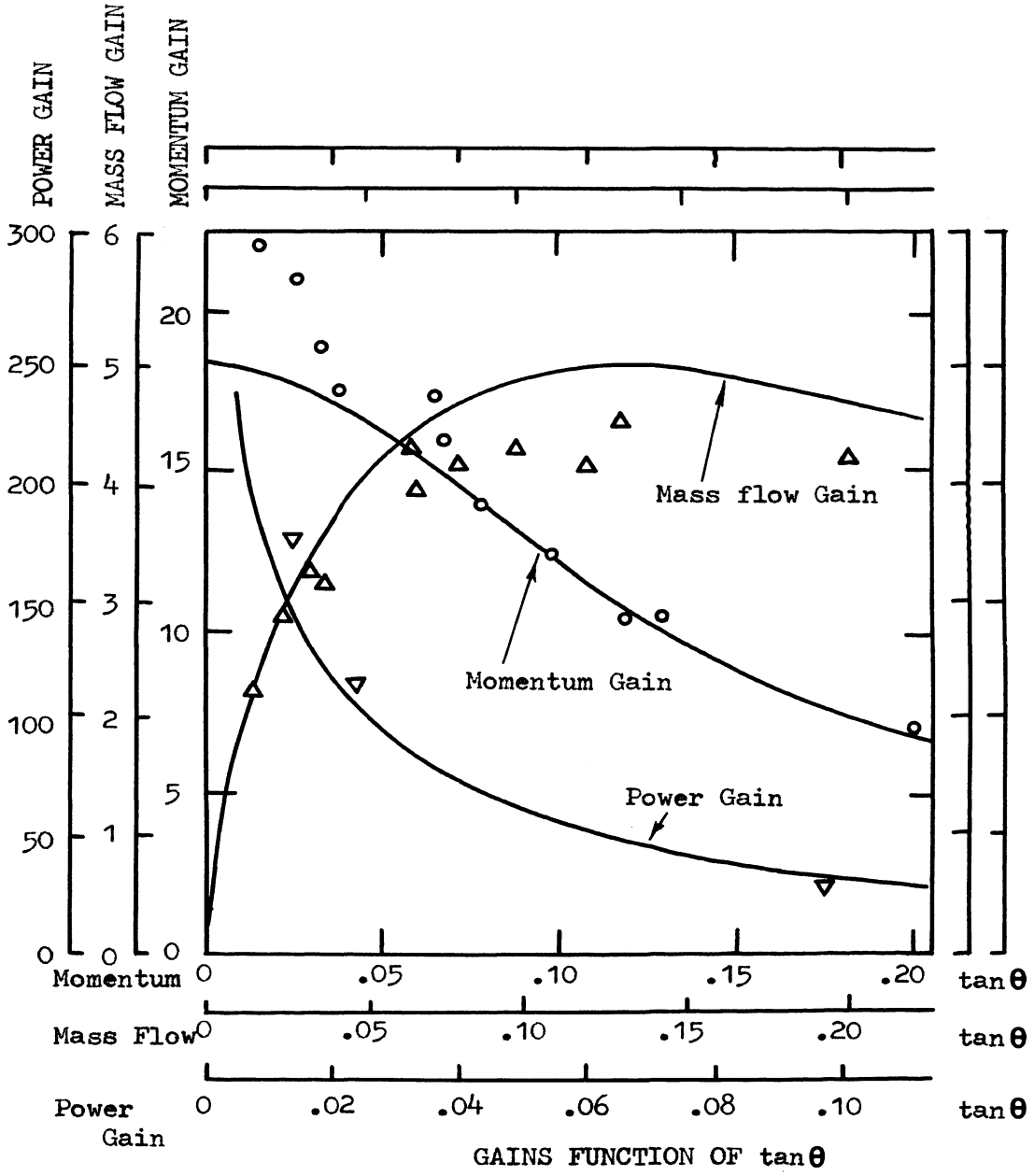

Fig. 42. Comparison of Theoretical and Experimental values of Gains

A unique configuration of a proportional amplifier (Fig. 43) has been given by Griffin [17] similar to his analysis for a bistable amplifier. Following are some of its improved features:

1. The maximum pressure gain obtainable for an ordinary proportional amplifier is 7 compared to 11 for the improved design (Fig. 44 a.).
2. The maximum normalized receiver output pressure was found to be 52 % while for an ordinary amplifier it is usually in the range of 40 - 50 % .
3. There is no drastic drop in output pressure in case of strong signals. Configuration is such that the power jet cannot be overdriven but in ordinary amplifiers there is such problem present.
4. Three stages of new amplifiers are capable of giving flat gain characteristics after saturation (Fig. 44 b.). The zero shift encountered could be removed partially by reducing aspect ratio and increasing supply pressure.

Constructionally, inclined ports are designed to limit power jet deflection with the disadvantage that high gain with this kind of amplifier should not be expected, although it is giving higher value of gain than those conventionally available. There is a small length of flat wall in the interaction region which does not let the power jet attach when overdriven because of its short length. A small offset of the interaction region's inclined walls serves two purposes:

1. To dissipate small pressure waves generated by power stream flow, that are peeled off by interaction region's

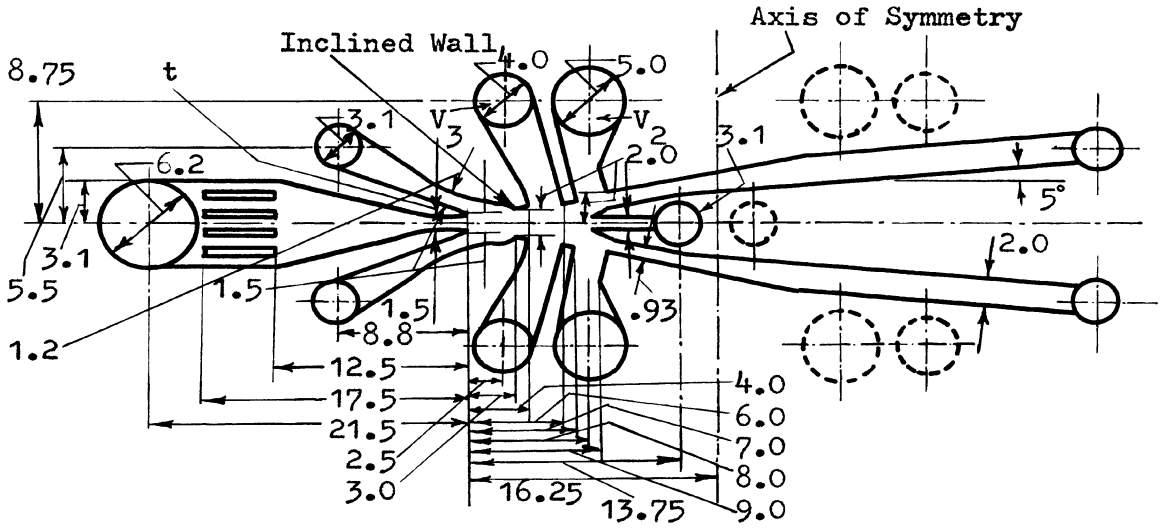

Fig. 43. Improved Proportional Amplifier. All linear dimensions to be multiplied by power nozzle width, 't'.

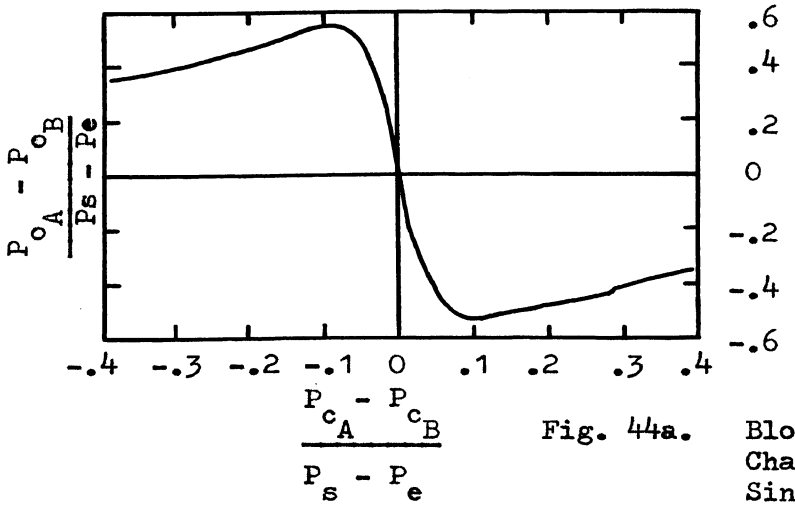

Fig. 44a. Blocked Receiver gain Characteristics for a Single Amplifier

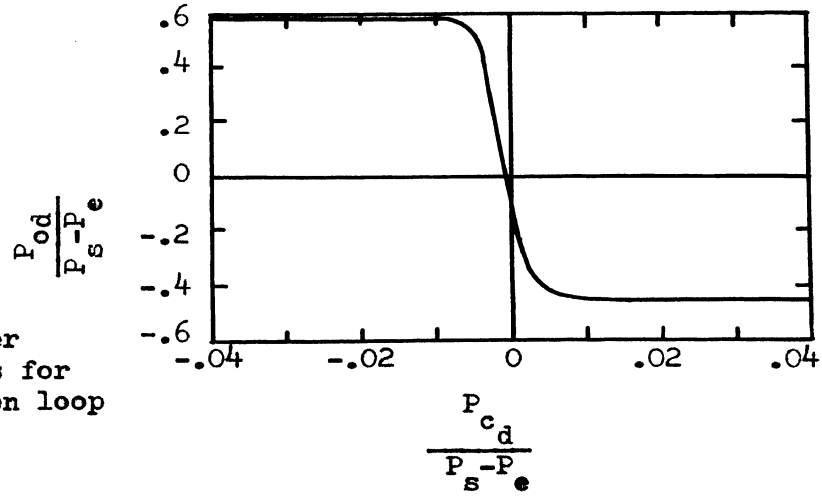

Fig. 44b. Blocked Receiver Characteristics for Three-stage open loop Gain Block

exits.

2. It reflects the small waves directly into the power stream rather than letting it travel up to the control port.

Cascading Amplifiers:

The gain of a single amplifier is not high as required for an operational amplifier and so cascading is required to obtain the necessary gain. Belsterling [18] provided insight for the problem. The design steps can be listed as follows;

1. Obtain the output characteristics of the first stage (Fig. 45). The curves (pressure vs. flow) are drawn for different differential control pressures.
2. Obtain the input characteristics of the second stage amplifier (Fig. 46). These characteristics are of a typical small vented jet interaction amplifier with 0.010 X 0.025 inch power nozzle width. Differential control curve is also shown (With a condition that $P_{c_A} + P_{c_B}$ = constant). This curve also indicates the operating limits for the amplifier controls.
3. Superimpose the above characteristics on each other (Fig. 47) which can tell exactly where the mismatch lies and possibly a rectification.

Following are the classifications of mis-matches, which should be checked one by one.

a. Matching operating bias points:

With superimposition of input-output characteristics (Fig. 48), it is observed that the operating bias

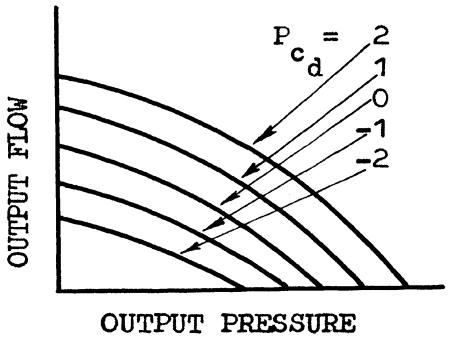

Fig. 45. First Stage Output Characteristics

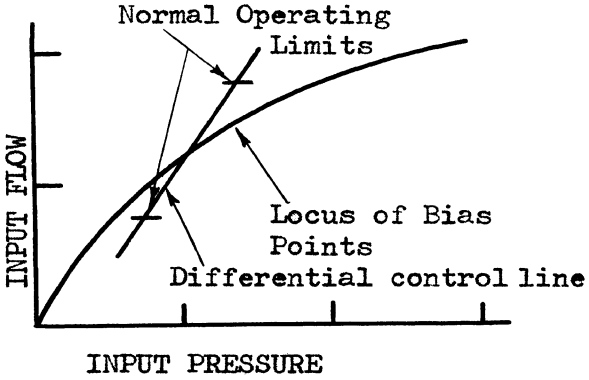

Fig. 46. Second Stage Input Characteristics

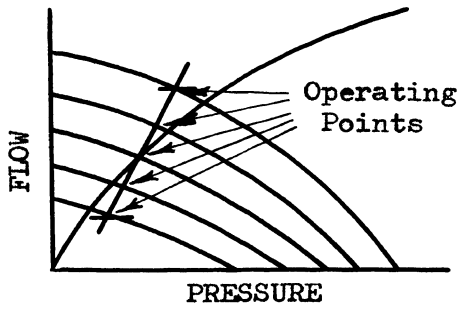

Fig. 47. Superimposition of Output-Input Characteristics

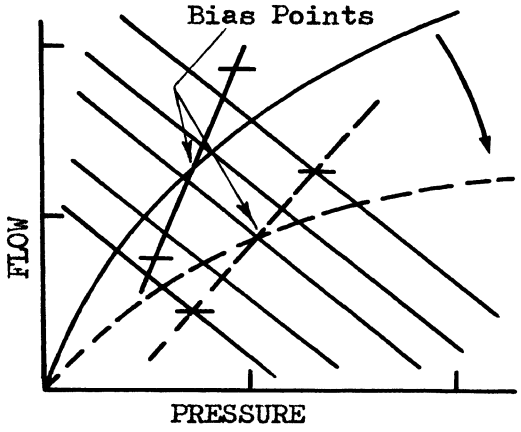

Fig. 48. Possible Mis-Match detection while Superimposition

points do not match because the input characteristics of the second amplifier is relatively steep. The possible matching is also shown in dotted lines. There are three ways to rectify:

i. The output bias level of the first stage amplifier is raised by increasing supply pressure, thereby all the output characteristics shift outwards (Fig. 49).

ii. Supply pressure of the second stage is reduced (Fig. 50).

iii. The effective input characteristics along with the differential control curve could be shifted by putting some restrictions in series and in parallel (Fig. 51 b.). The effect of restrictions on input characteristics is shown in Figure 51 a.

b. Matching operating ranges:

Figure 52 shows the mis-match in operating ranges of two amplifiers. The operating range of the second amplifier is greater than that of the first one. The mis-match is removed by putting a line to line shunt resistance i.e., by adding a restrictor between the two control inputs to the amplifier so as to rotate the differential control curve as desired.

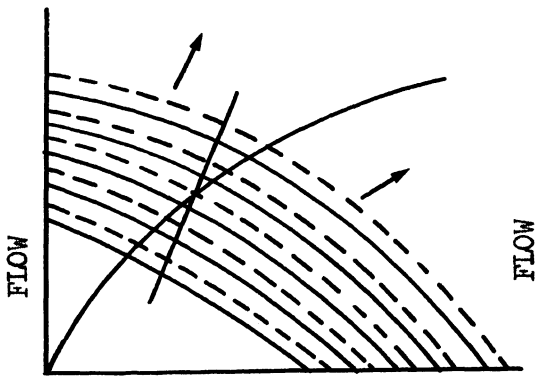

Fig. 49. Matching operating points by increasing supply pressure to the First Stage

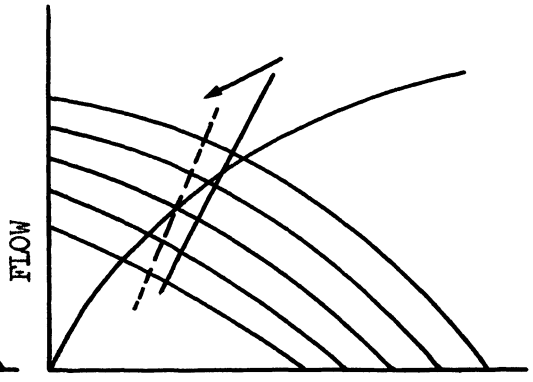

Fig. 50. Matching operating points by reducing supply to 2nd stage

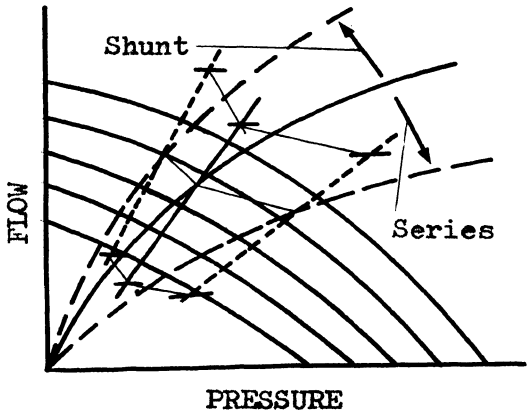

Fig. 51a. Effect of Shunt-Series Restrictors on matching points

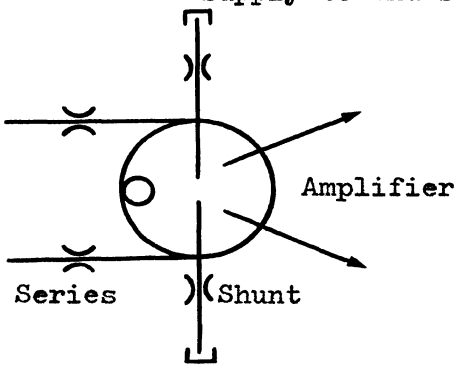

Fig. 51b. Location of Shunt-Series Restrictors

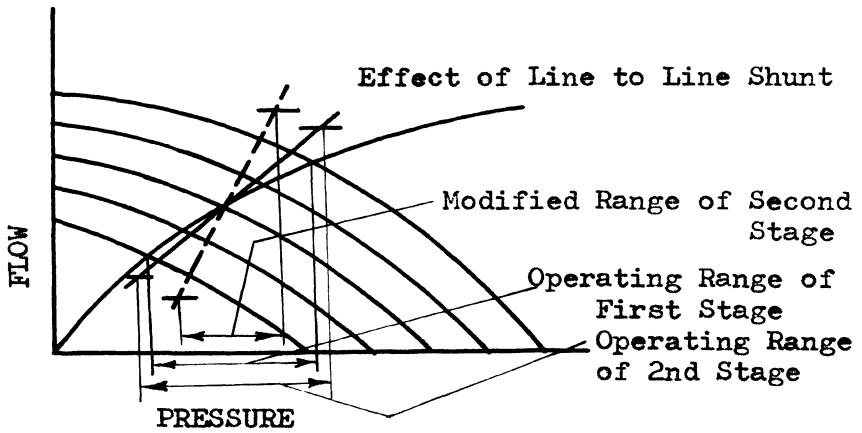

Fig. 52. Matching Operating Ranges by adding Restrictors

Fluidic Operational Amplifier:

After it became feasible to cascade amplifiers, fluidic operational amplifier came into existence. Doherty [19] presented the basic approach in obtaining different functions such as; integrating circuits, lead-lag or lag circuits along with the signal summing operations.

An operational amplifier circuit (Fig. 53) consists of an input resistor R_i, a feedback resistor R_f, a high gain five-stage amplifier with a gain of -K (K = 2000 approx.) and an amplifier control port resistance R_c. Flow at the summing junction is given by Kirchoff's laws, analogous to current flow:

$$W_1 + W_2 = W_3 \tag{22}$$

$$\frac{P_i - P_g}{R_i} + \frac{P_o - P_g}{R_f} = \frac{P_g}{R_c} \tag{23}$$

$$P_o = - K P_g \tag{24}$$

solving equations (22) and (23),

$$- \frac{P_o}{P_i} = \frac{R_f}{R_i} \left[\frac{K \left(1 \,/\, 1 + (R_f/R_i) + (R_f/R_c) \right)}{1 + K \left(1 \,/\, 1 + (R_f/R_i) + (R_f/R_c) \right)} \right] \tag{25}$$

$$\text{or,} \quad - \frac{P_o}{P_i} = \frac{R_f}{R_i} \left[\frac{G H}{1 + G H} \right] \tag{26}$$

where $G = K$

and $H = 1 \,/\, \left(1 + (R_f/R_i) + (R_f/R_c) \right)$

It is obvious from equation (26) that the transfer function is determined from the values of R_f and R_i when G.H, the loop gain is high.

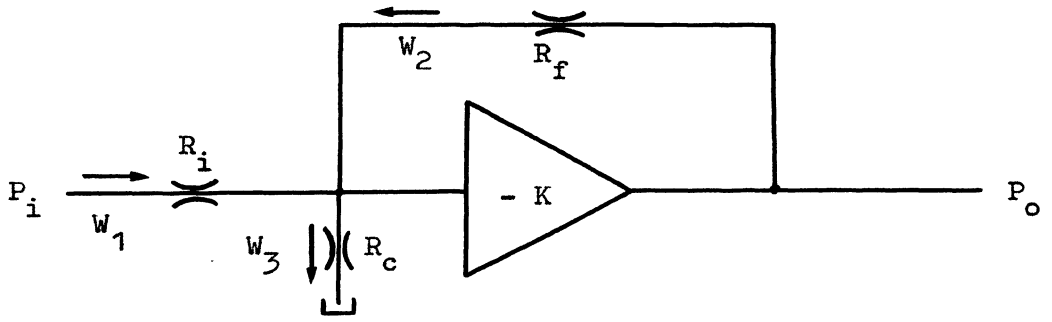

Fig. 53. The Basic Fluidic Operational Amplifier

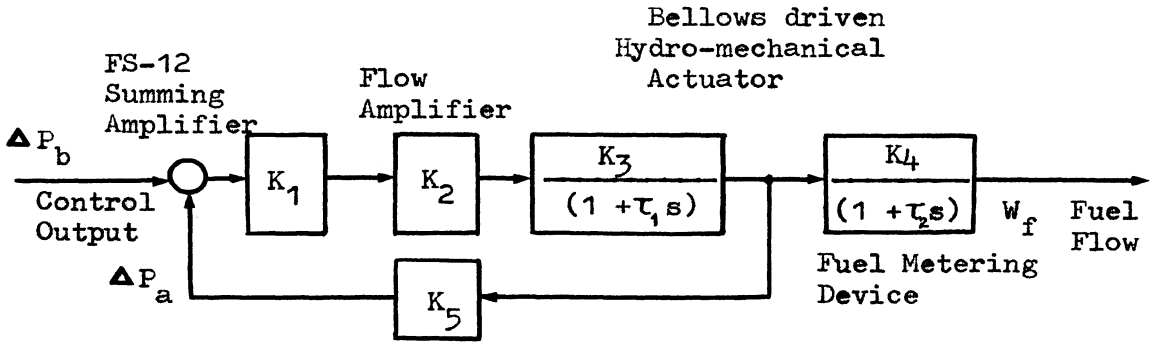

where K_1 = 45 psi/psi

K_2 = 1 psi/psi

K_3 = 3.8 Deg./psi

K_4 = 437 lb./Hr./Deg.

K_5 = 0.12 psi/Deg.

τ_1 = 0.03 sec.

τ_2 = 0.02 sec.

Fig. 54. FS-12, Summing Amplifier in J-79 Turbo-jet engine control

It has been claimed that an operationa amplifier model FS-12, developed at General Electric Company New York, has gain frequency independent up to approximately 200 cps. In its application as a summing amplifier in controlling fuel for J 79 turbo jet engine. The circuit diagram is shown in Figure 54 . The transfer function for the summing amplifier has been developed with reference to Figure 55 and equation (26).

$$\Delta P_o = \Delta P_a \frac{R_f}{R_a} \frac{G\,H}{1 + G\,H} + \Delta P_b \frac{R_f}{R_b} \frac{G\,H}{1 + G\,H}$$

If G.H, as defined earlier, is sufficiently large the above equation simplifies to :

$$\Delta P_o = \Delta P_a \frac{R_f}{R_a} + \Delta P_b \frac{R_f}{R_b} \qquad (27)$$

where ΔP_a and ΔP_b are two inputs, commanding signal and feedback position signal respectively.

Integrating circuit is obtained by means of a delayed (RC) positive feedback (Fig. 56) connecting the output of an operational amplifier (model FR-22 G.E.) to the imput summing junction. The approximate transfer function is given by;

$$\frac{\Delta P_o}{\Delta P_i} = \frac{R_f / R_i}{1 + \tau s} \qquad (28)$$

where τ is the integrating time constant and can be up to 60 seconds.

There are some more applications of fluidic operational amplifiers developed by General Electric Company to obtain functions such as lead-lag or lag and a recent feature about the use of a variable feedback resistor with its application, amplifier gain varies from 5 - 50.

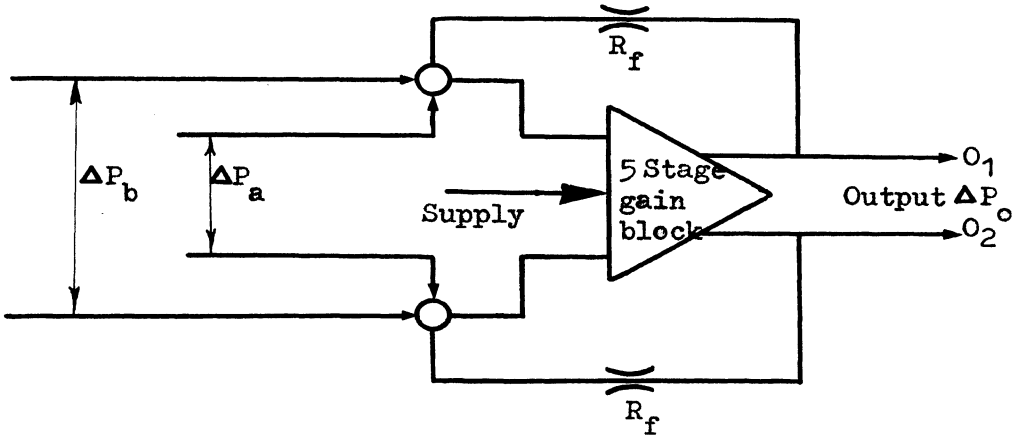

Fig. 55. A Summing Amplifier's fluidic circuit

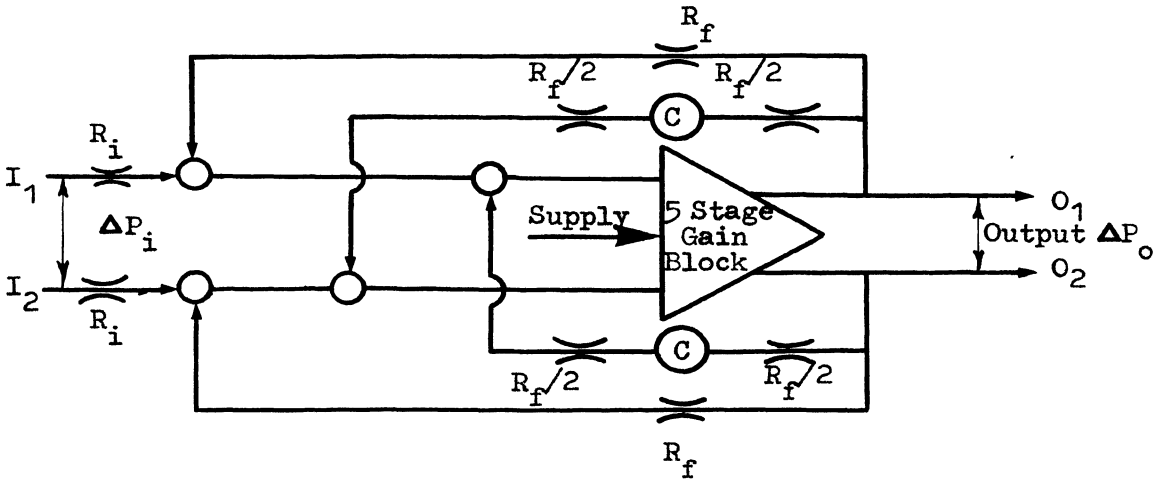

Fig. 56. An Integrating Fluidic Operational Amplifier Circuit

B. Vortex Amplifiers

The basic concept behind a vortex amplifier is of controlling and amplifying a fluid flow by using a secondary flow. Supply flow enters a cylinder and passed radially through a porous coupling element into a vortex chamber (Fig. 57) and leaves this chamber through an axial hole. Control flow enters tangentially into the vortex chamber and as a consequence a vortex motion is set up that restricts the output flow. This restriction is directly related to the strength of the control pressure. There are two disadvantages using a vortex amplifier:

1. The flow demand is hard to be reduced to zero.
2. Control pressure must be greater than the supply pressure, thereby, too much power drain.

Letham [20] made analysis for the pressure distribution in the vortex chamber, considering a differential fluid element radius r_t and radial thickness dr_t with tangential velocity U_t which is given by the following equation:

$$P_r = P_s + \frac{\rho U_0^2}{2n}\left[\left(r_t/r_0\right)^{2n} - 1\right] \qquad (29)$$

where

P_r = Pressure at any radius r_t in the vortex chamber

P_s = Supply pressure

ρ = Mass density of fluid

U_0 = Tangential velocity inside the vortex chamber

r_t = any radius in the vortex chamber

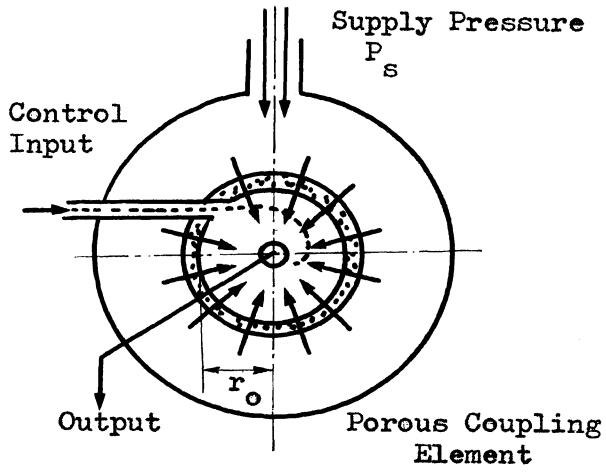

Fig. 57. Configuration of a Vortex Amplifier

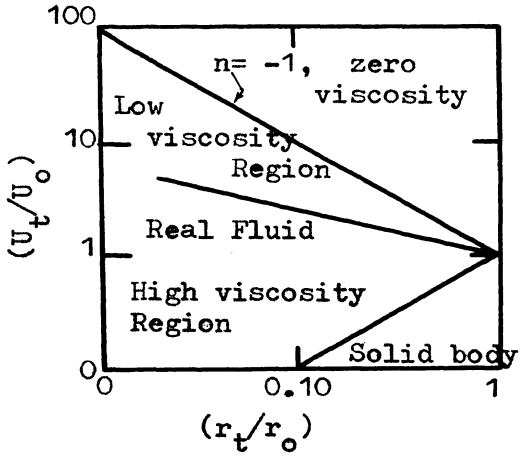

Fig. 58. Physical Significance of exponent 'n'.

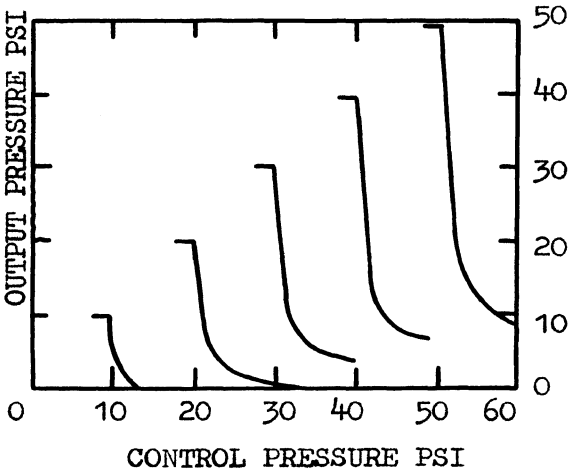

Fig. 59. Characteristic curves for a commercially available vortex amplifier.

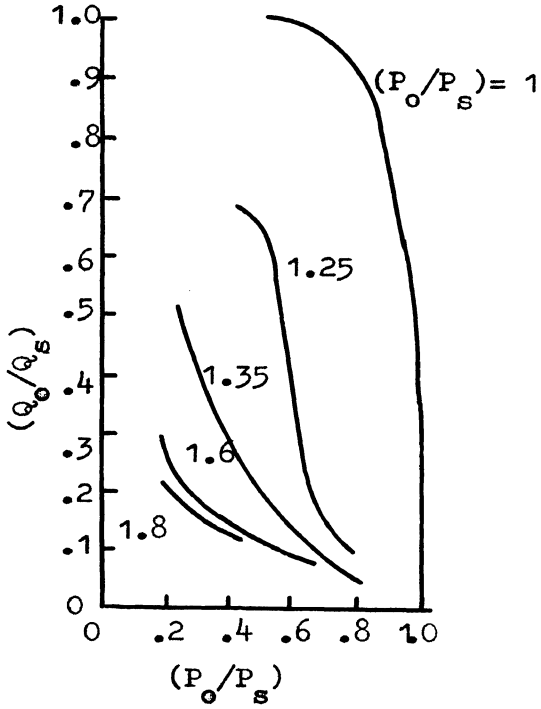

Fig. 60. Effect of downstream pressure on output flow

r_0 = Maximum vortex chamber radius

U_t, the tangential velocity at any radius is given by;

$$U_t = U_0 \cdot (r_t / r_0)^n \qquad (30)$$

where 'n' is an exponent, its physical significance is given in Figure 58.

The characteristic curves, for a commercially available vortex amplifier, appear in Figure 59. It is observed that the output pressure from the amplifier drops on application of the control signal. The effect is similar to the one in Turbulence Amplifiers but here the drop in pressure is more gradual as compared to the abrupt drop in turbulence amplifiers, that is why they are made to be used as digital devices and not proportional.

An unvented vortex amplifier is effected by the change in downstream pressure which is shown in Figure 60 by Larson [21] . Each curve corresponds to a constant ratio of control pressure to supply pressure. The curve with P_o/P_s ratio equal to one is for the case when there is no vortex present in the vortex chamber. Venting of amplifier is essential as the vent cavity provides a fixed static pressure in the receiver, thereby isolating the vortex chamber from downstream impedence changes.

Howland [22] introduced two configurations of vented vortex amplifiers along with their characteristics (Figures 61-62) with the difference that output receiving tube and the vent are located on the same side in one case and opposite in the other. When the vortex chamber is at full flow in the first geometry, the flow leaves the exit hole as a solid jet and is so collected by the receiver.

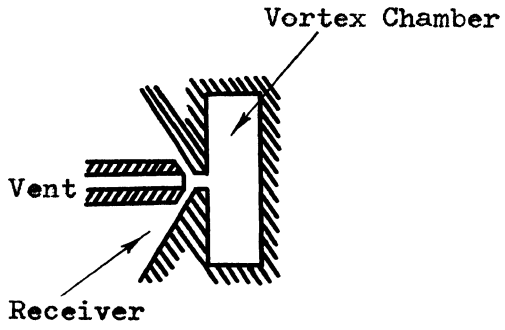

Fig. 61a. A Vortex Amplifier Receiver-Vent on same side

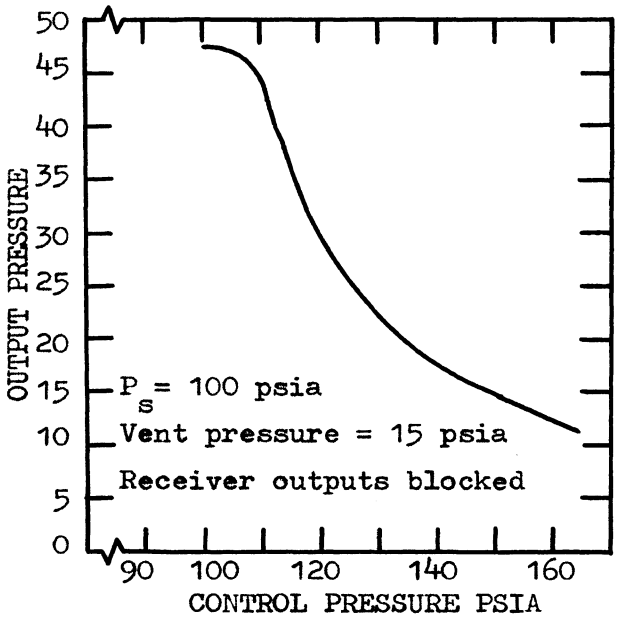

Fig. 61b. Transfer Characteristics

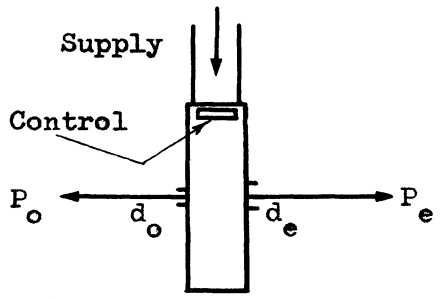

Fig. 62a. A Vortex Amplifier Receiver-Vent on opposite sides

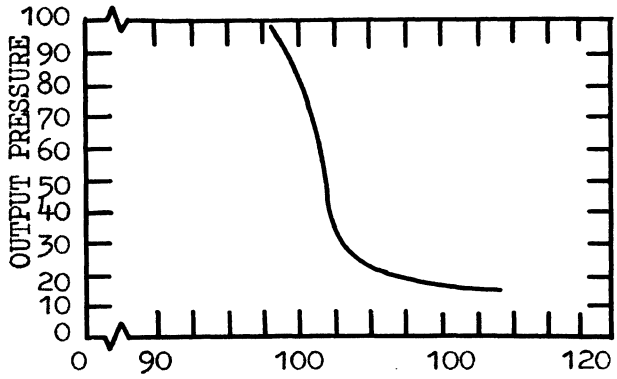

Fig. 62b. Transfer Characteristics

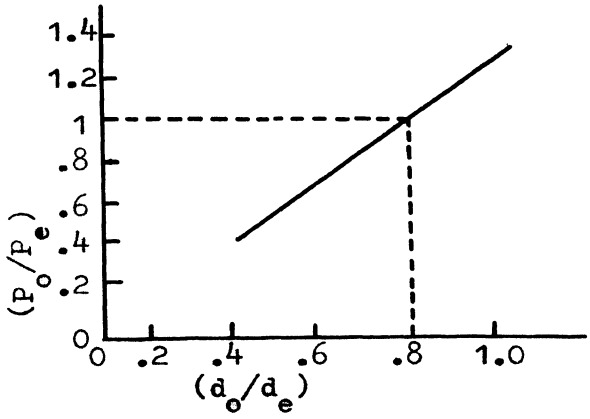

Fig. 62c. Effect of Vortex Geometry on Recovery Pressure

In the turn down condition it leaves in the form of a conical spray. In the second configuration, the load flow is taken from a hole in the opposite wall. The maximum dead ended pressure is close to the supply pressure and the minimum is obtained at full control pressure. Receiver pressure depends on parameters such as ambient pressure, P_e; outside diameter d_o and vent diameter d_e. Figure 62 c. illustrates how these effect the recovery pressure.

Vortex Amplifiers offer some unique applications for control valves in modulating flow and power. They also find use in chemical processing, natural gas control systems, engine fuel control, boiler system control etc. A non-vented amplifier can be used in a flow control system (Fig. 63). The flow sensor sends a feedback signal into the controller which appropriately sets the control signal to maintain the output flow. The controller is made up of fluidic amplifiers and performs the necessary summation, amplification and/or integration and/or differentiation. Vented amplifiers are especially suited for power amplification because they have the highest power recovery of all fluidic amplifiers and they are not size limited. In an application Larson [21] presented a circuit with function of servo valve (Fig. 64). In this circuit two vortex amplifiers are driven in push-pull by two jet-interaction amplifiers. When there is no input signal,

$$P_{o_A} = P_{o_B}$$

$$Q_{o_A} = Q_{o_B}$$

If a control pressure P_{c_A} is applied, P_{o_A} and Q_{o_A} decrease while P_{o_B} and Q_{o_B} increase. On application of P_{c_B} just the reverse happens. This circuit differs from the conventional servo valves that the input

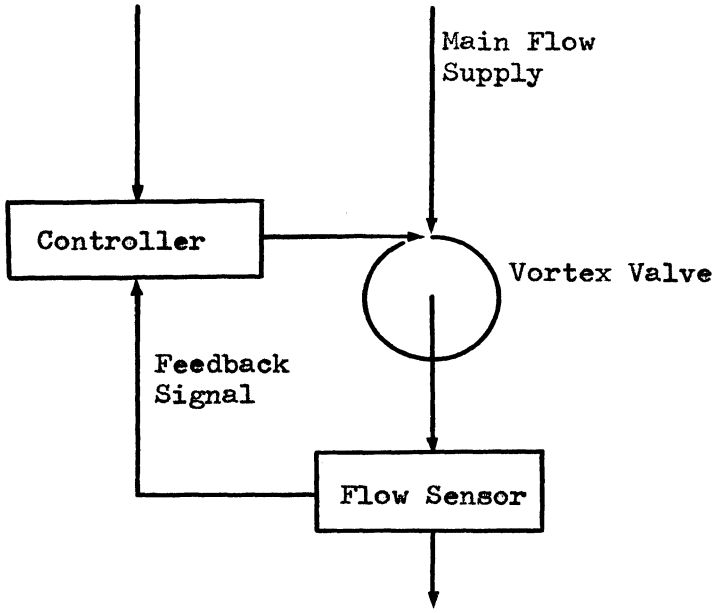

Fig. 63. A Flow Control System

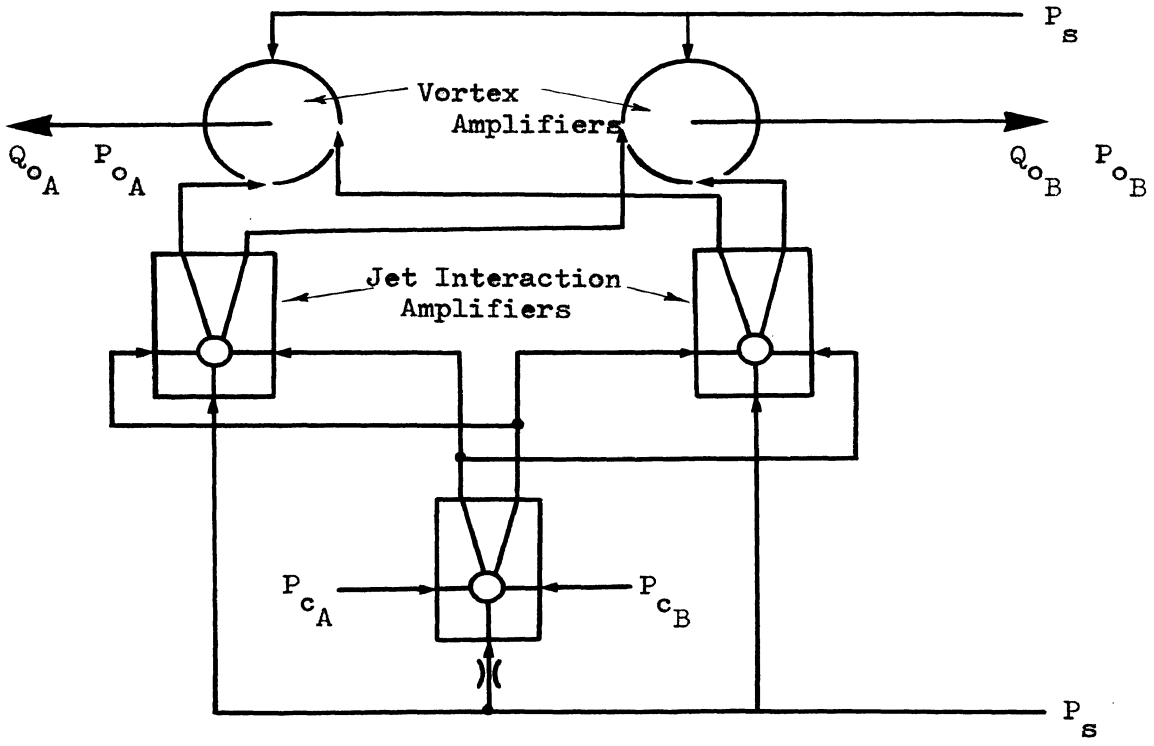

Fig. 64. A Fluidic Circuit for a Servo-Valve

signals are fluidic rather than electrical. Because of no moving parts this fluidic servo valve has a high frequency response of about 75 cps.

A lumped parameter approach by Boothe [13] and an equivalent electrical circuit presented by Belsterling [14] to predict characteristics of a jet interaction amplifier proved to be close. In a later reference Strunk and Bowman [15] found this technique to be valid until the resonance frequency of the output channel of the amplifier. Douglas and Neve [16] predicted gain curves considering different criteria for jet interaction such as momentum, mass flow and power interaction. Griffin [17] presented another efficient geometry for jet interaction amplifier. Cascading of amplifiers was explained to achieve higher gains so as to make use to obtain an operational amplifier. A fluidic operational amplifier does find its place in integrating, lead-lag or lag circuits along with its use as a summing amplifier. Vortex Amplifiers, which are basically proportional amplifiers were explained their operation, various characteristics with typical performance data and their applications.

IV FLUID SENSORS

A sensor is an element which is sensitive to changes in operating conditions such as temperature, pressure etc., and has an output that varies with changes in operating conditions. Fluidic circuits could be designed for various sensing operations. In this chapter some fluid sensors have been presented and also their practical design aspects have been studied. The Air Flow Velocity Sensor has been included and its experimental analysis appears in the next chapter.

A. Rotational Speed Measurement

There are two ways to measure rotational speed, using an analog fluidic device (jet interaction amplifier) or a digital device (Turbulence amplifier). In the analog device (Fig.65), the basic idea is that of a pitot tube principle. As the angular velocity of disc increases, air impinges on the openings in the disc edge thereby increasing static pressure inside the tubing which links to one of the control ports of an interaction amplifier. Thus, the pressure built up in the receiver of the amplifier is the analog of rotational shaft speed. Speed range for this device is limited by the disc diameter; a larger diameter helps accummulate more static pressure that makes the interaction amplifier reach its maximum gain (saturation) at an early stage. Although saturation could be readjusted by changing the biasing signal applied at the second control port of the amplifier but it would also change the caliberation for the rotational speed of shaft and the amplifier output. Response time of the sensor could be improved by having a minimum tube length to carry the control signal

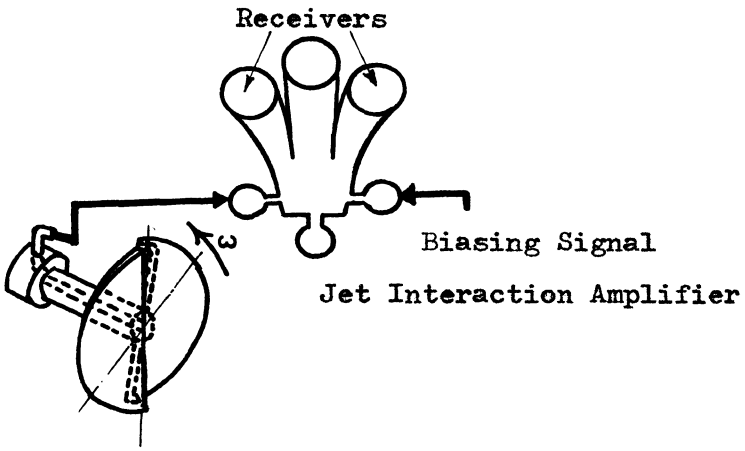

Fig. 65. Rotational Speed Sensor using a Proportional Device.

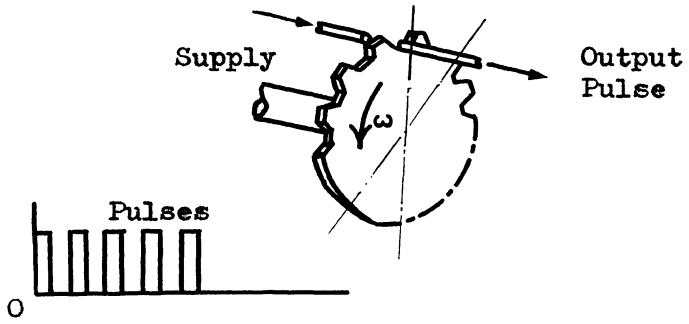

Fig. 66. Rotational Speed Sensor using a Digital Device.

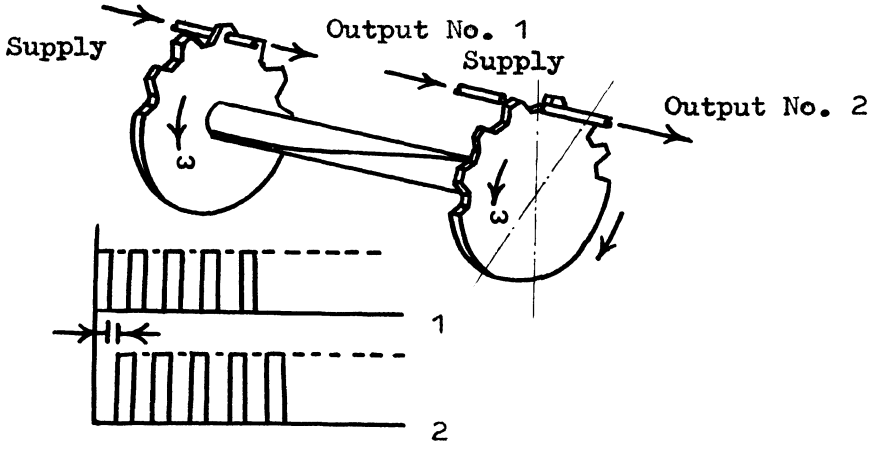

Fig. 67. Torque Measuring Sensor

and also using a small sized proportional amplifier. Frequency response of the amplifier is required to be good enough to handle fluctuations in the shaft speed.

On the other hand the digital device setup (Fig. 66) is relatively easier to build. Supply and receiver nozzles (turbulence amplifier) are placed across a rotating disc, in the form of a gear or perforations in the disc, mounted on the shaft. In the output tube pulses are formed that are counted and integrated with time to give the speed. The frequency response of the digital pulse counting device limits the maximum RPM that could be measured with this sensor. The square pulse output is only an ideal case i.e., with increase in the rotational speed, the pressure pulses in the receiving nozzle continue getting flattened to the point when it is hard to count the pulses. In other words the speed of the rotating disc is fast enough to make a solid screen in front of the supply nozzle. Speed range could further be increased to some extent by increasing pressure in the supply nozzle. Frequency response of the pressure pulse counting device essentially depends on the geometry of input-output nozzles, supply pressure, distance between the nozzles (thickness of rotating disc), and the diameter of the disc at the holes location, number of holes in that diameter circle and geometry of the holes.

B. Torque Measurement

The arrangement is similar to the one used for the rotational speed sensor with a digital device except, here two similar discs (gears or discs with perforations) are mounted on a rotating shaft, at a known distance apart (Fig. 67). This distance should be

less than the one producing a deflection equal to the angle between two consecutive holes in the disc. The two pulse counters at the two locations along the shaft tell a phase difference generated by the relative angular displacement of the two ends, which is a measure of torque when referred to the caliberation (phase difference vs. torque). The design considerations for this sensor are the same as for rotational speed sensor i.e., input-output nozzle diameter, supply pressure, distance between the nozzles, diameter of disc at holes location, number of holes in that diameter circle and hole geometry.

C. Temperature Sensor and Control System

A temperature sensing and control system developed by Gottron and Gaylord [23] at H.D.L. consists of two similar fluidic oscillators. These oscillators experience a change in frequency as a result of the temperature change. The difference in frequencies from the mixer, whose input links with the oscillators' output, is applied to an acoustic to pneumatic converter (Fig. 68). The output from the converter is operated upon by a digital logic circuit to yield a pulse of constant amplitude and duration. These pulses are integrated to obtain a 'd-c level' of flow or pressure that is a function of difference in frequency of the two oscillators and hence the temperature. The output may be applied to a servo-valve, a hydraulic valve or a reactor arm as per system requirement. Manual pre-set is the bias control to the first stage of proportional amplifiers corresponding to a pre-determined temperature maintenance. The fluidic oscillator frequency is given by:

$$f = (\gamma.R.T)^{1/2} / 4.1 \qquad (31)$$

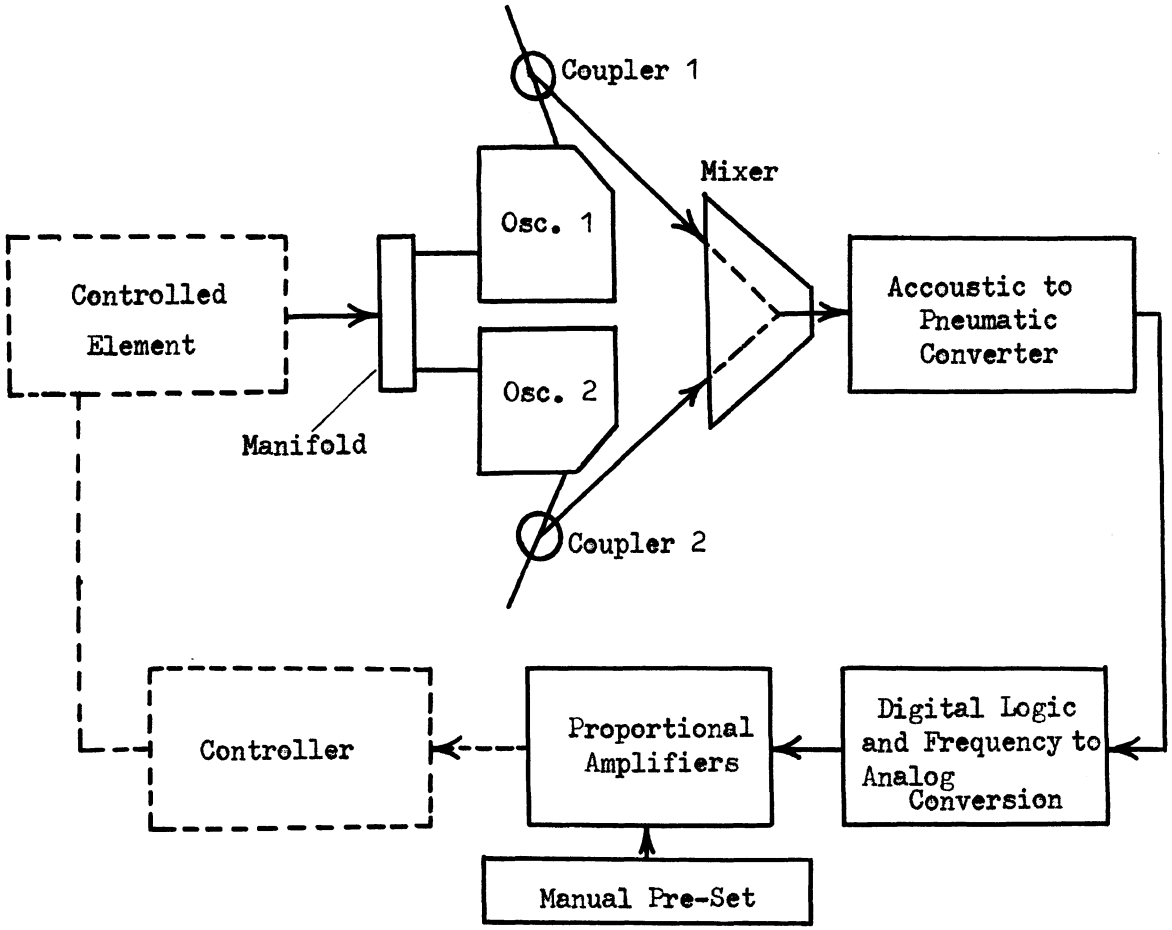

Fig. 68. Proportional Temperature Control System

where R = Gas constant

γ = Ratio of specific heats

l = Oscillator cavity length

The difference in frequency as a function of temperature is determined by;

$$f_1 - f_2 = \frac{\frac{\gamma.R}{4} \cdot T^{1/2} \cdot (l_2 - l_1)}{l_1 \cdot l_2} \qquad (32)$$

where subscripts 1, 2 correspond to the two oscillators.

The system sensitivity is the difference in sensitivities of the two oscillators.

$$\frac{df_1}{dT} - \frac{df_2}{dT} = \frac{\frac{\gamma.R}{4} \cdot (l_2 - l_1)}{2\, l_1 \cdot l_2 \cdot T^{1/2}} \qquad (33)$$

The temperature range tested was 21°-120° C during which the d.c. output level had a proportional change corresponding to a frequency difference. The system had a frequency response of 100 cps due to limitation of the frequency response of digital logic unit and frequency to analog conversion unit, although the other fluidic components are capable of frequency response up to 400 cps. Control range temperature is given by:

$$T^{1/2} - T_0^{1/2} = \frac{l_1 \cdot l_2}{\frac{\gamma.R}{4} \cdot (l_1 - l_2)} \left[(f_1 - f_2)_T - (f_1 - f_2)_{T_0} \right] \qquad (34)$$

where T_0 is corresponding to the manual pre-set temperature. The control range could be changed by resetting the temperature T_o. The output from the system is flow or pressure that could be used as a feedback signal as per need.

D. Liquid Level Sensor

A very simple but unique set-up (Fig. 69) for liquid level sensing was proposed by Letham [24] that monitors liquid level continuously. With gradual increase in liquid level the outlet resistance increases, thereby, back pressure in the supply tube builds up causing an increase in pressure and flow across the fluid resistor in to the output tube. This output could be used as control signal to maintain the liquid level as well as to shut off the supply to the sensor to save some power consumption. The optimum design requires its selection as regards the size of sensor with its supply pressure and geometry of the output resistor. Sensitivity (effective range of level sensing) is another important specification to be known.

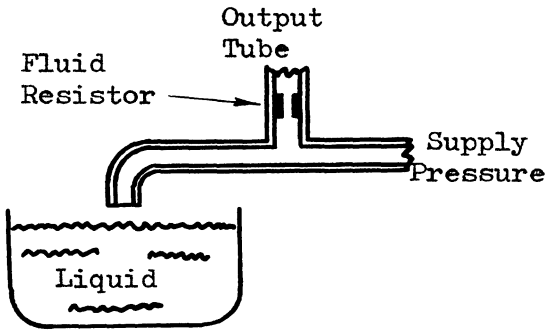

Fig. 69. Continuous Monitoring of Liquid Level

E. Air Flow Velocity Sensor

This sensor introduced by Sharpsteen [25] will be tested experimentally in the next chapter to find out its use. Basically, the phenomenon, as was hinted in chapter I, consists of studying the flow around a cylinder placed across an air flow (Fig. 3). The frequency of vortices f, cylinder diameter d, and the flow velocity V are related through Strouhal Number, which remains constant ($\simeq 0.21$) for flow velocities corresponding to Reynolds Number range of 10^3 to 10^5.

$$\text{Strouhal No.} = \frac{f \cdot d}{V} \qquad (35)$$

Knowing the frequency of vortices shed in the wake, the flow velocity can easily be calculated. To measure the frequency, a three-stage proportional amplifier will be used (although a bistable amplifier can also be used with equal success) by connecting the sensing holes drilled in the downstream side of the side of the cylinder where the separation of flow occurs, to the control ports of the amplifier. The amplified output will go to a transducer, a charge amplifier and finally to an oscilloscope. Comments will be made regarding the acuracy of this sensor as compared to the usual use of a pitot-tube manometer. It will also be decided out of the two tubes tested (½ " and 1 " outside diameters), which one is better to use.

V AIR FLOW VELOCITY SENSOR

Basically the phenomenon used in the development of sensor is the boundary layer separation and formation of Von Karman Vortex Street in the wake of a cylinder placed across an air flow. When the flow starts (low Reynolds Nos.) it is nearly frictionless. A fluid particle in the thin boundary layer consumes much of its kinetic energy on its path from D to E (Fig. 70) that it cannot climb the pressure hill from E to F. The external pressure reverses the flow which increases with the Reynolds No. A free vortex layer springs from each separation point that establishes a circulation and from which fluid in the form of vortices breaks away at regular intervals.

Von Karman does not claim to have discovered these vortices. Historically, the earliest picture in which he had seen them was in a church in Bologna, Italy where St. Christopher is shown carrying child Jesus across a flowing stream. Behind the saint's naked foot the painter indicated alternating vortices. Von Karman contributed two fold information. One that only the asymmetric arrangement of vortices could be stable (Fig. 71), and only for a certain ratio of the distance between the rows and the distance between two consecutive vortices in either row. Also, he connected the momentum carried by the vortex system with the drag, and showed how the creation of such a vortex system can represent the mechanism of the wake drag.

Roshko [26] has shown data (Fig. 72) on cylinders with diameters varying in the range of 0.00925 - 0.25 inches showing that the phenomenon of vortex shedding is not dependent on diameter selection.

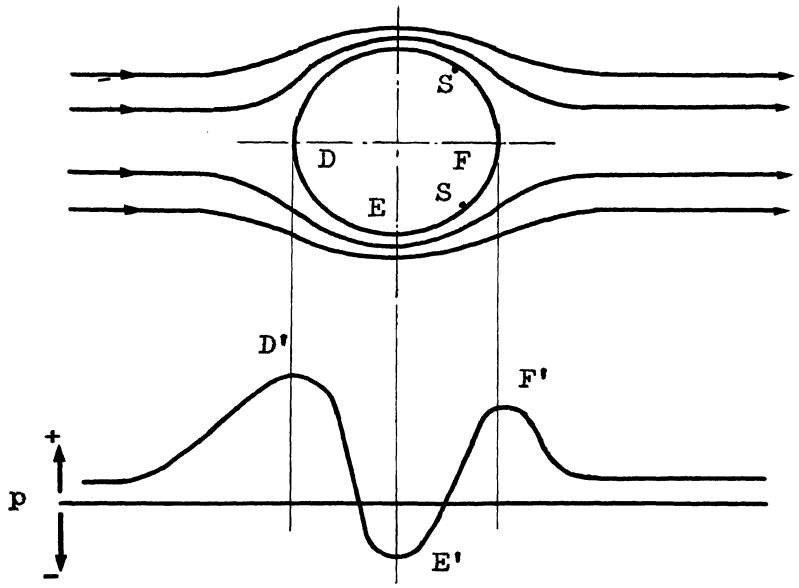

Fig. 70. Pressure Distribution in a flow around a cylinder

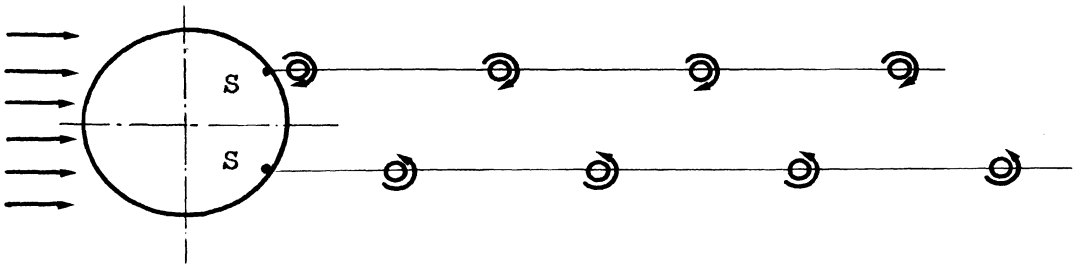

Fig. 71. A Stable Assymmetric Vortex Shedding Arrangement

There have been three characteristic ranges of Reynolds Nos. as regards the state of vortices.

Stable Range	$40 < R_e < 150$
Transition	$150 < R_e < 300$
Irregular	$300 < R_e < 10,000^+$

In the stable range Strouhal No. rises rapidly, in the irregular it is essentially constant and in the transition it is unstable. For working of the velocity sensor irregular range has been used when Strouhal No. remains constant. The vortex shedding mechanism and drag force experienced by a blunt body in the flow are closely related as is observed in Figure 72 that drag coefficient curve is a mirror image of the Strouhal No. curve during the irregular vortex shedding range. Drag is defined as the component of the total force exerted by a fluid stream on an immersed body parallel to the undisturbed initial velocity. It is non-dimensionalized by the dynamic head, thus;

$$C_D = D / \tfrac{1}{2} \rho . V^2 . A$$

where A is the frontal area exposed by the body to the flow direction. Drag is classified as follows:

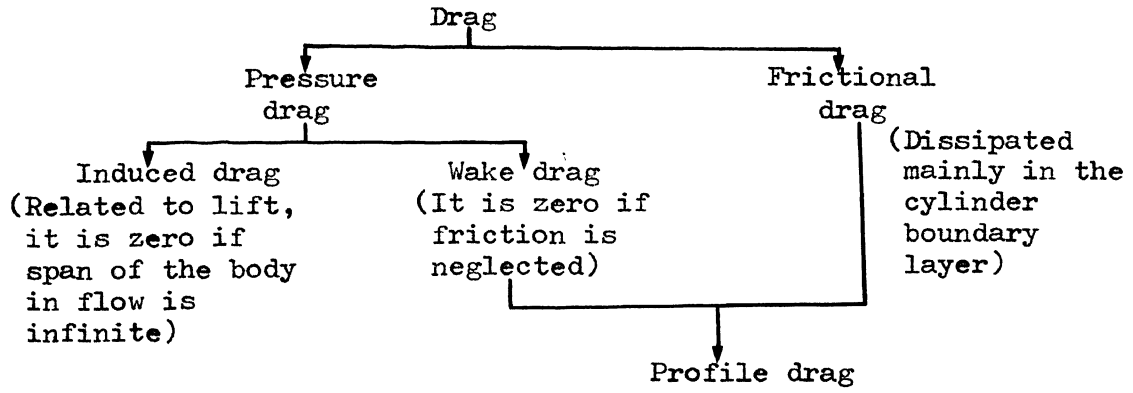

In the present case of a blunt body like a cylinder, wake drag

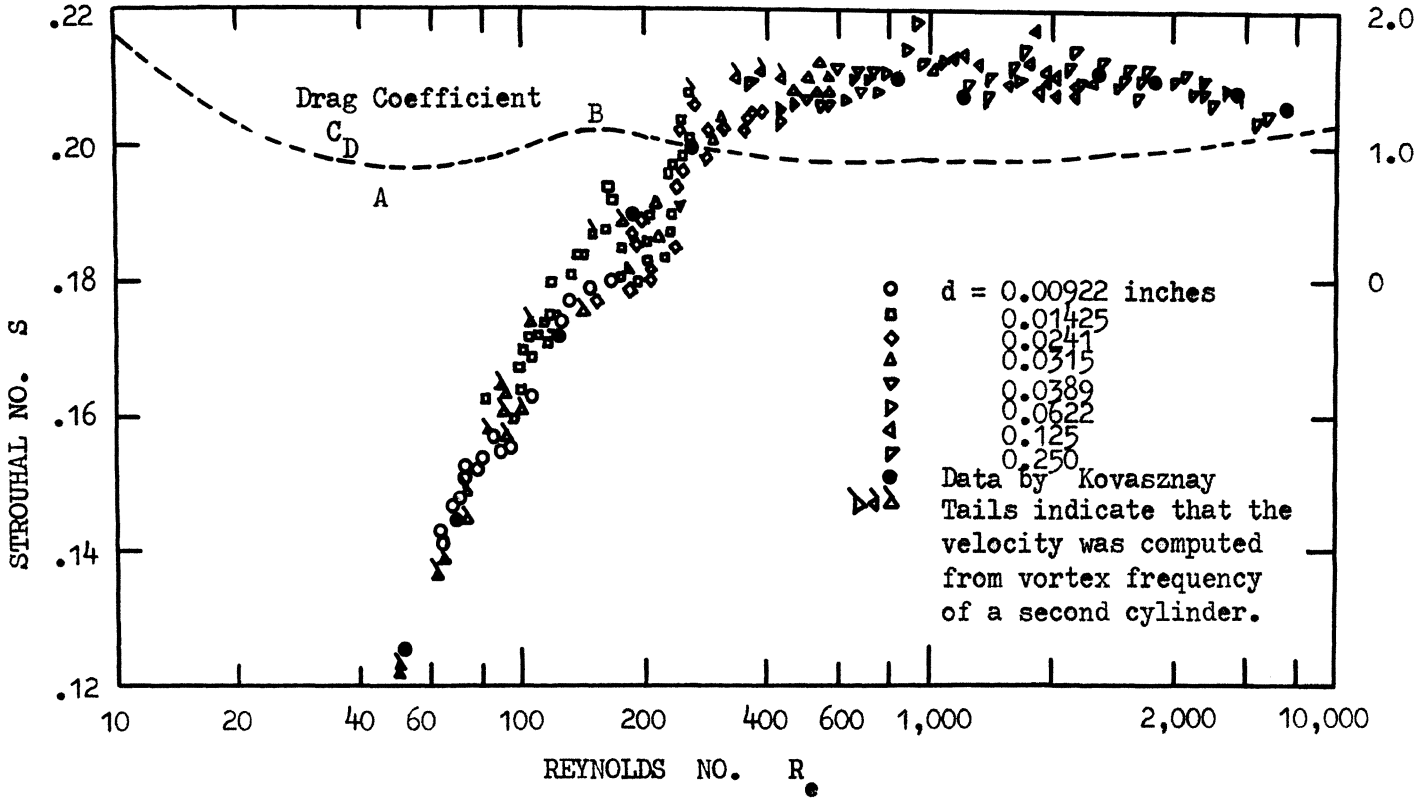

Fig. 72. Strouhal No. vs. Reynolds No. for circular cylinders

is dominating. It is also known as the Normal pressure drag. In some more data by Wieselberger [27], C_D the drag coefficient has been measured for cylinders with diameter ranging 0.00197" to 11.8 " (Fig. 73) and the Reynolds No. tested beyond 10^5. It is seen near $R_e = 5 \times 10^5$, there is a sudden drop in the drag coefficient as a consequence of the transition in the boundary layer. Transition causes the point of separation to move downstream which considerably decreases the width of wake. In the plot pressure drag coefficient and Strouhal No. vs. Reynolds No. (Fig. 72) following points are observed:

1. C_D, the drag coefficient is practically constant at the value $C_D = 1$.
2. The minimum point A is at a value of R_e close to that at which vortex shedding starts.
3. Maximum point B is in the transition range.
4. In the irregular range C_D is almost a mirror image of the Strouhal No. curve.

Effect of Blunt Body Surface Roughness:

The influence of roughness enters into the problem of turbulent skin friction. At low Reynolds No., it does not have a significant effect on skin friction. The physical reason being that below this limit the thickness of the laminar sublayer exceeds the height of irregularities of the roughness elements which are not able to produce additional turbulence in the main stream or in other words the surface is said to be hydraulically smooth.

With increasing Reynolds No. the laminar sublayer becomes thinner and thinner so that the roughness elements emerge and begin

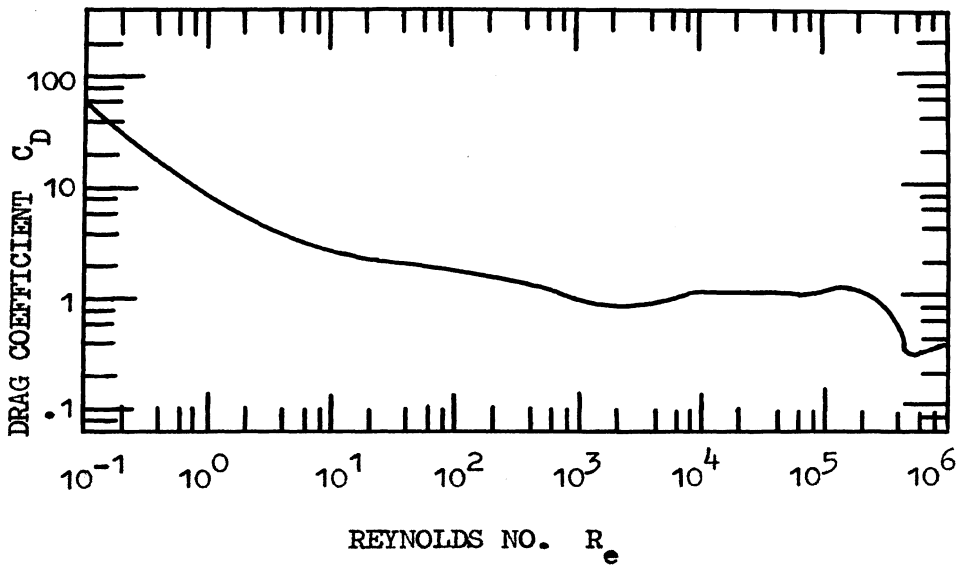

Fig. 73. Drag Coefficient for Circular Cylinders vs. Reynolds No.

to influence the main flow. Now the skin friction is given by the total frontal drag of these elements as every proturbance can be considered as a small blunt body that contributes its individual drag. The overall effect on the curve (Fig. 73) is to raise the first part of the curve till $R_e = 5 \times 10^5$ and the sudden drop in drag coefficient shifts to its left. This is because the transition moves beyond the separation point in the upstream making the boundary layer turbulent. As it is known that the turbulent boundary layer sticks better to the surface, thus moving the separation point further downstream. As result there is a narrow wake and hence a drop in the drag.

This experimental set-up is capable of working in the Reynolds No. range of 10^3 to 10^5. Keeping into mind the dependence of Strouhal No. on drag coefficient or in other words on the surface roughness, it is advisible to specify the roughness of the tubes under test. In the present work the tubes are assumed to be smooth.

Experimental Component Description:

Clear, cast lucite (acrylic) tubes of ½ " and 1 " outside diameters were used with 1/16 " and 1/8 " respective wall thickness. It is placed vertically in the middle of test section of the wind tunnel. From top and bottom it is vented to downstream pressure. In the middle of tube there was initially one hole (1/8 " diameter) to sense the vortices. Later depending on the best signal detection, the second hole was also drilled. The holes were found to be 115° downstream, close to the boundary layer separation point.

A G.E. 3-stage proportional amplifier model MG-11 was used to

amplify the pressure pulses due to the shedding of vortices. Three custom designed proportional elements are cascaded in a close coupled arrangement to minimize signal phase shift and excessive line connections. Individual supply pressures are adjusted internally for optimum performance. The manufacturer specified the following characteristics:

Supply pressure	5 - 15 psig
Maximum signal gain	100 : 1 (dead ended input)
Null bias	negligible
Operating frequency	0 - 3,000 cps
Signal to noise ratio	100 : 1 below 25 cps

A quartz pressure transducer (KISTLER model 603 A) was used to transduce the pressure signals to electrical signals. The transducer contains an accelerometer positioned with in the pressure sensitive quartz column to cancel out effectively spurious acceleration signals over a wide frequency range. It measures very fast transients under most environmental conditions. Response time is near micro-second.

KISTLER model 566 Multirange Charge Amplifier was connected between the pressure transducer and the oscilloscope. This model employs an electrometer tube input followed by a transistorized voltage amplifier. Use of an electrometer tube in the input stage makes the amplifier insensitive to accidental input overloads.

A stiff plastic tube of 1/8 " I.D. and 1/4 " O.D. was employed for the supply flow to the fluid amplifier while for its input-output connections a flexible tube of 1/16 " I.D. and 1/8 " O.D. was used. One output of the amplifier was blocked and the other connected to the transducer. The length of input-output tubing is preferred to

be as short as possible to reduce the inductive and capacitive effects present in a fluid line.

Experimental Procedure:

The two tubes (1/2 " O.D. and 1 " O.D.)used in the making of the fluid sensor were tested in two sets of data each, corresponding to single and double sensing holes.

First, the 1/2 " O.D. tube with single sensing hole was placed in the flow (Fig. 74 a.) and rotated in order to get the best vortex signal on the oscilloscope. This angular position of the sensing hole (115° with the leading nose of the tube) was noted and subsequently vortex frequency is noted. A pitot tube was placed in the centre of the duct after removing the vortex sensor tube to determine the corresponding velocities used for the velocity sensor. A second sensing was then drilled in the tube corresponding to second separation point (115° with the leading nose of the tube) and all the above mentioned steps were repeated. Next, the second tube (1 " O.D.) is similarly tested for the same velocity range with single and double control ports. Velocity in the wind tunnel varies from 25 fps to 75 fps in five steps. Thus, five runs in each set make the total data consisting of 20 runs which are repeated for pitot tube. Using above data, Strouhal No will be evaluated separately for each run and then from the mean Strouhal No. value, the velocities of flow will be predicted.

Strouhal No. and Reynolds No. appearing in Table I were evaluated corresponding to the experimental data (Appendix A) consisting of frequency measurements and the pitot tube velocities. Strouhal No. will be evaluated using equation (35).

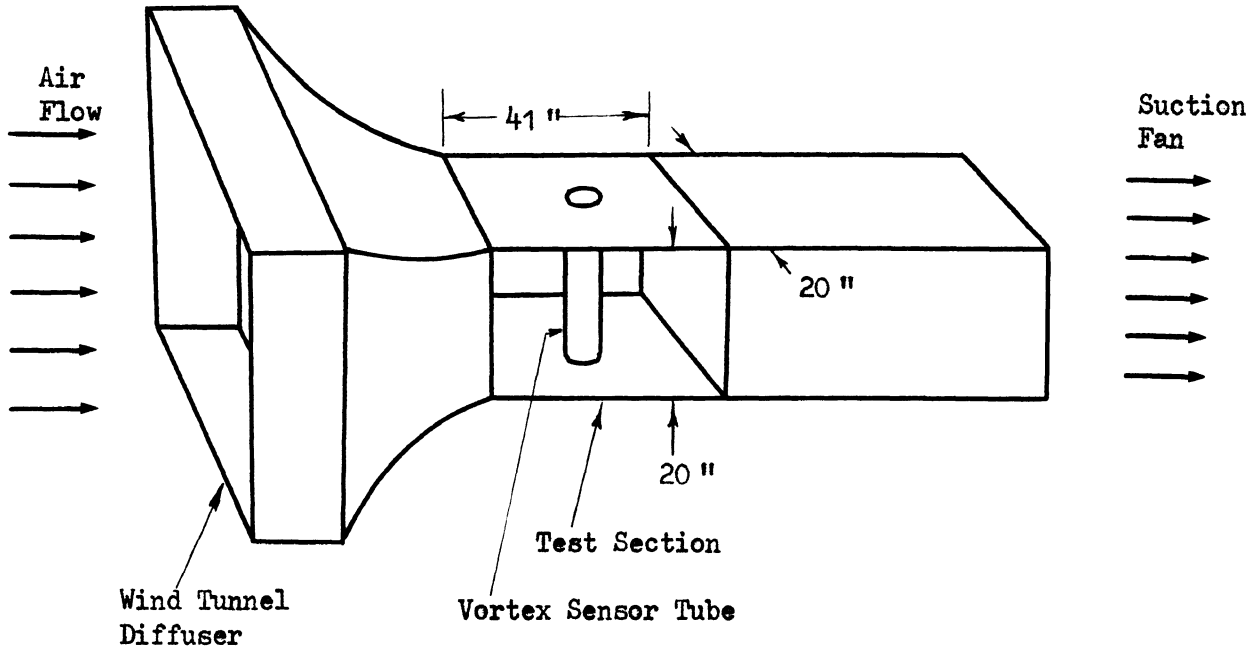

Fig. 74a. Vortex Sensor Tube set-up in Wind Tunnel

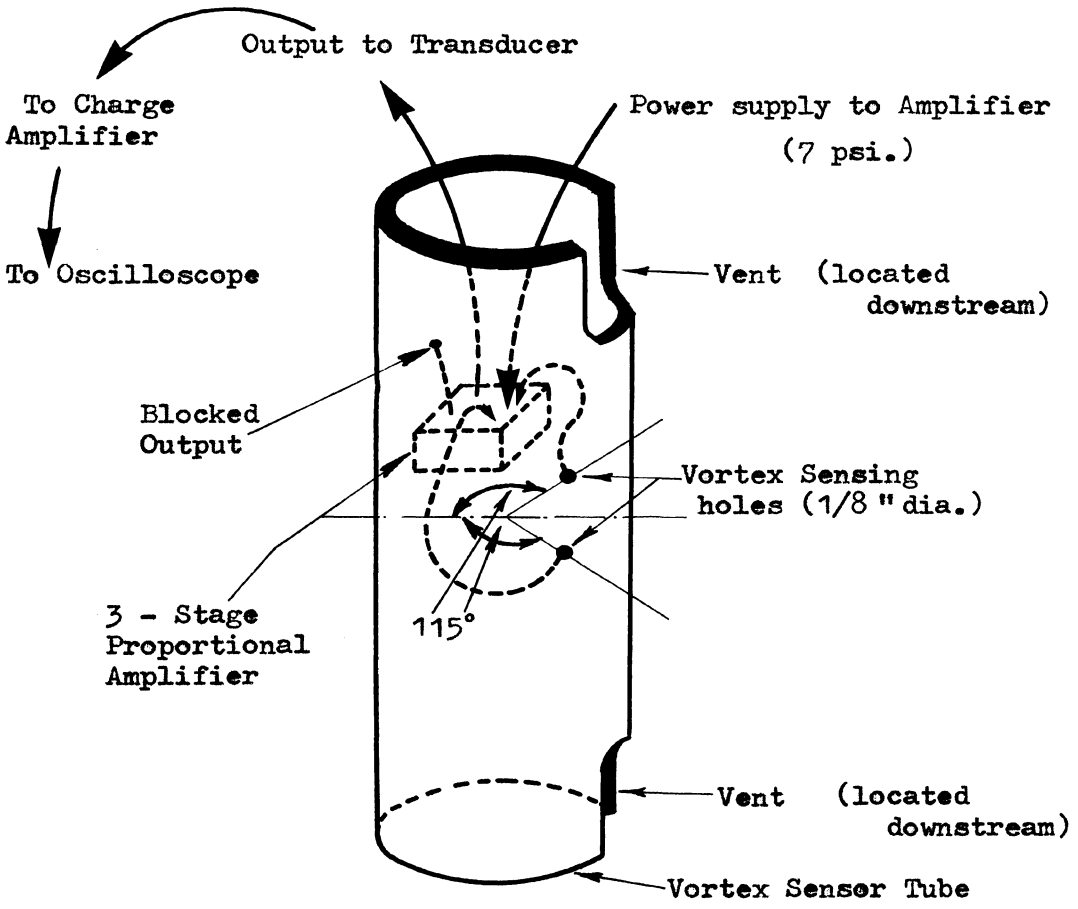

Fig. 74b. An Exploded View of the Vortex Sensor Tube

Reynolds No. R_e, is given by;

$$R_e = \frac{\rho.V.d}{\mu} \qquad (36)$$

where V is the pitot tube velocity in fps, 'd' the tube diameter μ is the viscosity of air and corresponding to the mean room temperature of 81.25°F, it is taken to be 0.383×10^{-6}. ρ, the density of air has been evaluated corresponding to static pressure inside the duct and the room temperature. It is given by the following expression,

$$\rho = P_S / R.T$$

where P_S is the static pressure inside the duct, R is the gas constant and T is the absolute room temperature.

There are some uncertainties associated with Strouhal No. and Reynolds No. (ω_S and ω_{R_e}) due to uncertainties in reading data such as inacuracy in reading the frequency of vortices (ω_f), diameter of the sensor tube (ω_d), velocity of air flow using pitot tube (ω_V) and also the errors involved in reading the room temperature (ω_T) and finally error involved in reading barometer (ω_P).

The expressions for ω_S and ω_{R_e} appear as follows:

$$\omega_S = \sqrt{(\omega_f \cdot \partial S/\partial f)^2 + (\omega_d \cdot \partial S/\partial d)^2 + (\omega_V \cdot \partial S/\partial V)^2}$$

where ω_f is calculated taking in to consideration the accuracy of reading oscilloscope screen and it is taken to be one fourth of a cycle for the full screen.

ω_d is the inaccuracy in reading sensor diameter, or in other words it is the least count of the micrometer which is 0.001 " or 0.000083 feet.

Table I. Evaluation of Strouhal Nos. and Reynolds Nos. for various data

Set NO.	Run No.	Static Pressure P_S, in. of Hg.	Temperature	Static Pressure P_S, psi	Air Density	Velocity head in. of water	Velocity V, fps	Strouhal No.	Reynolds No.
I 1/2" tube single control	1.	29.136	543.0	14.3103	0.002211	0.222	32.31313	0.19419	7804.24
	2.	29.1198	543.0	14.3023	0.002210	0.445	45.76181	0.19197	11046.21
	3.	29.1015	543.0	14.2933	0.002209	0.685	56.79434	0.20624	13700.68
	4.	29.0700	543.0	14.2778	0.002206	1.095	71.84589	0.19797	17312.87
	5.	29.0465	543.0	14.2663	0.002204	1.405	81.41580	0.19525	19603.08
II 1/2" tube double control	6.	28.9974	539.0	14.2422	0.002217	0.171	28.32242	0.22156	6858.39
	7.	28.9840	539.0	14.2356	0.002216	0.360	41.10399	0.21373	9948.90
	8.	28.9660	539.0	14.2268	0.002215	0.582	52.27921	0.20805	12645.92
	9.	28.9396	539.0	14.2138	0.002213	0.942	66.54128	0.20118	16081.13
	10.	28.9176	539.0	14.2030	0.002211	1.232	76.12656	0.20332	18383.63
III 1" tube single control	11.	29.0948	540.0	14.2895	0.002220	0.171	28.30167	0.18550	13781.52
	12.	29.0820	540.0	14.2838	0.002219	0.360	41.07272	0.21474	19992.30
	13.	29.0640	540.0	14.2750	0.002218	0.582	52.23940	0.20100	25411.98
	14.	29.0368	540.0	14.2616	0.002215	0.940	66.42076	0.20235	32280.30
	15.	29.0180	540.0	14.2523	0.002214	1.200	75.07082	0.20141	36460.57
IV 1" tube double control	16.	28.8906	543.0	14.1898	0.002193	0.154	27.02710	0.22129	12996.75
	17.	28.8760	543.0	14.1826	0.002192	0.342	40.28673	0.21372	19363.22
	18.	28.8610	543.0	14.1752	0.002190	0.547	50.96306	0.22251	24481.91
	19.	28.8360	543.0	14.1629	0.002188	0.890	65.03465	0.21312	31214.65
	20.	28.8108	543.0	14.1506	0.002186	1.230	76.48779	0.20866	36679.75

ω_V is the inaccuracy in pitot tube velocity. The least count for the inclined manometer (20° to horizontal) is 0.05 inch or 0.0171 inch for a verticle scale. This inaccuracy is added in the velocity head for each reading and the corresponding velocities are calculated and hence the difference gives the uncertainty in the pitot tube velcity.

$$\omega_{R_e} = \sqrt{(\omega_P \cdot \delta R_e/\delta P)^2 + (\omega_V \cdot \delta R_e/\delta V)^2 + (\omega_d \cdot \delta R_e/\delta d)^2 + (\omega_T \cdot \delta R_e/\delta T)^2}$$

where ω_V and ω_d have already been explained. ω_P is the least count for the vernier scale mounted on the barometer equal to 0.002 inches of Hg. or 0.000983 psi. ω_T is the least count of the thermometer and is equal to 0.5°F. ω_S and ω_{R_e} appear in Table II.

There were 20 runs in all to evaluate Strouhal No. and the Reynolds No. range tested was from 7,000 to 37,000. A plot with ordinates Strouhal No. vs. Reynolds No. appears in Figure 75.

In order to find the mean value of Strouhal No.,

let $f_n(a) = A$, the mean value of strouhal no., and let $f_n(x)$ is any data point on the plot. The subscript 'n' varies from 1 to 20, the number of runs.

Then

$$f_n(x) - f_n(a) = \text{deviation}$$

The mean value for Strouhal No. will be obtained by minimizing the function J.

$$J = \sum_{n=1}^{20} \left[f_n(x) - f_n(a) \right]^2$$

Table II. Percentage uncertainties in Strouhal Number and Reynolds Number

Run No.	ω_f	ω_V	ω_S	ω_{R_e}	% ω_S	% ω_{R_e}
1.	5	1.12141	0.00930	270.941	4.79	3.47
2.	5	0.87067	0.00583	210.422	3.04	1.90
3.	5	0.7043	0.00446	170.385	2.17	1.24
4.	5	0.5587	0.00328	135.608	1.66	0.78
5.	5	0.4941	0.00282	120.386	1.44	0.61
6.	5	1.38248	0.01304	334.836	5.89	4.88
7.	5	0.9648	0.00712	233.712	3.34	2.35
8.	5	0.76264	0.00500	184.863	2.40	1.46
9.	5	0.60116	0.00362	146.076	1.80	0.91
10.	5	0.53671	0.00307	128.375	1.51	0.70
11.	1.25	1.38115	0.00970	676.960	5.23	4.91
12.	2.5	0.96383	0.00712	469.518	3.32	2.35
13.	2.5	0.76178	0.00494	371.326	2.46	1.46
14.	5	0.60168	0.00653	293.959	3.23	0.91
15.	5	0.53268	0.00573	260.936	2.84	0.72
16.	1.25	1.46090	0.01248	702.619	5.64	5.40
17.	2.5	0.99460	0.00736	478.372	3.44	2.47
18.	2.5	0.79082	0.00501	380.576	2.25	1.55
19.	5	0.62232	0.00672	300.093	3.15	0.96
20.	5	0.53026	0.00563	256.550	2.70	0.70

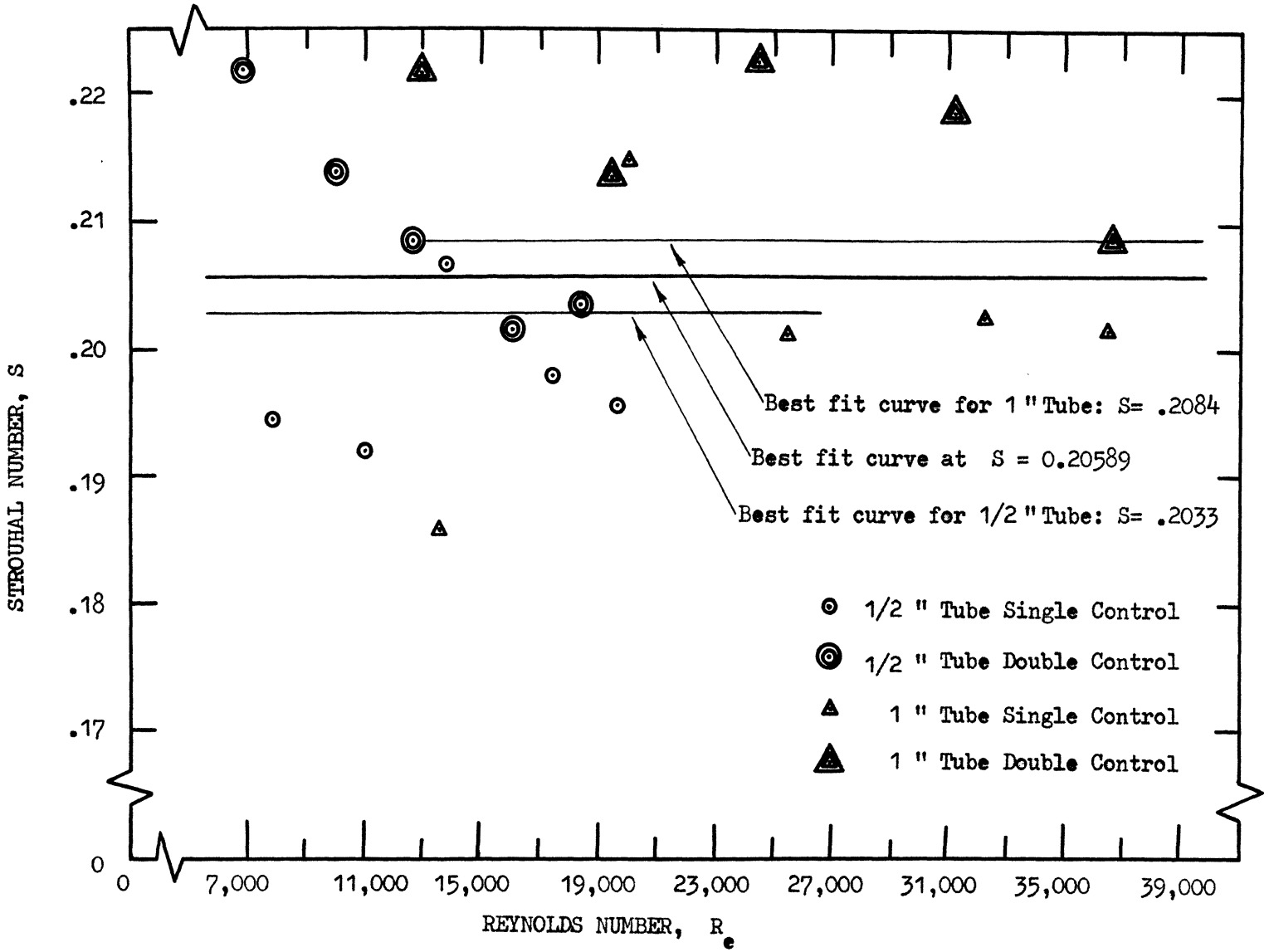

Fig. 75. A Plot of Strouhal No. vs. Reynolds No. Corresponding to the the Experimental Data on the Vortex Sensor

$$\text{or} \quad A = \frac{\sum_{n=1}^{20} f_n(x)}{20}$$

$$= \frac{4.11776}{20} = 0.20589$$

The mean value of Strouhal No. is shown in the plot (Fig. 75) along with mean values corresponding to 1/2 " and 1 " diameter tubes. These are found to be o.2033 and 0.2084 respectively. For the sensor velocity predictions these Strouhal No. values will be made use of to find out which one of the two tubes gives close results.

Next a plot with variables pitot tube velocity vs. vortex frequency is presented (Fig. 76) which is used to find fluctuations in pitot tube velocity and the velocity obtained from the mean slope of this plot and the available frequency data. The mean slope K (assuming a linear functional relationship), is given by:

$$K = \frac{\Sigma V.f}{\Sigma f^2}$$

The respective values of K for 1/2 " and 1 " diameter tubes are as follows;

$$K_{1/2"} = 1/4.815704$$

$$K_{1"} = 1/2.477748$$

The velocities obtained from this plot (Fig. 76) are assumed to be more accurate than the pitot tube velocities (Table III) since the mean slope of the plot deals in larger fluctuations to smooth out than the uncertainty present in the pitot tube velocities.

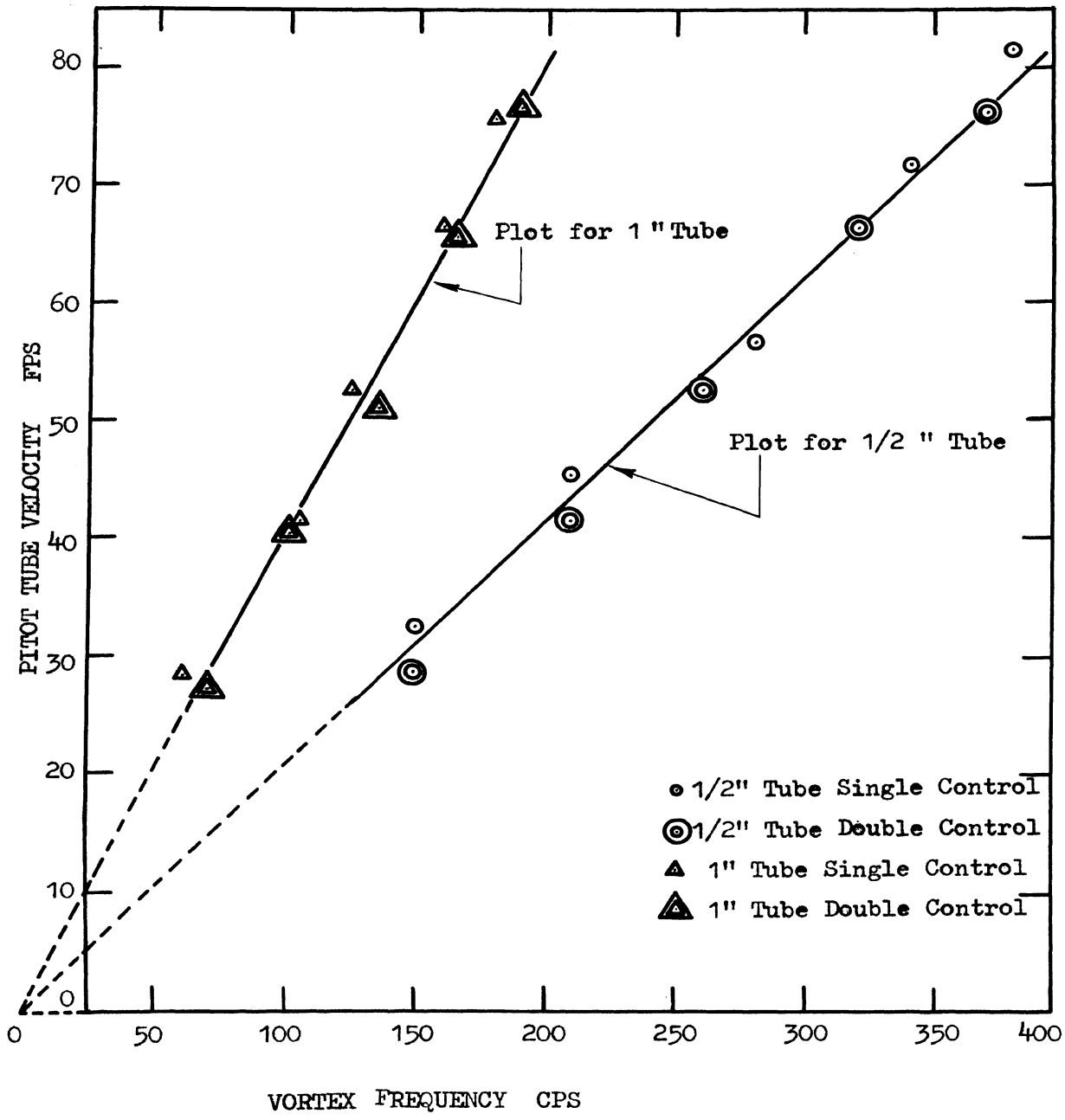

Fig. 76. A Plot of Pitot Tube Velocity and Vortex Frequency

Table III. Comparison of Pitot tube velocities and the velocities obtained from the plot of pitot tube velocity vs. vortex frequency

Run No.	f	Pitot tube velocity	Velocity from the plot	error	ω_V
1.	150	32.31	31.15	1.16	1.121
2.	210	45.76	43.61	2.15	0.871
3.	280	56.79	58.14	- 1.35	0.704
4.	340	71.85	70.60	1.25	0.559
5.	380	81.42	78.91	2.51	0.494
6.	150	28.32	31.15	- 2.83	1.382
7.	210	41.10	43.61	- 2.51	0.964
8.	260	52.28	53.99	- 1.71	0.763
9.	320	66.54	66.45	0.09	0.601
10.	370	76.13	76.83	- 0.70	0.527
11.	62.5	28.30	25.23	2.07	1.381
12.	105	41.07	42.38	- 1.31	0.964
13.	125	52.24	50.45	1.79	0.762
14.	160	66.42	64.58	1.84	0.602
15.	180	75.07	72.65	2.42	0.533
16.	71.2	27.03	28.74	- 1.71	1.461
17.	102.5	40.29	41.37	- 1.08	0.995
18.	135	50.96	54.49	- 3.53	0.791
19.	165	65.03	66.60	- 1.57	0.622
20.	190	76.49	76.69	- 0.20	0.530

Table IV. Comparison of Vortex Sensor velocities and the velocities obtained from the plot of pitot tube velocity vs. vortex frequency

Run No.	f	Sensor Velocity	Velocity from the plot	error	ω_V
1.	150	30.80	31.15	- 0.35	1.121
2.	210	43.20	43.61	- 0.41	0.871
3.	280	57.50	58.14	- 0.64	0.704
4.	340	70.00	70.64	- 0.64	0.559
5.	380	78.20	78.91	- 0.71	0.494
6.	150	30.80	31.15	- 0.35	1.382
7.	210	43.20	43.61	- 0.41	0.964
8.	260	53.50	53.99	- 0.49	0.763
9.	320	65.80	66.45	- 0.65	0.601
10.	370	76.10	76.83	- 0.73	0.527
11.	62.5	25.20	25.23	- 0.03	1.381
12.	105	42.20	42.38	- 0.18	0.964
13.	125	50.30	50.45	- 0.15	0.762
14.	160	64.40	64.58	- 0.18	0.602
15.	180	72.40	72.65	- 0.25	0.533
16.	71.2	28.60	28.74	- 0.14	1.461
17.	102.5	41.20	41.37	- 0.17	0.995
18.	135	54.30	54.49	- 0.19	0.791
19.	165	66.40	66.60	- 0.20	0.622
20.	190	76.40	76.69	- 0.29	0.530

These velocities will then be used as reference for the sensor velocities. The sensor velocities are calculated by the Strouhal Number expression already described. The exact diameters of the two tubes are 0.502 " and 1.008 ". Thus the sensor velocities are compared with the respective velocities evaluated from the mean slope of the plot of pitot tube velocity vs. frequency of vortices shed (Table IV). The errors obtained using the sensor are considerably less than the uncertainty in the pitot tube velocities. Further it is observed that the errors for 1 " diameter tube are smaller as compared to the 1/2 " diameter tube.

Comments as regards the Velocity Range of Vortex Sensor and its tube diameters:

The feasibility of the velocity sensor was due to the fact that Strouhal No. remains constant in the Reynolds No. range of 10^3 to 10^5. Corresponding to this range 1/2 " diameter sensor tube could be operated in the velocity range of 4.04 fps to 404 fps while for 1 " tube it is 2.02 - 202 fps. Due to the limited velocity range available from the wind tunnel (25 -75 fps approx.), the sensor could be tested for the Reynolds No. range of 7,800 to 19,600 in case of 1/2 " tube and 13,000 to 36,700 for 1" tube. The two Reynolds No. ranges tested are although different but have an overlap from 13,000 to 19,600.

The Strouhal No. evaluations indicate consistent values irrespective of the tube diameters, however, separate mean Strouhal No. values were used to determine the individual performance of the tubes. 1 " tube proved to be better due to following points.

Large diameter tubes are useful for low velocities. Observing the Reynolds No. range, 1 " tube could probe lower velocities as compared with 1/2 " tube for the same Reynolds No.

A pitot tube-manometer set has increasing uncertainty as lower velocities are approached due to inaccuracy in reading manometer. For a flow velocity of 25 fps there has been found to be an error of 1.5 fps which further increases with lower velocities. It is recommended to use a vortex sensor in the range from 25 fps to further lower velocities. Although the 1/2 " tube is supposed to have a greater sensitivity i.e., larger Δf for the same ΔV (Fig. 76), still 1 " tube was found to have smaller errors associated than those with 1/2 " tube. The smaller tubes are limited by the frequency response of the fluidic circuit due to higher frequency of vortex shedding. A few more tubes with larger diameter (say 1½ " or 2 " or may be 3 " too) are suggested to be tested to decide upon a particular tube for a certain velocity range.

VI SUMMARY AND CONCLUSIONS

A study of the Air Velocity Sensor, using a three staged proportional amplifier to sense the vortices shed in the wake of a cylinder placed in a flow, indicates that it gives a precise measurement of velocity. Two different(1/2 " and 1 ") diameter tubes were used. It has been concluded in the previous chapter that 1 " diameter tube is better as for as acuracy is concerned and also more effective for low velocities. The usual way to measure velocity of air through the use of a pitot tube, starts loosing accuracy as lower velocities are approached. This error is mainly caused due to uncertainty in reading the manometer correctly.

Working range of Reynolds No. is 10^3 to 10^5 during which Strouhal No. remains constant. In the present work the sensor was tested for a Reynolds No. range of 7,000 to 37,000. The mean value for Strouhal No. from the plot of Strouhal No. vs. Reynolds No. (Fig. 75) came out to be 0.2058 and in particular for 1/2 " tube it was 0.2033 and for 1 " tube it was 0.2084 . Using these values, velocities were calculated, the velocities obtained using 1 " tube agreed closely with the values obtained when using the best slope of the curve of pitot tube velocity vs. frequency of vortices shed (Fig. 76). The limitations for the velocity range as well as the frequency range have been discussed corresponding to each tube.

In early part of this thesis report, literature has been collected for the fluidic components such as bistable and proportional amplifiers which include turbulence and vortex amplifiers respectively. These components have been described with a fair amount of detail

regarding their characteristics, cascading of amplifiers and special designs with new efficient configurations. An application of jet-interaction amplifier as an operational amplifier, has been included and analysed. The fluidic component whose function is similar to the electronic component, consists of fluidic resistors and capacitors. Sensors have been dealt with separately. Sensors such as rotational speed sensor, torque measurement, temperature sensing and control and an air velocity sensor has also been included.

The air velocity sensor has been found to sense velocities precisely and in particular the 1 inch diameter tube proved to be better. Sensor accuracy depends mainly on the correct evaluation of mean Strouhal No. value from the plot of Strouhal No. vs. Reynolds No. The uncertainty in Strouhal No. (p. 89) consists of uncertainties due to inaccurate observation of frequency (ω_f), tube diameter measurement error (ω_d), the least count of micrometer, along with the assumption that the tube has uniform outside diameter and finally the error in the pitot tube velocity (ω_V) due to inaccurate reading of manometer. Out of the above mentioned errors, the error due to velocity is maximum, appreciable in frequency and negligible for tube diameter variations. The error in velocity measurement could be reduced by using a more sensitive pitot tube and also using lighter fluid in the manometer as compared to water and further reducing the angle of inclination of the manometer tubes from 20° to say 15° to the horizontal. The accuracy for the scope screen was judged to be one fourth of a cycle. It should be tried to accommodate a maximum number of cycles on the screen without loosing much accuracy so that the overall error introduced in frequency (ω_f) is minimized.

Taking above points into considerations, Strouhal No. value obtained will be more exact with less uncertainty. In the present analysis, a maximum uncertainty for Strouhal No. came out to be 5.9 % (Table II.).

The control holes drilled in the two tubes are of same diameter (1/8 "). It needs further investigation regarding their individual usefulness that how does a 1/8 " hole disturb the flow around cylinders of different diameters, and what is its effect on the boundary layer separation point and the frequency of vortices shed.

The analysis has been extended to calculate the drag force per unit length of sensor tube (Appendix B). Making use of the expressions for drag and Strouhal No., drag force is found to be proportional to square of the vortex frequency. The constant of proportionality is easy to find. A plot with variables drag force and $(\text{frequency})^2$ (Fig. B1), is a straight line. Drag is further connected with velocity since velocity and frequency are linearly related to each other. This approach could be used to determine drag force experienced by other blunt bodies such as a flat plate or one with a tringular section with one of the edges facing the flow.

With reference to work done by Fage Johansen [28] a new constant S' has been introduced (Appendix B) which is similar to Strouhal No. with the difference that instead of the tube diameter, d', the distance between free vortex layers is used. The new constant S' has been claimed to remain more steady as compared to Strouhal No. for essentially the same Reynolds No. range. A further analysis shows that using a value of 0.142 for S', the velocity of vortices moving downstream remains half of the main flow velocity for R_e = 300 to 20,000$^+$.

BIBLIOGRAPHY

1. Anderson, Blain W., The Analysis and Design of Pneumatic Systems, John Wiley & Sons Inc., New York, 1967.

2. Warren, Raymond W., Fluid Amplifiers, McGraw-Hill Book Company, New York, 1966.

3. Lush, P. A., " Investigation of the Switching Mechanism in a Large Scale Model of a Turbulent Re-attachment Amplifier ", Proceedings of the Second Cranfield Fluidic Conference, January, 1967, Paper A-1.

4. Borque, C. and Newman, B. G., " Re-attachment of a Two-Dimensional Incompressible Jet to an Adjacent Flat Plate ", Aeronautical Quarterly vol. 11, 1960, 201 - .

5. Harda, M., Ozaki, S. and Hara, Y., " Output Characteristics of Wall Attachment Elements ", Proceedings of the Third Cranfield Fluidics Conference, May, 1968, Paper F-2.

6. Sarpkaya, T., " The Performance Characteristics of Geometrically Similar Bistable Amplifiers ", Transactions of ASME Journal of Basic Engineering, June 1969, 257 - 261.

7. Griffin, William S., " Bistable Fluid Jet Amplifier with Low Sensitivity to Receiver Reverse Flow ", Proceedings of the Fluid Amplification Symposium vol. III, October, 1965.

8. Belsterling, Charles A., " Digital and Proportional Jet Interaction Devices and Circuits ", Fluidics Quarterly vol.I, no. 2, January, 1968, 60 - 66.

9. Hayes, W. F. and Kwok, C., " Impedance Matching in Bistable and Proportional Amplifiers through the Use of a Vortex Vent ", Proceedings of the Fluid Amplification Symposium vol. I, October, 1965, 331 - 358.

10. Auger, Raymond N., " How to Use Turbulence Amplifiers for Control Logic ", Control Engineering, June, 1964, 89 - 90.

11. Auger, Raymond N., " Turbulence Amplifier Design and Application ", Proceedings of the Fluid Amplification Symposium vol. I, October, 1962, 357 - 361.

12. Metzger, Eric E. and Lomas, Charles G., " Turbulence Amplifier for Integrated Two-Dimensional Fabrication ", Proceedings of the Fluid Amplifiaction Symposium vol. II, October, 1965, 363 - 370.

13. Boothe, Willis A., " A Lumped - Parameter Technique for Predicting Analog Fluid Amplifier Dynamics ", ISA Transactions vol. IV, no. 1, 1965, 84 - 92.

14. Belsterling, Charles A. and Tsui, Ka Cheung, " Analyzing Proportional Fluid Amplifier Circuits ", Control Engineering, August, 1965, 87 - 92.

15. Strunk, R. D. and Bowman, D. E., " Frequency Response of a Proportional Fluid Amplifier ", Paper edited by Society of Automotive Engineers, Inc., the Authors are from Engineering Research Div., Deere & Co.

16. Douglas, J. F. and Neve, R. S., " Investigation into the Behaviour of a Jet Interaction Proportional Amplifier ", Proceedings of the Second Cranfield Fluidics Conference, January, 1967, Paper C-3.

17. Griffin, William S., " A Fluid - Jet Amplifier with Flat Saturation Characteristics ", Transactions of ASME Journal of Basic Engineering, December, 1969, 734 - 738.

18. Belsterling, Charles A., " Digital and Proportional Jet Interaction Devices and Circuits ", Fluidics Quarterly, vol. I, no. 2, January, 1968, 61 - 71.

19. Doherty, Martin C., " Applying Fluidic Operational Amplifiers ", ISA Transactions vol. VIII, no. 4, 1969, 287 - 292.

20. Letham, Daryl L., " Fluidic System Design, Vortex Amplifiers ", Machine Design, July 21, 1966, 178 - 181.

21. Larson, Ralph H., " Vortex Amplifier Parameters ", Instruments and Control Systems, vol. XXXVIV, October, 1966, 105 - 110.

22. Howland, G. R., " Performance Characteristics of Vortex Amplifiers ", Proceedings of the Fluid Amplification Symposium vol. II, October, 1965, 208 - 213.

23. Gottron, Richard N. and Gaylord, Wilmer, " A Temperature Control System using Flueric Components ", Proceedings of the Fluid Amplification Symposium vol. III, October, 1965, 245 - 258.

24. Letham, Daryl L., " Fluidic System Design, Application Circuits", Machine Design, March 16, 1967, 203.

25. Sharpsteen, James S., " Fluid Amplifier Measures Flow Velocity ", Control Engineering, January, 1966, 103.

26. Roshko, A., " On the Development of Turbulent Wakes from Vortex Streets ", NACA Report no. 1191, 1954.

27. Schlichting, H., Boundary-Layer Theory, McGraw-Hill Book Company, New York, 1960, 16 - 19.

28. Fage, A. and Johansen, F. C., " On the Flow of Air behind an Inlined Flat Plate of Infinite Span ", Proceedings Royal Society (London), ser. 4, vol. 116, September 1, 1927, 170 - 197.

VITA

The author, Gian Sagar Aneja, was born on January 5, 1948 in Rohtak, India. After his secondary education in New Delhi, India, he passed the Pre-Engineering examination from the Panjab University in 1965. Then he joined the Punjab Engineering College, Chandigarh, India. He received a Bachelor's degree in Mechanical Engineering with first class in May, 1969.

He has been enrolled in the graduate school of the University of Missouri-Rolla, U.S.A. since January, 1970.

APPENDIX A

EXPERIMENTAL DATA

Set: I

Tube Diameter = 1/2 "

Single Control Port

Atmospheric Pressure = 29.152 inches of Hg.

Room Temperature = 83° F

Location of Control Port = 115° downstream

Magnification of Vertical Scale on Oscilloscope = 20 mv.

Velocity Range corresponding to the available

Reynolds No. Range = 4.04 - 404 fps

Corresponding Frequency Range = 19.2 - 1920 cps

Angle of inclination of the Manometer Board = 20° to horizontal

Set: II

Tube Diameter = 1/2 "

Double Control Port

Atmospheric Pressure = 29.010 inches of Hg.

Room Temperature = 79° F

Set: III

Tube Diameter = 1 "

Single Control Port

Atmospheric Pressure = 29.108 inches of Hg.

Room Temperature = 80° F

Velocity Range corresponding to the available

Reynolds No. Range = 2.02 - 202 fps

Table V. Vortex Frequency and Pitot tube Velocity Measurements

Set No.	Run No.	% Wind Tunnel opening	Time setting on scope m. sec.	No. of cycles on scope screen	Vortex Frequency 'f' cps	Vel. head inclined in.	Vel. head Vert. in.	Pitot tube velocity fps
I.	1.	25	5	7 ½	150	0.65	0.222	32.313
	2.	37 ½	5	10 ½	210	1.30	0.445	45.765
	3.	50	5	14	280	2.00	0.685	56.794
	4.	75	5	17	340	3.20	1.095	71.846
	5.	100	5	19	380	4.10	1.405	81.416
II.	6.	25	5	7 ½	150	0.50	0.171	28.322
	7.	37 ½	5	10 ½	210	1.05	0.360	41.104
	8.	50	5	13	260	1.70	0.582	52.279
	9.	75	5	16	320	2.75	0.942	66.541
	10.	100	5	18	370	3.60	1.232	76.127
III.	11.	25	20	12 ½	62.5	0.50	0.171	28.302
	12.	37 ½	10	10 ½	105	1.05	0.360	41.073
	13.	50	10	12 ½	125	1.70	0.582	52.239
	14.	75	5	8	160	2.75	0.940	66.421
	15.	100	5	9	180	3.50	1.20	75.071
IV.	16.	25	20	14 ¼	71.2	0.45	0.154	27.027
	17.	37 ½	10	10 ¼	102.5	1.00	0.342	40.287
	18.	50	10	13 ½	135	1.60	0.547	50.963
	19.	75	5	8 ¼	165	2.60	0.890	65.035
	20.	100	5	9 ½	190	3.60	1.23	76.488

Set: IV

Tube Diameter = 1 "

Double Control Port

Atmospheric Pressure =28.902 inches of Hg.

Room Temperature = 83° F

The experimental data to measure Vortex Frequency and Pitot tube Velocity appears in Table V. consisting of the above four sets. Figures A1 and A2 are the pictures to evaluate the vortex frequencies for the test run no. 2 and 20.

Evaluating P_S, the Static Pressure in the Test Section of the Wind Tunnel:

From the pitot tube data (Table VI.) ΔP, the velocity head and $(P_S - P_e)$ are noted, where P_e is the ambient pressure. A straight line plot with these two variables is then used as a reference to determine P_S for the previous data (knowing ΔP and the atmospheric pressure corresponding to any set, P_S can easily be evaluated, the results appear in Table VI.). The knowledge of P_S is necessary in order to have an accurate estimate of air density inside the test section which was used to evaluate different Reynolds No. corresponding to each run in the data.

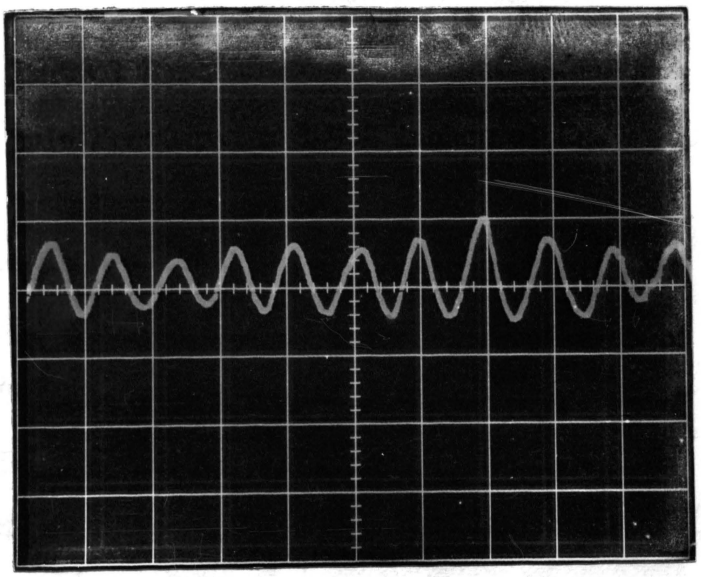

Fig. A1. Vortex Frequency Photograph corresponding to Test Run No. 2.

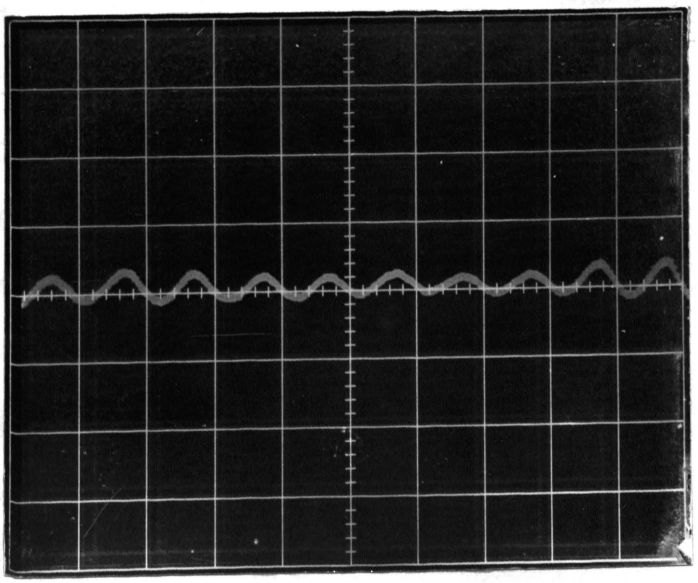

Fig. A2. Vortex Frequency Photograph corresponding to Test Run No. 20.

Table VI. Pitot tube Data

Run No.	ΔP, in. of water	ΔP, in. of Hg.	$(P_s - P_e)$ in. of Hg.	P_e in. of Hg.	P_s in. of Hg.
1.	0.222	0.0156	- 0.016	29.152	29.136
2.	0.445	0.0328	- 0.0332	29.152	29.1198
3.	0.685	0.0505	- 0.0505	29.152	29.1015
4.	1.095	0.0805	- 0.0820	29.152	29.0700
5.	1.405	0.1035	- 0.1055	29.152	29.0465
6.	0.171	0.0126	- 0.0126	29.010	28.9974
7.	0.360	0.0258	- 0.0260	29.010	28.9840
8.	0.582	0.0428	- 0.0440	29.010	28.9660
9.	0.942	0.0694	- 0.0704	29.010	28.9396
10.	1.232	0.0908	- 0.0924	29.010	28.9176
11.	0.171	0.0126	- 0.0132	29.108	29.0948
12.	0.360	0.0258	- 0.0260	29.108	29.0820
13.	0.582	0.0428	- 0.0440	29.108	29.0640
14.	0.940	0.0692	- 0.0712	29.108	29.0368
15.	1.200	0.0884	- 0.0900	29.108	29.0180
16.	0.154	0.0113	- 0.0114	28.902	28.8906
17.	0.342	0.0252	- 0.0260	28.902	28.8760
18.	0.547	0.0403	- 0.0410	28.902	28.8610
19.	0.89	0.0655	- 0.0660	28.902	28.8360
20.	1.23	0.0906	- 0.0912	28.902	28.8108

APPENDIX B

DRAG FORCE AND VORTEX FREQUENCY RELATION

C_D, the coefficient of drag is given by;

$$C_D = D / \tfrac{1}{2} . \rho . V^2 . A$$

where

D = Drag force per unit length of sensor tube

ρ = Density of Air

V = Velocity of Air

A = Projected area per feet length of sensor tube

or, $D = (\tfrac{1}{2} . \rho . A . C_D) . V^2$ (B-1)

also

$$S = f . d / V$$

or $V = f . d / S$ (B-2)

Substituting the value of 'V' from equation (B-2) in (B-1),

$$D = (\tfrac{1}{2} . \rho . A . C_D) . (f . d / S)^2$$

$$= \frac{\rho A . C_D . d^2}{2 . S^2} \cdot f^2$$

It is known that, $\rho \simeq$ Constant

A = Constant

$C_D \simeq$ Constant

d = Constant

S $\simeq$ Constant

Therefore, $D \propto f^2$

$= K . f^2$

where $K = \rho . A . C_D . d^2 / 2 . S^2$, S= 0.2058

Table VII. shows the values of 'K' and hence the drag force experienced.

Table VII. Evaluation of Drag Force experienced by the Sensor tubes

Run No.	Air Density	Diameter 'd' inches	C_D from literature	$K \cdot 10^{-6}$	f^2	$D = K.f^2 . 10^{-6}$ per feet of sensor tube
1.	0.002211	0.502	1.10	2.0897	22500	0.05026
2.	0.002210	0.502	1.20	2.290	44100	0.09852
3.	0.002209	0.502	1.20	2.289	78400	0.17514
4.	0.002206	0.502	1.20	2.2859	115600	0.25824
5.	0.002204	0.502	1.20	2.2838	144400	0.32257
6.	0.002217	0.502	1.05	2.0101	22500	0.05026
7.	0.002216	0.502	1.15	2.2008	44100	0.09852
8.	0.002215	0.502	1.20	2.2952	67600	0.15101
9.	0.002213	0.502	1.20	2.2931	102400	0.22875
10.	0.002211	0.502	1.20	2.2911	136900	0.30582
11.	0.002220	1.008	1.20	18.6239	3906.25	0.07221
12.	0.002219	1.008	1.20	18.6155	11025	0.20380
13.	0.002218	1.008	1.20	18.6072	15625	0.28884
14.	0.002215	1.008	1.20	18.5820	25600	0.47323
15.	0.002214	1.008	1.20	18.5736	32400	0.59893
16.	0.002193	1.008	1.20	18.3974	5069.44	0.09371
17.	0.002192	1.008	1.20	18.3890	10506.25	0.19421
18.	0.002190	1.008	1.20	18.3723	18225	0.33689
19.	0.002188	1.008	1.20	18.3555	27225	0.50327
20.	0.002186	1.008	1.20	18.3387	36100	0.66732

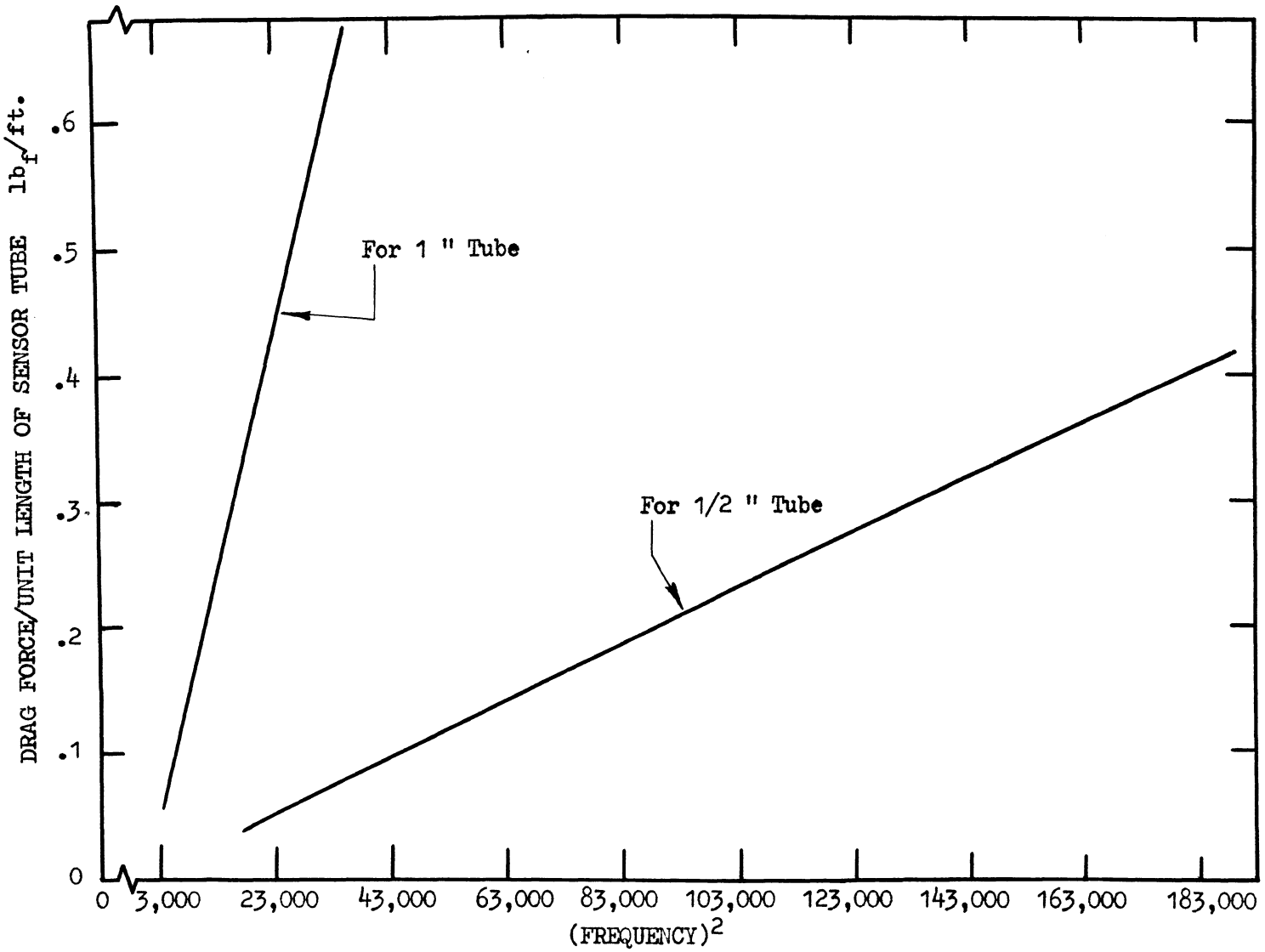

Fig. B1. A Plot of Drag Force experienced by Sensor tubes vs. Square of the Vortex Frequency

Defining a new constant S':

In the present work it is assumed that Strouhal No. remains constant in the Reynolds No. range of 10^3 to 10^5. Fage and Johansen[28] have made an interesting observation by defining a new constant S', in place of Strouhal No. It is defined as,

$$S' = f.d'/V \qquad \text{(B-3)}$$

where

d' = distance between the free vortex layers instead of the usual cylinder diameter

V = Stream Velocity

f = Frequency of vortices shed

S' was found to be rising till R_e = 300 and after that it was practically constant.

$$S' = 0.140 \quad \text{at} \quad R_e = 300$$

$$= 0.143 \quad \text{at} \quad R_e = 20{,}000^+$$

In evaluating S', f and V are already known and d' is related empirically to 'l', the distance between the two consecutive vortices in the same row.

$$d'/l = 0.281 \qquad \text{(B-4)}$$

f, the vortex frequency could also be written as;

$$f = \frac{V - u}{l} \qquad \text{(B-5)}$$

where 'u' is the velocity of vortices with respect to the flowing liquid.

From equations (B-4) and (B-5),

$$d' = 0.281 \cdot \frac{V - u}{f}$$

Therefore, S' is given by;

$$S' = \frac{f}{V} 0.281 \frac{V - u}{f}$$

$$= 0.281 \quad 1 - \frac{u}{V} \qquad \text{(B-6)}$$

In the above expression to evaluate S', the problem lies in the measurement of 'u', the velocity of vortices moving downstream.

Assuming a value of 0.142 for S', d' the distance between free vortex layers for the experimental data has been calculated (Table VIII) using equation (B-3).

Table VIII. Evaluation of distance between free vortex layers for the Sensor tubes

Run No.	d' inches	Run No.	d' inches	Run No.	d' inches	Run No.	d' inches
1.	0.367	6.	0.322	11.	0.770	16.	0.653
2.	0.372	7.	0.334	12.	0.678	17.	0.670
3.	0.342	8.	0.341	13.	0.712	18.	0.642
4.	0.360	9.	0.355	14.	0.706	19.	0.675
5.	0.365	10.	0.352	15.	0.717	20.	0.685

An interesting fact is obtained from equation (B-6) and assuming a value of 0.142 for S'.

$$\frac{0.142}{0.283} = 1 - \frac{u}{V} = 0.505 \simeq \frac{1}{2}$$

or,

$$\frac{u}{V} = 1/2$$

The above equation shows that in the Reynolds No. range of 300 to 20,000^{+} the velocity of vortices moving downstream remains half of the main stream flow velocity.

Fage and Johansen [28] have claimed the new constant S' could be a better choice in place of the usual Strouhal No. Also, as a follow up analysis, the calculation of ' d' ', could be a valuable set of data for the further work as regards the vortices shedding structure is concerned for a particular tube diameter. Once d' is found accurately for a particular size tube, f can be measured by the technique presently used and S' is already known to be constant for a pre-determined velocity range, the velocity could thus, be estimated with a better precision.